NASA
CR
132316
c.1

LOAN COPY: RE
AFWL (.S
KIRTLAND AFB
NASA CR-132316

0062745

TECH LIBRARY KAFB, NM

FINAL REPORT

ON THE DESIGN AND TEST OF A LIQUID INJECTION ELECTRIC THRUSTER

By: Theodore A. Jones
John T. Kenney
E. Howard Youmans

Prepared under Contract No. NAS1-11382 by
GENERAL ELECTRIC CO.
Philadelphia, Pa.

for

NATIONAL AERONAUTICS AND SPACE ADMINISTRATION

TECH LIBRARY KAFB, NM
0062745

TABLE OF CONTENTS

LIST OF TABLES

LIST OF FIGURES

LIST OF FIGURES (cont'd)

ACKNOWLEDGEMENTS

During the course of this program, many people have provided me with assistance, support and counseling in the design, operation and care of electric thrusters. Their counsel was based on long-standing past association with SPET and its creator, Dr. A. LaRocca. Of particular note are Mr. Pete Malherb and Drs.C. H. Marston and A. T. Tweedie.

For those directly associated with the program, the services of Mr. E. Hansen in the design and debugging of the Control Logic Box and other electronics is gratefully acknowledged. In performing work starting with the design and fabrication of Configuration #2, through a long, agonizing and detailed compilation of test data and analysis thereof, a special debt is owed to my co-author, Mr. Jack Kenney. My other co-author, Mr. Ted Jones, worked tirelessly and with great imagination, diligence and inventiveness during all phases of the program. I acknowledge this with deep thanks. A special thought and acknowledgement is extended to my General Electric management chain for their most appreciated and never-ending support of this program.

And, finally, a sincere expression of thanks to Mr. John Dahlgren, the program technical monitor for NASA at JPL for his encouragement, understanding and help throughout the program.

E. Howard Youmans
Program Manager
30 July 1973

I. SUMMARY

This program was sponsored by NASA under contract number NAS1-11382. During the course of the program, a liquid injection electric thruster (LINJET) was designed and tested. The results of the tests were very encouraging with thruster performance levels well in excess of design goals. Thruster characteristics demonstrated included thrust output of over 4440 micronewtons (1000 micropounds [μlbf] at 5Hz), impulse bits greater than 3000 micronewton seconds/pulse (675 μlbf-sec/pulse) and impulse bit to energy ratios in excess of 300μ newton-seconds per joule (67.5 μlbf-sec/watt).

Supporting activities to the engine design and test included a five-million pulse life test on the main capacitor, a 46-million pulse test on the trigger electronics, design and fabrication of a zero resistance torque connector for use with the torsional pendulum thrust stand, design and fabrication of a logic box for control of engine firing, and a physical and chemical properties characterization of the perfluorocarbon propellant.

While the results were encouraging, testing was limited, as many problems existed with the design. The most significant problem was involved with excessive propellant flow which contributed to false triggering and shorting. Low power active thermal control of the propellant storage cavity, coupled with a re-evaluation of the injection ring pore size and area exposed to the main capacitor discharge are areas that should be investigated should this design be carried forward.

The performance of the LINJET described herein cannot be considered conclusive toward establishing a breakthrough in pulsed plasma technology without additional verification. Some of the performance data exceeded what might be termed as a reasonable breakthrough in the state of the art. However, until further testing is performed the results presented in this report exemplify a significant improvement in the performance of presentday pulsed plasma technology .

In the near future it is anticipated that MIT Lincoln Labs in Lexington, Mass., will perform additional laboratory tests on the LINJET engine for NASA.

II. INTRODUCTION

Since the late fifties, General Electric has performed a number of studies and contracts concerning various forms of advanced space propulsion systems. Those early efforts included some of the initial work on ion engines, arc rockets, resistojets and low density arc rockets and analyses of different fuels and their related loss mechanisms.

Since 1962, the Company has concentrated on the development of a family of electric propulsion devices generically called "SPET" for Solid Propellant Electric Thruster. These thrusters have several modes of operation ranging from a subliming rocket, detonator, resistojet, arc jet and supersonic arc jet to the pulsed plasma jet. During the later phases of this period, the main thrust of the activity was aligned to the pulsed plasma mode of operation, and it was during this time that many of the concepts of the program being reported herein were initially investigated.

The funding for the above work was from both governmental contract and company discretionary sources at about a 1:1 mixture ratio. The current work was sponsored by NASA, with contract administration by Langley Research Center and technical direction by the Jet Propulsion Laboratory.

It is felt that this program, using a liquid propellant, represents the start of a new generation of electric thrusters. The progenitor being SPET and the progeny being LINJET for Liquid Injection Electric Thruster.

III. REQUIREMENTS

The requirements for this program, as delineated in the Statement of Work, were intentionally broad in character for the following reasons: 1) maximum advantage would be taken of past work by other investigators; 2) the basic philosophy was to be of a hardware/empirical approach, as opposed to a rigorous analytical study eventually leading to a design; 3) it was to be the implementation of a single point design which, based on precedence and limited sub-scale testing, offered the greatest chance of success; and 4) it was to be a program to demonstrate a concept that had been previously conceived and subjected to limited testing in sub-scale models in the laboratory.

In general, the thruster design was to incorporate the following features:

1. A centrally located coaxial trigger electrode assembly that ablated a teflon surface by a low-energy capacitive discharge.
2. A trigger assembly that was to be segmented into a least three sections, and each section was to be fired in an indexed, sequential timeline.
3. A propellant that was a waxy perfluorocarbon, and that was to feed or be injected in the region of main capacitor discharge by capillary flow (wicking) through a porous membrane.
4. A total of six thermistors; two to measure temperature at the anode (or cathode) of the main capacitor, with the remaining four to measure propellant temperatures at selected locations.
5. A heating element for controlling propellant temperature.

The conventional parameters used in measuring performance of a thruster were also stated as goals, again reflecting the latitude and broad scope of the contract in allowing the contractor to develop a concept rather than meet a particular set of rigid requirements. The performance goals presented are listed in Table III-1.

TABLE III-1 - PERFORMANCE GOALS

THRUST (AT 5 Hz)	2.224 NEWTONS (500 MICROPOUNDS)
IMPULSE BIT	0.4448 NEWTON-SECONDS (100 MICRO-POUND-SECONDS)
IMPULSE BIT TO ENERGY RATIO	0.02224 NEWTON-SECONDS PER JOULE (5 MICROPOUNDS-SECONDS PER JOULE)
SPECIFIC IMPULSE	1000 SECONDS
TOTAL IMPULSE	4448 NEWTON-SECONDS (1000 POUND-SECONDS)

Further goals for the program were established either by implication, considering the type of device and potential applications, or by desire to facilitate future experimentation. Included in this category were:

1. The capability to operate for 10^7 pulses.
2. The mechanical design of the thruster would be such that various parts could be changed, modified or adjusted without major disassembly or machining.
3. Since the thruster was to be a laboratory concept demonstration device, little if any effort would be expended for design as a piece of flight hardware.
4. Typical application of this hardware would be on an orbiting space vehicle in zero or a very low gravity environment. Hence, for earth-bound testing, the one-G field had to be considered.
5. Design for any type of dynamic environment (other than "normal" man handling) was not a consideration.

The program requirements can be summarized by saying that it was desired to build a piece of laboratory type equipment to a new and basically untried concept. The design was to contain generic types of trigger and propellant feed mechanisms, and the conventional measures of performance were stated as goals selected from past work as readily attainable.

IV. ENGINE DESCRIPTION AND OPERATION

The Liquid Injection Electric Thruster (LINJET) is composed of two major elements: 1) the thruster and 2) the electronics--including trigger circuit, main capacitor, instrumentation, and heater. An overall external view of the assembled engine is shown in Figure IV-1.

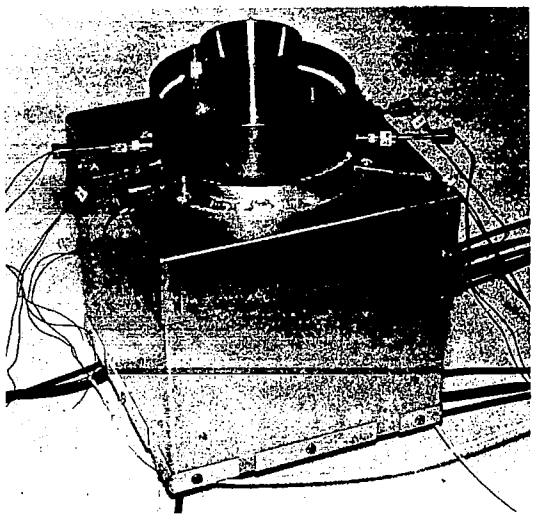

FIGURE IV-1 - LINJET ENGINE ASSEMBLY

The concept of the thruster was to use a set of electronics to discharge a low-energy capacitor in vacuum across a piece of teflon. The ionic particles generated would be of sufficient volumetric density to breakdown the interelectrode gap of a high-energy capacitor. The cathode of the main capacitor (or the anode--it works either way) was to be a porous material impregnated with the waxy perfluorocarbon material used as the propellant. The energy of the main capacitor discharge would ablate the propellant on the surface of the porous material, ionizing it and electromagnetically accelerating the plasma to ambient through the exhaust nozzle. Measurable thrust would be created as a reaction to the high exhaust velocity of the ablated particles. Propellant would be replaced at the surface of the porous material by capillary action (wicking) but, theoretically, not flow beyond the surface line due to surface tension forces. The porous material would be continuously fed with propellant by virtue of having one side directly exposed to the propellant reservoir.

The firing rate of the main capacitor is variable, and for this program was restricted to between 0.01 Hz and 5.0 Hz.

V. ENGINE DESIGN

A. Thruster System

Cross-section views of the thruster, including the trigger assembly, are presented in Figures V1 and V2. Figure V-1 delineates the design used for the bulk of the testing. Figure V-2 is the final design that evolved during the course of the program.

The principal differences between the two are in the design of the trigger assembly, the method of sealing the porous metal injection ring, and in the design of the insulating path to minimize the build-up of carbonaceous deposits on the internal surfaces. The following discussion will describe the final design with appropriate remarks directed toward the evolutionary process in those three areas.

The nozzle section is threaded into the support ring until it bottoms against the porous material injection ring used for propellant feed. The annular volume formed by these parts is the propellant tank, which is capable of holding approximately 450 grams (one pound) of propellant when a 6.35mm (0.25 inch) thick injection ring is used.

Since the injection ring is one electrical terminal in the discharge of the main capacitor, the mechanism used to seal the interfaces between the injection ring and the other parts must also provide good electrical conductivity. The evolution of the sealing mechanism for the design is given in Table VI-1. For the final design, delineated in Figure V-2, a formed compression ring of 0.5mm (.020 inch) diameter 24K gold wire was used at each interface.

The main capacitor is built with a continuous ring outer terminal. A contoured ceramic insulator separates the two terminals. The flanged base of the thruster support ring is bolted to the outer terminal of the capacitor, providing a low resistance, low induction connection between the capacitor terminal and the injection ring. A copper pintle within an externally contoured ceramic column insulator is threaded onto the center post terminal of the capacitor. The column insulator bears against the contoured ceramic capacitor insulator and the underside of the copper pintle. The cylindrical section of the head of the pintle is coplanar with the injection ring to provide the discharge gap during thruster operation.

A slot was milled in the base of the column insulator to permit feed-thru of the flat copper conductor to the center terminal of the capacitor.

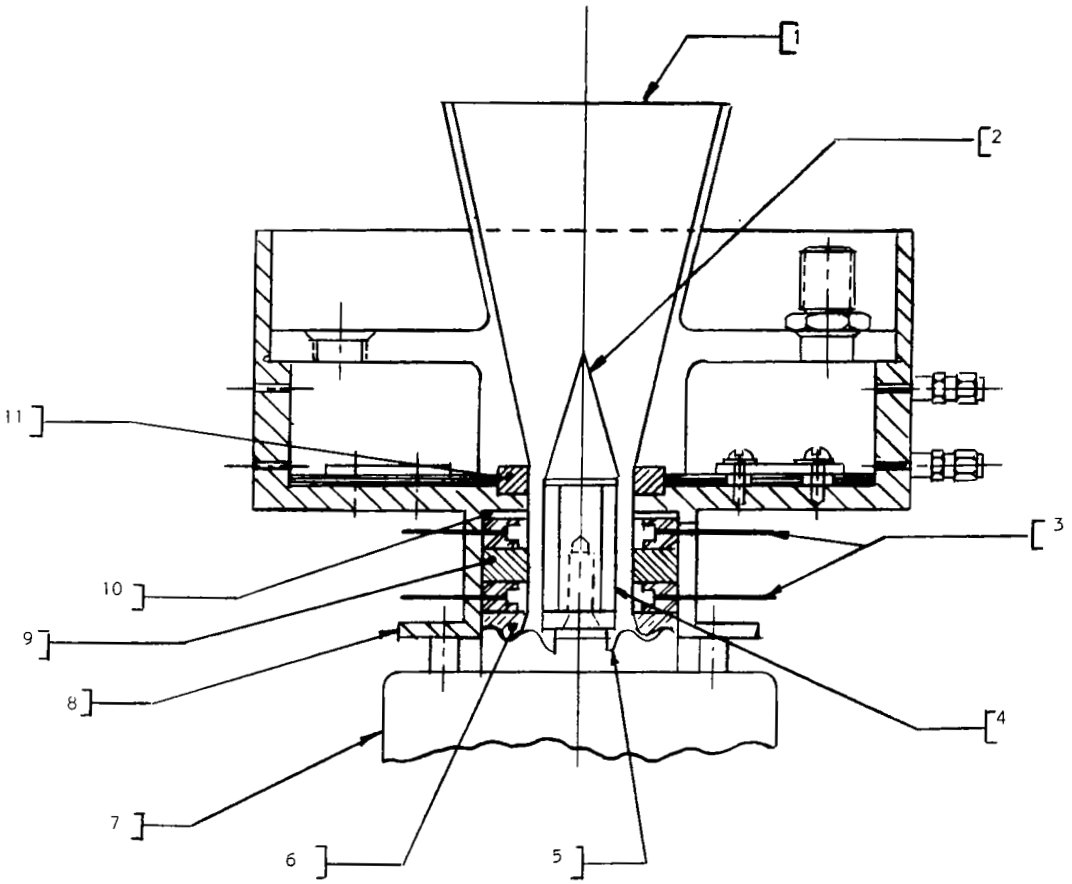

PART NO.	PART IDENTIFICATION
1	Nozzle/Propellant Chamber
2	Pintle
3	Trigger Electrodes
4	Insulator (Ceramic)
5	Lead, High Voltage
6	Spacer (Ceramic)
7	Main Capacitor ∿ 25. mfd
8	Thruster Housing
9	Teflon Fuel Wafer (Trigger)
10	Insulator (Ceramic)
11	Porous Injection Ring

FIGURE V-1 - INITIAL LINJET ENGINE CONFIGURATION

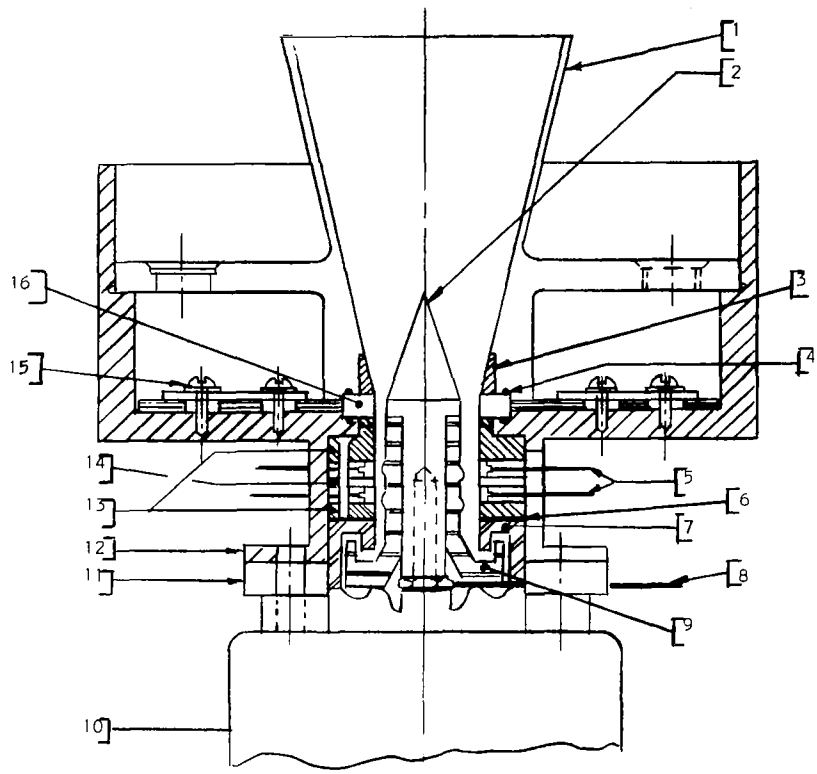

PART NO.	PART IDENTIFICATION
1	Nozzle/Propellant Chamber (STN STL)
2	Pintle
3	Insulator, Nozzle (Ceramic)
4	Seal Rings (24K Gold)
5	Trigger Electrodes (Copper - RTV)
6	Shims (As Req'd) (Mylar)
7	Insulator/Standoff (Nylon)
8	Lead, High Voltage (Copper)
9	Insulator, Pintle (Ceramic)
10	Capacitor 25. MFD
11	Spacer Ring (Copper)
12	Support Ring/Housing (Brass)
13	Insulator Rings, Trigger (G-10)
14	Fuel Wafer, Trigger (Teflon)
15	Propellant Feed Screens (STN. STL)
16	Injection Ring (Porous STN. STL.)

FIGURE V-2 - FINAL LINJET ENGINE CONFIGURATION #2

The trigger assembly is made up of five pieces; an upper insulator, a lower insulator, two trigger rings, and a solid Teflon ring which provides fuel for the trigger assembly. Each trigger ring consists of four electrodes located in a cruciform pattern and encapsulated in RTV silicone rubber. In the final design, clearance holes are provided in the upper insulator, the two trigger rings and in the Teflon ring while tapped holes are provided in the lower insulation ring. In this manner, the trigger may be built up as a separate sub-assembly - independent of stack up tolerances. This permits check-out of the trigger elements to assure proper operation prior to engine assembly.

In the original design the compressive load on the trigger elements and the Teflon ring was obtained when the support ring was bolted to the capacitor. This required careful and time-consuming shimming to assure surface contact between the support ring and the capacitor without having voids between any pieces in the stack. This problem is not eliminated in the final design, but it is reduced and the initial pressure in the trigger assembly is preset and checked on the bench.

The trigger assembly is slipped into the bore in the lower section of the support ring. Four slots milled in the support ring base (see Figure V-3) permit feed-through of the electrical conductors from the trigger electronics to the trigger segments.

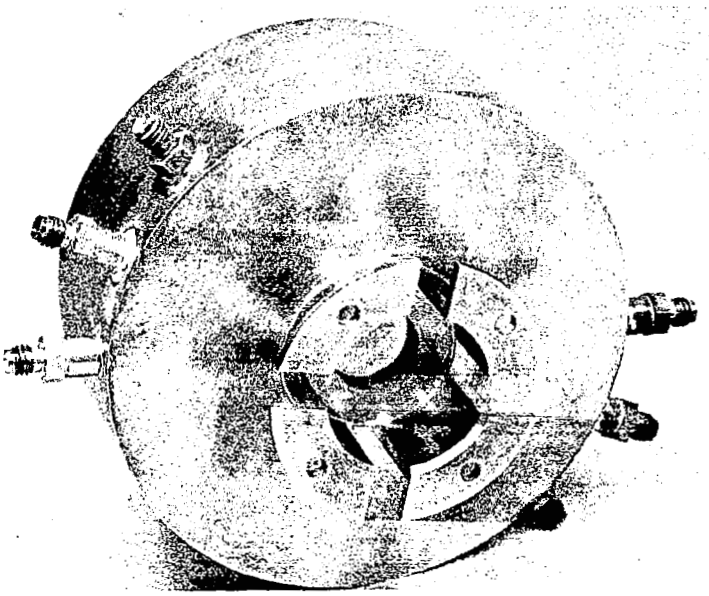

FIGURE V-3 - TRIGGER HOUSING IN AFT END OF ENGINE SUPPORT RING

The bottom nylon insulator provided two functions in the design. First, it supports the trigger assembly by bearing against the ceramic insulator of the main capacitor and against the bottom insulator of the trigger assembly. Appropriate shims are inserted between this piece and the trigger assembly to give correct dimensional correspondence at assembly. The second function is to provide a baffle arrangement with the column insulator surrounding the pintle (capacitor center terminal).

It had been found in previous programs, and reaffirmed during this program, that the internal surfaces become coated with a carbonaceous residue from the ablated propellant. It is electrically conducting and, in a relatively short operating time, will effectively short-out the main capacitor. During test, this manifests itself as either "false triggering" or electrically shorting the main capacitor. In false triggering, the main capacitor will discharge without external stimulation at a rate proportional to the value of the capacitor charging resistor and the resistance of the carbon conducting path. The point at which this occurs is a function of the voltage applied to the main capacitor.

To interrupt the surfaces susceptible to coating by the discharge, the "labyrinth" sealing arrangement pictures in Fig. V-2 was employed.

During engine test, it was necessary to fire the engine horizontally--that is, the thrust axis would be perpendicular to the gravity vector. This presented a design problem not found in the normal application in a zero-g environment of feeding propellant to the porous injection ring once the level of propellant receded below the level of the injection ring. This was accomplished by placing several flat screens in the bottom of the support housing to act as a capillary feed device. Seventeen screens were used that were a line-to-line fit with the inside diameter of the support housing and the outside diameter of the porous feed ring. Each screen was cut from 10 micron pore size, Rigidmesh stainless steel flat sheet. Brass brushings, precisely machined in length, permitting 0.0127mm (.0005 in.) nominal gap between screens, were used as spacers between the support ring and a perforated steel cover plate. Threaded screw holes were tapped in the support housing and clearance holes drilled in the perforated steel plate and screens. The assembly was made by laying the screens in the bottom of the support housing and aligning the clearance holes with the threaded holes. The spacers were inserted through the screen and the perforated retaining ring placed over top with all clearance holes aligned. Screws with washers were used to clamp the assembly together. An exploded view of this hardware is shown as Fig. V-4.

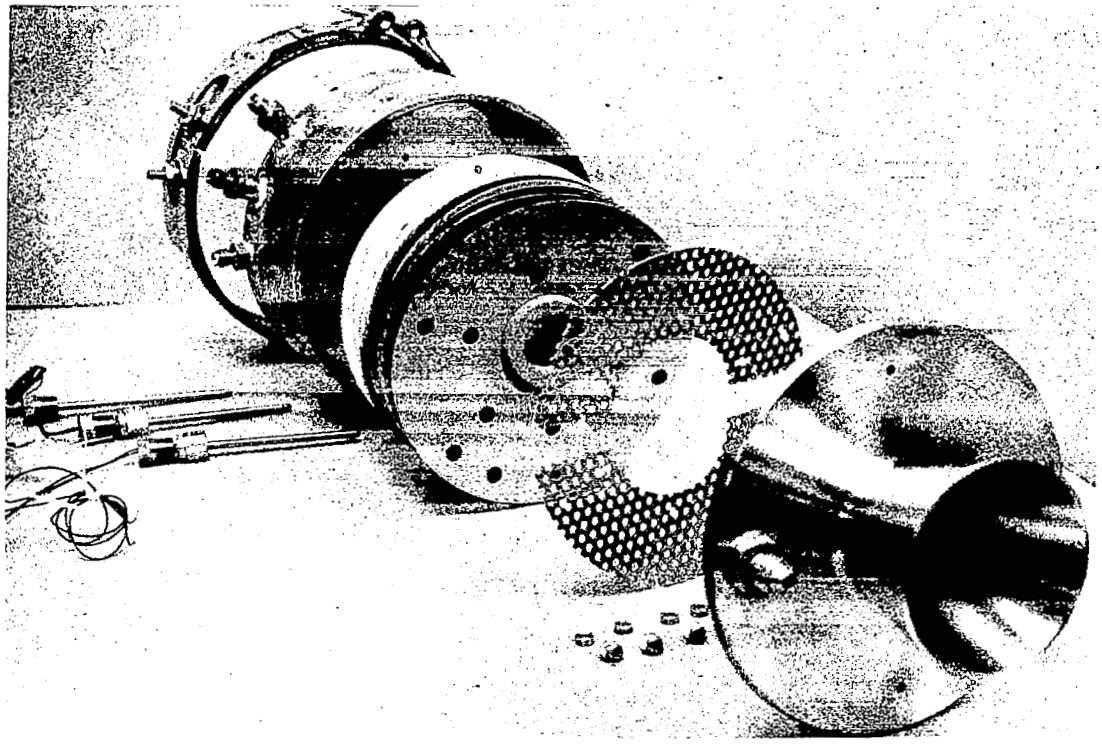

FIGURE V-4 - EXPLODED VIEW OF PROPELLANT FEED SYSTEM

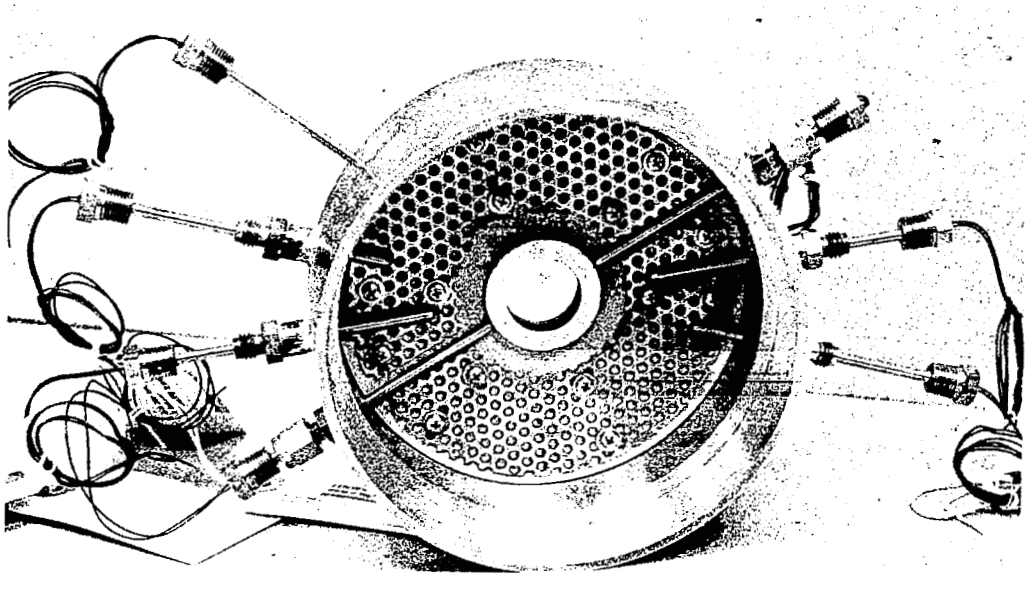

FIGURE V-5 - FEED SYSTEM, THERMISTOR AND SUPPORT RING ASSEMBLY

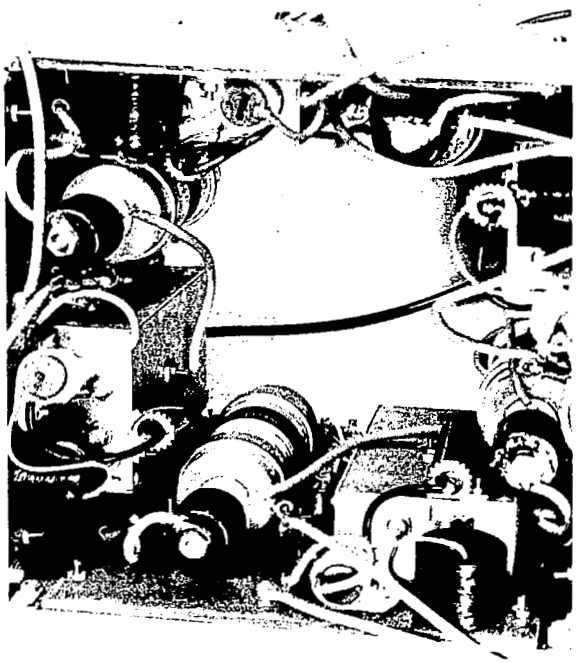

FIGURE V-6 - FORWARD END OF TRIGGER BOARDS ASSEMBLED

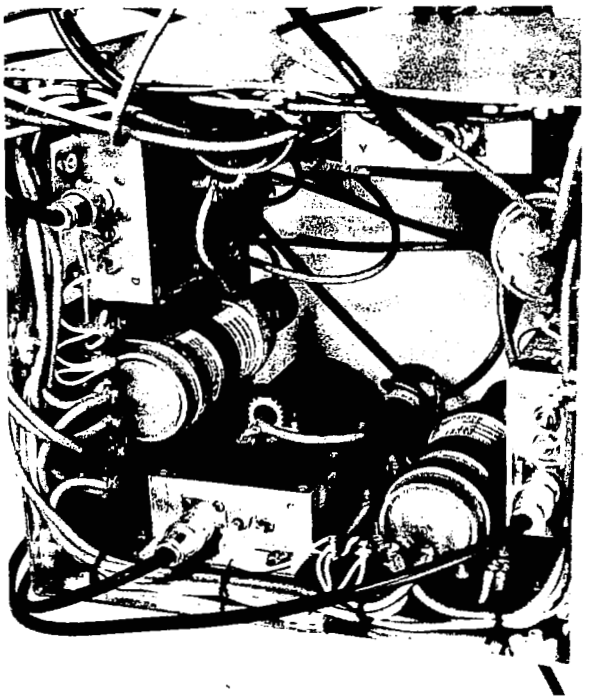

FIGURE V-7 - AFT END OF TRIGGER BOARDS ASSEMBLED

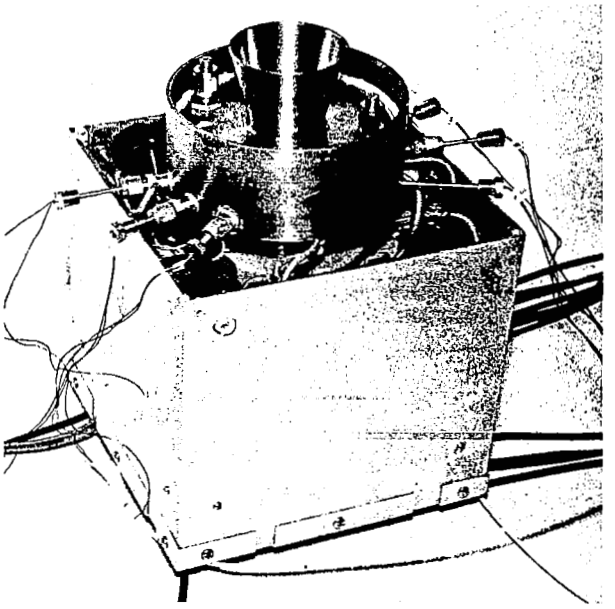

FIGURE V-8 - LINJET ENGINE ASSEMBLY LESS FORWARD COVER

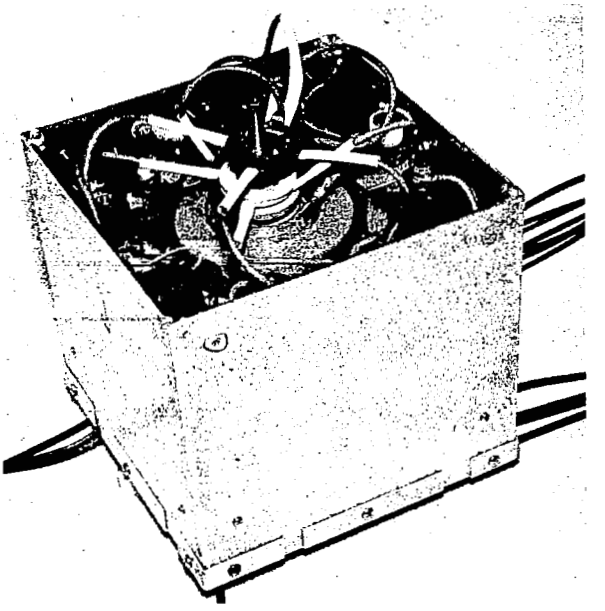

FIGURE V-9 - ORIGINAL DESIGN OF LINJET ENGINE ASSEMBLY

Six thermistors were used to measure temperature of the propellant and were arranged in two sets of three with each thermistor 180° apart from its counterpart. Axially, they all lay against the capillary feed screens in slots machined in the perforated retaining ring. Radially, there was a pair against the outside diameter of the porous feed ring and a pair at the 1/3 and 2/3 radially outward points. Swagelock fittings were used for the retention and sealing at the point of penetration of the support ring wall. Fig. V-5 shows an assembly of the feed system and the thermistors in the support housing.

Each of the four trigger electronic boards were mounted on the inside of an 20.32cm (8 inch)square open-ended aluminum box as shown in Fig. V-6 and V-7. A subassembly was made of the main capacitor and support housing with trigger elements in place. This was inserted into the box as shown in Fig. V-8 and held in place by an aft cover plate with a cylindrical insert to support the capacitor and a forward split cover that bolted to the box and clamped to the support ring. Electrical connections between trigger electronics and terminals and power feed to the main capacitor were made internally prior to installation of the forward cover. The control signal and power wires for the trigger circuit are fed through access ports in the aft cover. (The original method is shown in Fig. V-9 where the trigger elements and trigger Teflon propellant ring were separate items that had to be aligned at assembly.)

An electrical heater (see last item in Fig. V-4) in the form of a metallic ring may be clamped to the outside diameter of the support ring if required. Due to limitations in electrical pin connections when the engine was on the thrust stand for test, the heater was not used in most of the tests.

Propellant loading was accomplished using the two fittings on the nozzle section and an ordinary grease gun. The propellant is a stiff wax at room temperature. To liquify it for engine loading, the temperature was raised to above 60°C (140°F). The liquid propellant was poured into the grease gun and then pumped into the engine through one of the nozzle fittings until it flowed out the other fitting. The pump was then disconnected, and both fittings capped. For the later tests, the propellant was deaerated by placing the engine with the electric heater on it in a vacuum chamber. The propellant was heated above the melting point with one of the fittings uncapped. The pressure was reduced and any entrapped air exhausted through the fitting, usually as a froth of propellant and air. When flow stopped, the heater was turned off, and the unit allowed to cool in vacuum. During test, one fitting, with suitable plumbing, was left open to vent the propellant tank to ambient pressure.

The quantity of propellant loaded was determined by accurately weighing the hardware before loading the propellant and after deaerating. Accuracy of the weighing system was ± 0.0227 grams (.00005 lbs.)

B. Trigger Circuit

The trigger circuit used to fire the main capacitor is shown in Fig. V-10 and is designed to accept a square wave pulse from the logic control box while rejecting noise pulses from adjacent circuits. The input circuit consists of a blocking diode and a zener diode which rejects any pulse below a five volt level or any negative noise spikes. The following two stages are used for differentiation and current amplification which produces a sharp pulse to fire the SCR.

When the SCR is turned on, capacitor C is discharged through the primary windings of the transformer. The transformer in turn suppiles a high voltage signal to ignite the spark gap. The spark gap acts as an on/off switch for the primary trigger capacitor and trigger segment circuit. When the spark gap fires, the charged trigger capacitor is placed directly across the trigger terminals producing an arc which ablates and ionizes a piece of solid Teflon between them. These particles, located in the area of the main capacitor electrodes, provide a conducting path for the main capacitor to discharge its stored energy.

It will be noted that there is a 1.0 ohm resistor in the trigger capacitor discharge line. This was included to reduce the discharge current when it was found during the life test cycle that the Teflon trigger propellant ring was severly ablated after three days of testing.

Each of the trigger capacitors is discharged each time the main capacitor is fired. They are discharged sequentially around the ring with a 0.5 millisecond delay between discharge across each segment. Further, the first pulse of the four pulse train is indexed around the ring 90° from the start of the last train. This system provided two important functions in engine operation: 1) using four trigger pulses for each main capacitor discharge provided quad redundancy in obtaining at least one trigger pulse for each main capacitor firing; 2) it had been observed in previous work that a single trigger pulse is sufficient to fire the main capacitor. With this in mind, it was felt that the main capacitor would be discharged by the first pulse of the triggger pulse train. To prevent continuing discharge of the main capacitor at the same location on the pintle and the injection ring, the first pulse of the trigger pulse train was indexed sequentially to the trigger electrodes around the trigger ring assembly by electronic means.

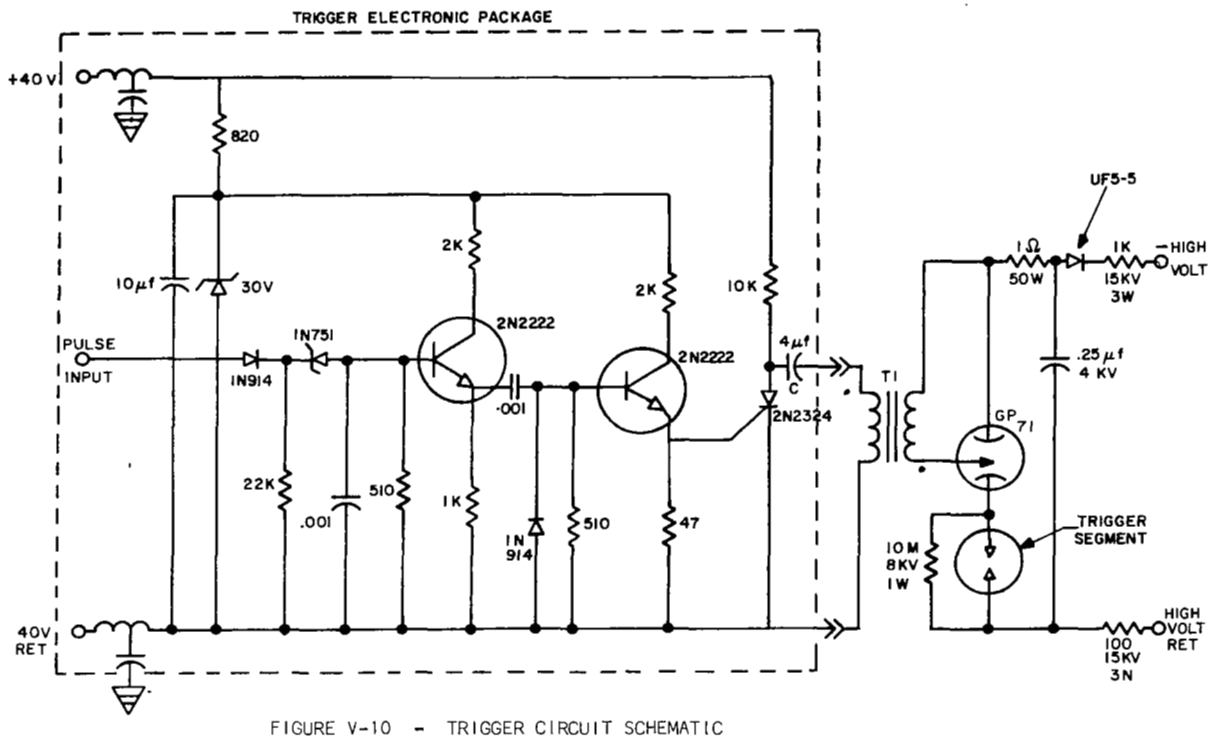

FIGURE V-10 - TRIGGER CIRCUIT SCHEMATIC

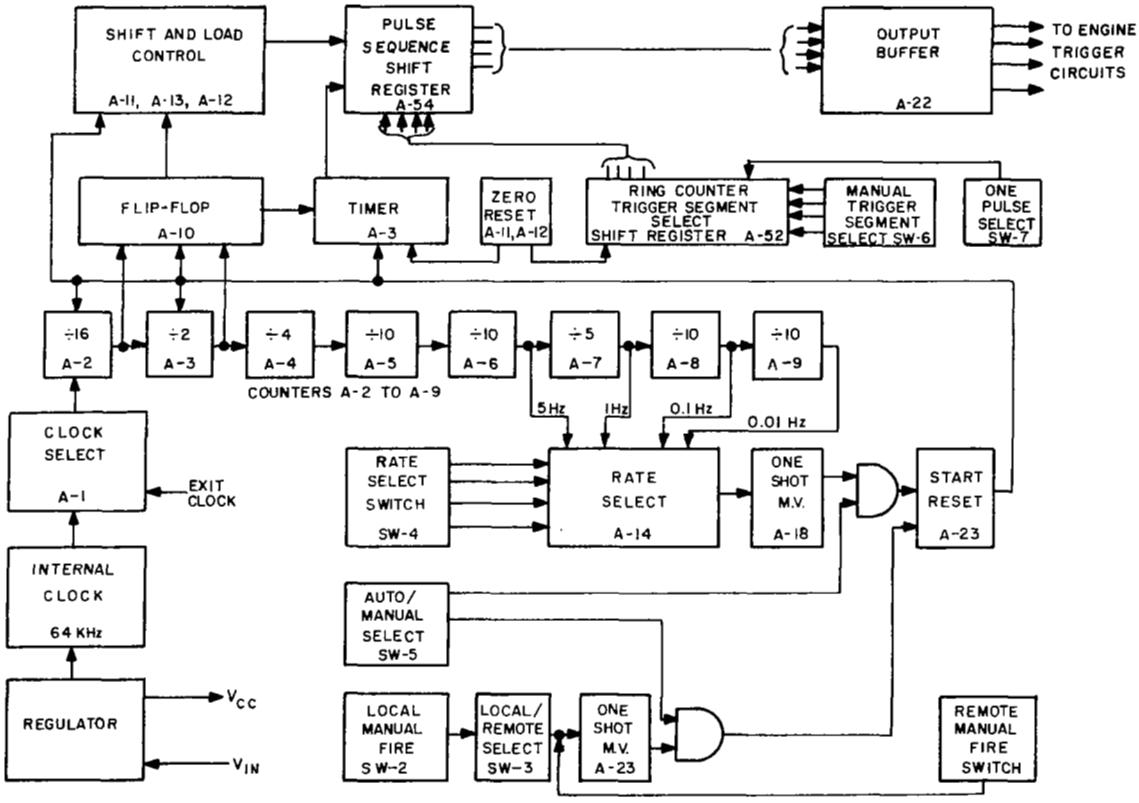

FIGURE V-11 - BLOCK DIAGRAM CONTROL LOGIC BOX

Both points were demonstrated during engine testing. On several occasions, it was determined that one or more of the four trigger elements was inoperative, but the main capacitor discharged. Also, visual observation of the main capacitor discharge showed that the point of initiation of the arc did, in fact, move in the programmed manner.

(Details of the system to provide these features are included in Appendix C.)

C. Fire Control Logic Box

The electrical operation of the LIN JET engine is controlled by the Fire Control-Logic Box. A block diagram of the Fire Control Logic box is shown in Figure V-11. The logic box provides for the following functions:

1. Selection of trigger firing rates of 5, 1, 0.1 or 0.01 Hz when operating on the 64 KHz internal clock or other proportional trigger rates where operating on an external clock.
2. Automatic firing at the selected trigger pulse rate or manual firing at any pulse rate that the test conductor chooses.
3. Local or remote manual firing control.
4. Automatic sequencing of the lead trigger pulse of the four pulse train to each of the four trigger segments to prevent repetitive initiation of the main capacitor discharge at the same location within the engine, or manual override of the automatic sequencing so that the lead pulse of the trigger train will always occur at a selected trigger segment. In addition to the manual override, provision is made to have only one trigger segment fire rather than having a four pulse train.

A complete description of the circuits and the operation of the Fire Control Logic Box is contained in Appendix C.

D. Engine Temperature Control Circuit

The temperature control circuit consists of a four-resistor bridge circuit with the temperature control thermistor as one leg of the bridge as shown in the temperature controller schematic, Fig. V-12. Two series connected potentiometers are used to establish the operating set point for the heater. One pot is used for coarse settings between 25°C and 82°C, while the second pot provides fine settings between 49°C and 82°C. A toggle switch is used to select the coarse or fine temperature control range.

The output from the bridge is fed to a high gain operational amplifier with a hysteresis loop provided to fix the temperature swing about any set point at ± 1.5°C.

The operational amplifier provides current to a relay driver. The relay contacts are the direct control in the heater circuit.

The temperature control circuit is included in the logic control box and required 115V AC and + 15V and - 15V DC for proper operation.

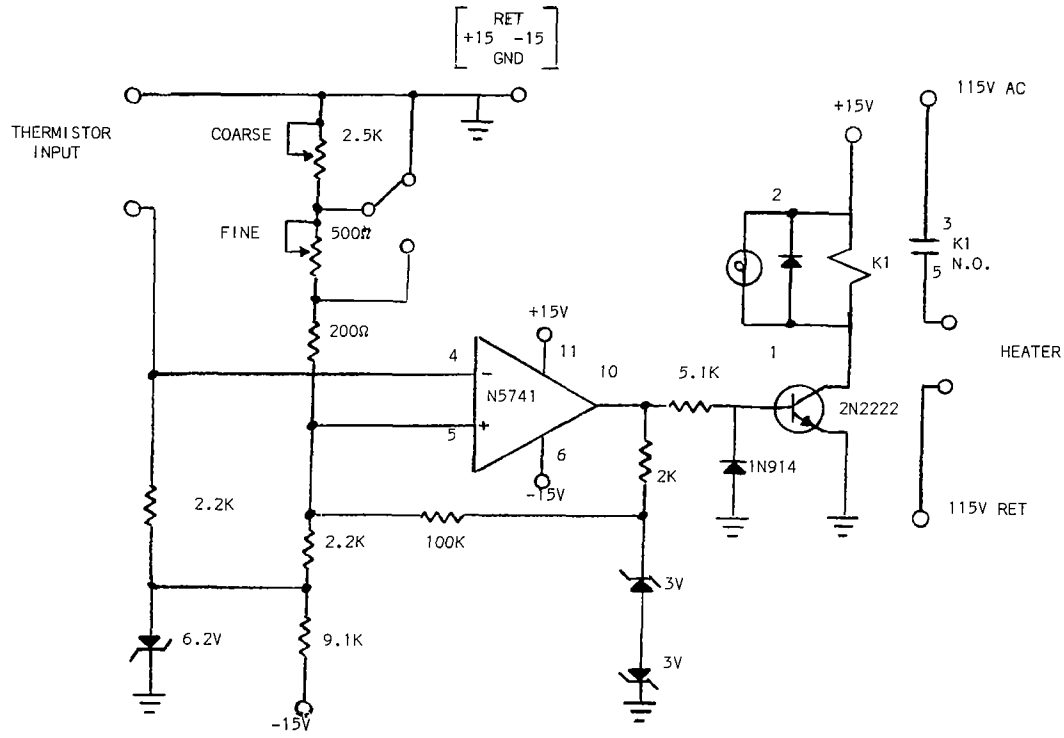

FIGURE V-12 - HEATER CONTROL CIRCUIT SCHEMATIC

E. Thrust Measurement System

The system used in measuring the engine thrust was a simple torsional pendulum, shown in Figure V-13. It is a highly modified version of a system that had been used on previous programs. The principle parts are three-legged base, a two-element support frame, an engine support platform suspended by the wire (the torsion member), a deflection measurement assembly, and an interface connector (IFC).

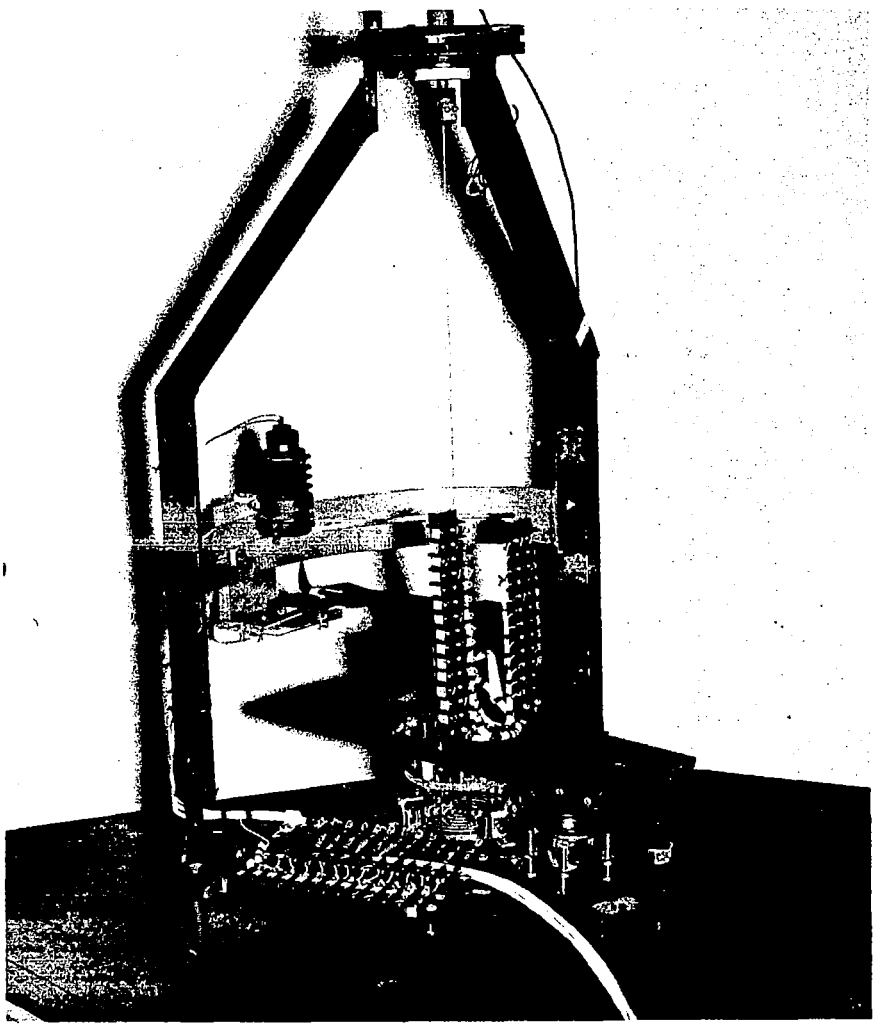

FIGURE V-13 - TORSION PENDULUM THRUST STAND

The base holds the stationary half of the IFC, provides a mounting location for the wiring terminal boards (used as a convenient interface between the test chamber and the IFC), and mounting for the support frame. The three legs of the base are adjusting screws which were used to align the two halves of the IFC.

The two-element support frame is the structural member that supports the weight of the engine and counterbalance and the fixed end of the torsional wire. The deflection measuring system is mounted on these members.

At the apex of the support frame is the wire clamping and adjusting mechanism. The thumb screw on top moves the wire axially adjusting the elevation of the engine support platform. The lever rotates the wire about its axis so that the deflection system can be zeroed. On the bottom of the mechanism is the friction clamp for holding the wire. The wire and clamp are electrically isolated from the frame so it could be used as the high voltage lead to the main capacitor during engine testing.

The engine support platform is the moveable end of the torsional pendulum. It is supported in the top center by the wire through a friction clamp (hidden behind the terminal boards in Fig. V-13). The engine is mounted on one side of center firing horizontally at a fixed perpendicular distance from the wire. Counterweights are placed on the other side to balance the load. Adjusting the position of the weights allows leveling of the engine. A pointer for the deflection measurement is on this side of the platform. On the underside are the mobile elements of the IFC. Terminal strips are also mounted on the support platform to provide an accessable electrical interface between the engine and the IFC.

The deflection measurement system consists of a light source, a series of light sensitive silicon devices (Solar Cells), and a graduated scale, all mounted on the support frame. The light source impinges on the solar cells causing a measurable voltage output proportional to the amount of cell area exposed to the light. During engine firing, the pointer arm on the engine support platform rotates, proportional to thrust, shading the solar cells, changing the exposed area and hence the voltage output. Therefore, thrust is measured by solar cell voltage. The system can be calibrated by holding the pointer at indicated angular deflections inscribed on the graduated scale and the voltage measured. Such calibrations were made pre and post-engine test with little variation noted. During test, deflections as small as 0.1 degree were measured.

The final element of the thrust measurement system is the IFC shown in Figure V-14. It provided the necessary electrical connections for the main capacitor power, trigger capacitor power, and trigger segment signals, and the useful but not essential connections for propellant heater power and control, and data from eight thermistors. In total, 24 wires were needed to operate the engine and obtain useful data, and to cross the torsional interface in a manner that would not affect the operation of the pendulum. After review and analysis of several systems, it was decided to use a liquid metal for a contact between the moving parts. Elemental Gallium (99.9% pure) was selected because of the comparatively low melting point, 29.75°C (87°F), its ability to supercool to below-normal room ambient, the very low vapor pressure of $1.X10^{-33}$mm of Hg at the melting point, and a low specific resistance of 25.8 μohms-cm (for the liquid).

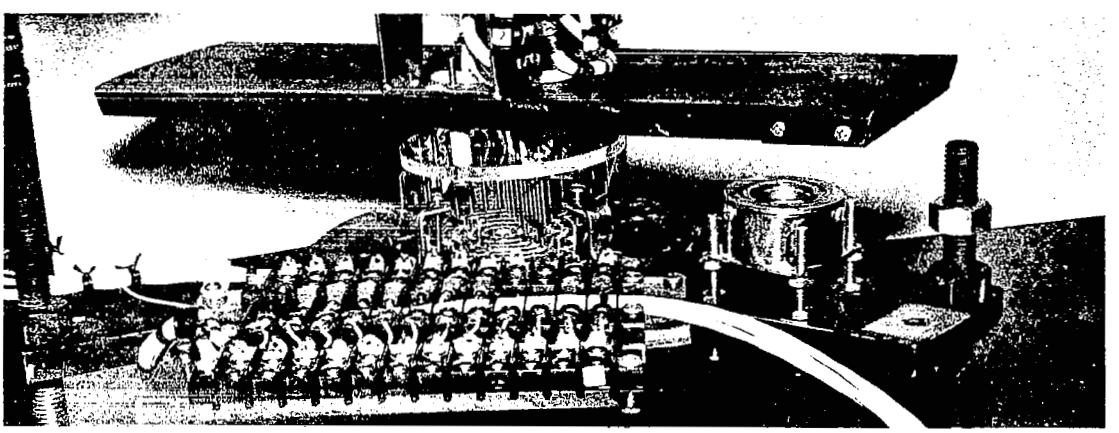

FIGURE V-14 - INTERFACE CONNECTOR

The design of the IFC used a system of four concentric rows of 60° circular arc segments plus a center hole machined into a plastic disk. These non-interconnected galleries held the liquid Gallium. From the opposite side of this disk, threaded holes were tapped through the plastic and into each gallery. Stainless steel studs were threaded into the holes flush with the bottom of the gallery, providing a connection between the liquid metal and the wire lead (Stainless steel was used because Gallium combines with most other metals). This piece was mounted to the thrust stand base plate. A second plastic disk was made with similar studs located on center with each gallery. It was mounted to the moving engine support platform. The studs extended well beyond the faces of the disk. One end was used to connect to the engine wiring. The opposite end was drilled to accept a 0.35mm (0.015 inch) diameter by 12.7mm (half-inch) long stainless steel pin. In operation, the pin would be immersed into

the center of the liquid Gallium filled gallery, thus completing the electrical path from the outside world to the engine mounted on a torsional pendulum.

Thus, the design provided electrical continuity through ± 30° of rotation. It was realized that the element of viscous damping had been introduced, but it is interesting to note that in the differential equation of motion for a torsional pendulum:

$$\frac{Jd^2e}{dt^2} + \frac{de}{dt} + ke = 0$$

(Inertia-acceleration) (damping-velocity) (position)

that, at an equilibrium position, when acceleration and velocity are zero, the forces on the system are represented by the displacement from its null position. The damping coefficient only affects the rate at which angular position is changed.

From test data, the system worked quite well. The damping coefficient turned out to be near critical so that there were minimal oscillations when changing position. Several examples of the position vs. time trace are presented in the test section (Section VI) of this report.

In the initial fabrication of the IFC, the Gallium galleries were nominally 3.18 mm (.125 inch) wide. The task of aligning the 24 pins into these slots bordered on the impossible. Therefore, the decision was made to make a new gallery disk with 6.35 mm (.25 inch) wide galleries within the same external envelope. The existing pin disk would be retained but pins were eliminated and realigned to correspond with the new gallery configuration. Because of the reduced pin availability, four thermistors and the heater power and control lines were eliminated. The loss of these functions was not critical as the principal temperature of the injection ring was still being recorded and the heat to melt the propellant was generated by discharging the main capacitor for a period of time in a "pre-test warm-up" and monitoring the injection ring temperature. Typically, this warm-up time was about one hour but was variable as it is obviously a function of the firing rate and the frequency of discharge.

During the time period when the engine was changed from configuration #1 to configuration #2, the IFC was also modified to add on the eight channels which had been deleted when the width of the gallery was increased. This was accomplished by adding bolt-on rings of galleries and pins around the existing disks.

In the post-test data analysis, it is required to translate the measured parameters, in this case, angle, into the engine performance parameters of thrust and impulse bit. This system was analyzed as shown in Section VI.

VI. TEST PROGRAM

A. Propellant Characterization

As required by the Statement of Work, the physical and chemical properties of the selected propellant were to be measured and reported. The original intent of this activity was to provide quantitative data for material comparison and reorder purposes. It was expanded, however, to include tests to determine the capillary flow characteristics of various materials and configurations. These data would be used in the analytical flow feed study (See Appendix A), eventually leading to a material selection and size of the injection ring.

Appendix B presents in detail the tests conducted, method of testing, and data obtained.

B. Capacitor Life Test

The main capacitor used in this program is nominally rated at 25 microfarads (μf) and 6000 volts. It was manufactured by Maxwell Laboratories, Inc., as their catalog No. 30109.

The purpose of this test was to determine if there was any degradation of the part when it was used as a high current pulse source. The plan was to use a test configuration as shown in a block diagram, Figure VI-1, where a spark gap, triggered by a transformer output, would act as high current switch to discharge the energy of the main capacitor into the load. It was also part of the plan to discharge the capacitor at a 5 Hz rate until 10^7 pulses were accumulated.

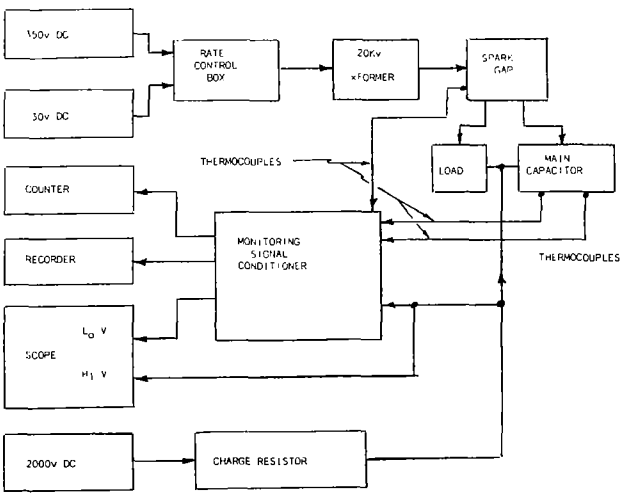

FIGURE VI-1 - BLOCK DIAGRAM - LINJET MAIN CAPACITOR LIFE TEST

The actual set up is shown in Figures VI-2 and VI-3. All components were close coupled to reduce the resistive and inductive loads. Fans were used for forced cooling of the set up, but the temperature of the spark gap still exceeded 93.2°C (200°F).

Data was accumulated using a multipoint recorder for temperature, an electromechanical counter for monitoring the number of main capacitor discharges and a Tektronix Oscilloscope, with camera, for viewing and recording the discharge waveform.

Figure VI-4 is a schematic of the control circuit and the capacitor under test. The circuit consists of an adjustable unijunction oscillator which provided the pulses used to turn on an SCR. For this test, 350 VDC was used to charge C1, through a 3.9K resistor. When a pulse is applied to the SCR, this charge is dumped through the primary windings of T1, producing a 20KV pulse across the secondary windings. Meanwhile C2, the 28μf test capacitor has been charged to 2KV. The transformer signal fires the spark gap which acts as a closed switch in the capacitor discharge circuit. A 0.025 ohm load was added to this loop to simulate the condition expected in the engine life test.

A test set up was also made to check the capacitor parameters at the start of test and periodically during the life cycle. Figure VI-5 is the set up that was used. It will be noted that the set up is similar to the life test set schematic (Figure VI-4) except a coaxial fixture is used so that the capacitor internal values of inductance and resistance can be measured.

The results of the testing performed are presented in detail in Appendix D as extracted from the test log, and from various oscilloscope pictures and the data reduced from those pictures. In summary, approximately 5.2M pulses were recorded before testing was terminated. It will be noted from the contents of Appendix D that initial efforts were exploratory in nature trying to get the equipment to operate. Further, for a significant portion of the test, the peak discharge current was on the order of 9000 amperes. Revisions to the set up reduced the resistance and increased the current to over 17,000 amperes. At the 5 Hz rate this was too high a load on the spark gap and two failures occurred.

Testing was discontinued after the second spark gap failed because: 1) the main point of the program was to build and test an engine not life test capacitors; 2) during the first 4.1M pulses there was no measurable change in capacitor parameters as measured with the coaxial cavity; 3) oil was leaking out of the capacitor at the center post either due to a mechanical failure of the lead solder joint between center post and ceramic insulator or due to overheating from the close coupled hot spark gap.

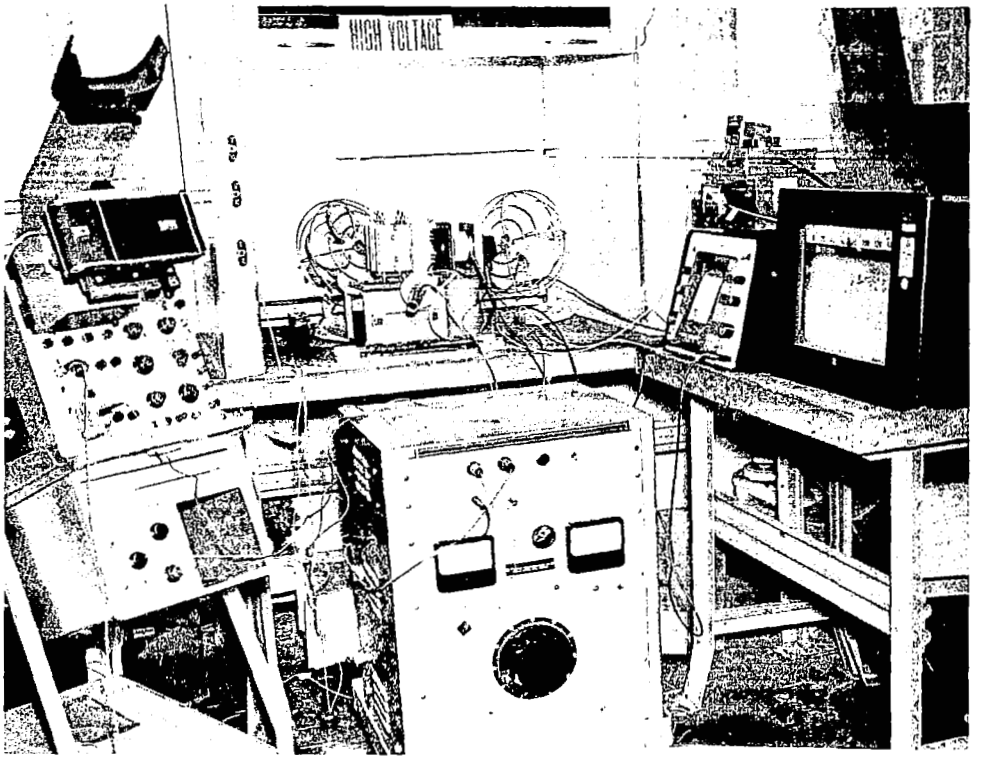

FIGURE VI-2 - TEST SET UP FOR MAIN CAPACITOR LIFE TEST

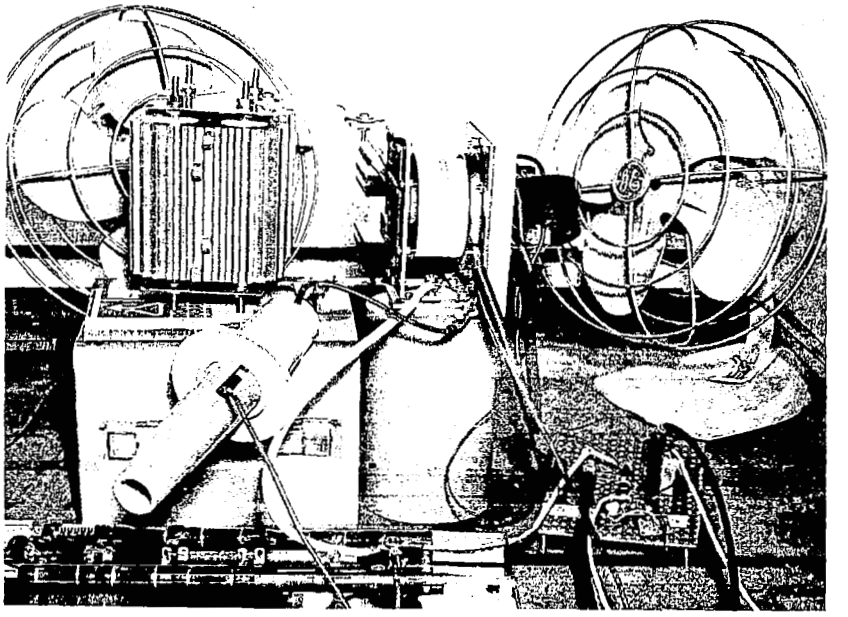

FIGURE VI-3 - MAIN CAPACITOR LIFE TEST CONFIGURATION

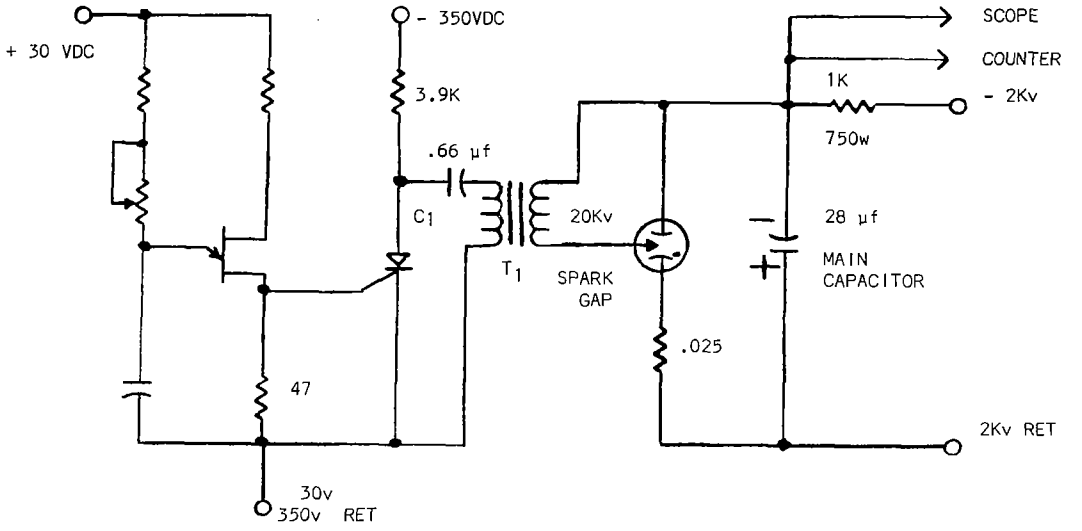

FIGURE VI-4 - MAIN CAPACITOR LIFE TEST SCHEMATIC

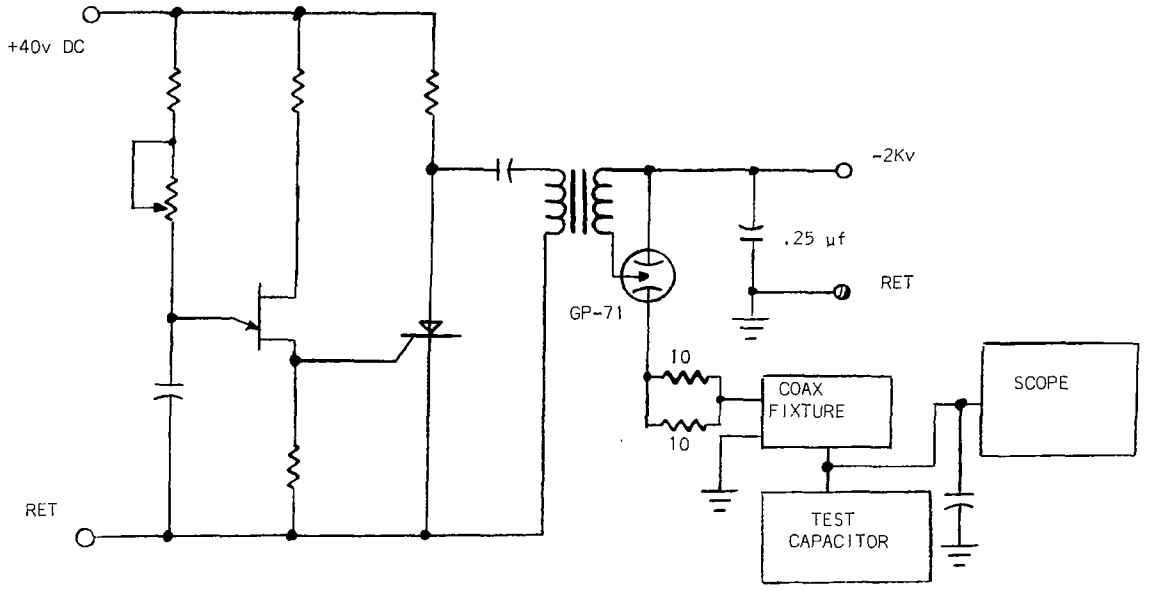

FIGURE VI-5 - CAPACITOR PARAMETER MEASUREMENT SCHEMATIC

C. Trigger Circuit and Trigger Segment Life Tests

The objective of the trigger tests was to determine the combination of materials and physical configuration of a trigger segment which could be operated with predictable, consistent results for a life of several million pulses over a range of voltages and pulse rates. Life tests would also be conducted on the trigger pulse circuit electronics, the trigger capacitor and the spark gap.

The block diagram of the trigger segment test is shown in Figure VI-6 and the schematic of the trigger pulse circuit is shown in Figure VI-7.

The test program consisted of a development test series and an extended life test.

Development Tests

In the development tests combinations of the following materials were assembled and tested.

Trigger Electrodes: Encapsulated in RTV Silicone with smooth and serrated faces.

Fuel:

a. Solid Teflon circular segments with thickness of 0.85 mm (.033 in) and 1.6 mm (.063 in).

b. Fiberglass reinforced Teflon tape (nominal thickness 0.1 mm) built up in layers to produce variable thicknesses.

Primer: Carbon dust mixed in Flourocarbon grease in varying proportions to produce a desired resistivity.

A summary of the results of the development test series is given in Table VI-1.

The results of the development tests showed that the configuration of the mechanical portion of the trigger segment had little effect upon trigger operation, except in the case of the graphite-coated tape. This configuration was an unstable mechanical assembly with slip planes between each layer of the Teflon tape. With time, the assembly would slip with resultant failure. (See Fig. VI-6)

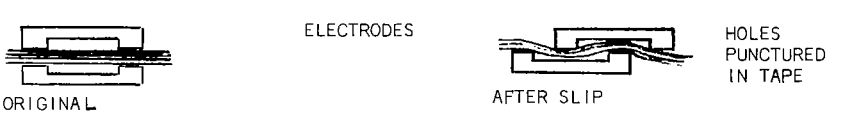

FIGURE VI-6 - TRIGGER TERMINAL FAILURE MODE

The significant variable was the resistance of the primer material. Very high resistance resulted in poor performance. When the resistance was reduced from 1.0 Megohm to 0.1 Megohm, consistent satisfactory operation was achieved.

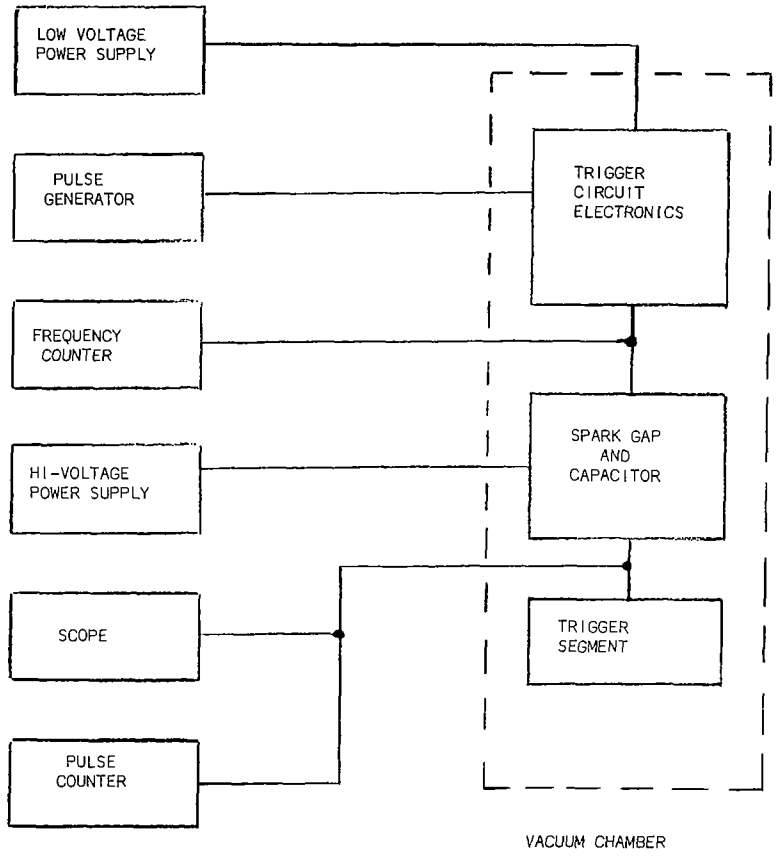

FIGURE VI-7 - BLOCK DIAGRAM - TRIGGER CIRCUIT LIFE TEST

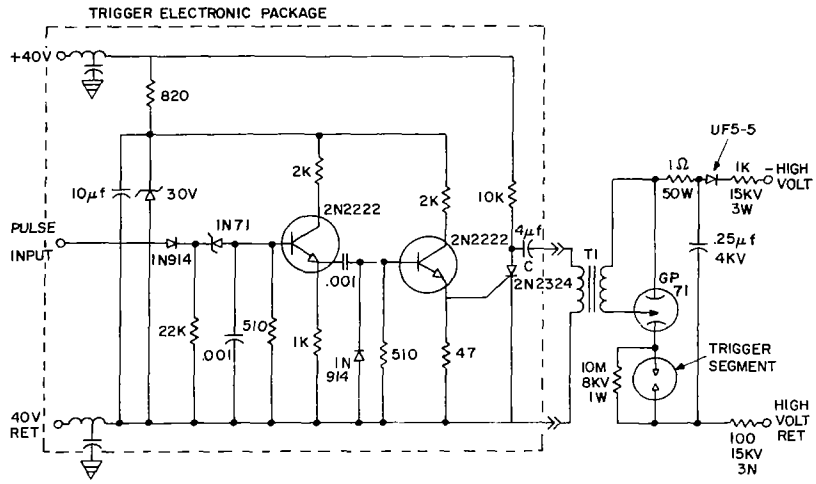

FIGURE VI-8 - TRIGGER SEGMENT LIFE TEST SCHEMATIC

TABLE VI.1 SUMMARY OF TRIGGER SEGMENT DEVELOPMENT TESTS

TEST NO.	CONFIGURATION ELECTRODE	TEFLON	APPLIED VOLTAGE	PULSE RATE APPLIED	ACTUAL	PRIMER RESISTIVITY	COMMENTS
1	Smooth	.033 Solid	2000 to 2800	2.5 to 5.0	Var.	1 Meg	Erratic operation accumulated 2.016 x 10^6 pulses operated primarily at 2400v
2	Smooth	.062 Solid	3000	5.0	Var.	1 Meg	Poor operation, 50000 pulses
3	Serrated	.033 Solid	1600 to 2400	1.25 to 5.0	Var.	1 Meg.	Performance varied between very erratic to very good; accumulated 1.444 x 10^6 pulses; much ablation of teflon
4	Serrated	.062 Solid	1700 to 2400	5.0	Var.	1 Meg.	Poor operation; 35000 pulses
5	Serrated	.033 Solid	1800 to 2800	5.0	Var.	1 Meg.	Erratic; 6,000 pulses
6	Serrated	.033 Solid	1600 to 4000	5.0	Var.	0.5 Meg.	Erratic; 1.238 x 10^6 pulses; varied R&C in electronics (cap discharge)
7	Serrated	.033 Solid	1200 to 2600	5.0	Var.	1.0 Meg.	Erratic; best operation ∿ 2200 volts, but much ablation. Varied R&C. 255,000 pulses.
8	Serrated	16 layers 4 mil tape	1300 to 2000	5.0	Var. 5.0 @ 2000V	0.5 Meg	Erratic operation below 2000V. Good @ 2000V. 1.867 x 10^6 pulses. Shorted gap. Layers graphite gated.
9	Serrated	16 layers 4 mil tape	1700 to 2200	5.0	Var.	0.56 Meg.	Erratic to smooth operation. Failed 3 times due to slippage of assembly. Graphite-coated layers 1.116 x 10^6 pulses.
10	Serrated Smooth	Solid .062	1200 to 2400	5.0	Var.	20K Ω	Erratic. 658,000 pulses.
11	Serrated Smooth	.062 Solid	1800 to 2250	5.0,2.5 1.25	5.0,2.5 1.25	100K Ω	Smooth operation. 8.544 x 10^6 pulses at 1800V. Change HV Pwr. Supply;operated smoothly at 2250V for 2.067 x 10^6 pulse.

TABLE VI.2 SUMMARY OF TRIGGER SEGMENT LIFE TESTS

TEST NO.	CONFIGURATION ELECTRODE	TEFLON	APPLIED VOLTAGE	PULSE RATE APPLIED	ACTUAL	COMMENTS
1	Smooth	.062 Solid	1875 2500	5.0	Var	Operated well for 0.4 x 10^6 pulses @ 1875V. Became erratic; gradually increased voltage to 2500V over 1.297 x 10^6 pulses. Total 1.695 x 10^6 pulses. 100K Ω primer.
2	Smooth	.062 Solid	1800V	5.0	5.0	Operated for 13.994 x 10^6 pulses. Shut down and re-started six times during 34-day test period. 100KΩ primer.
2a	Smooth	.062 Solid	2250	5.0	5.0	Operated well for 12.24 x 10^6 pulses with 8 stops and restartes. Power failure in bldg. on one occasion shut down system, but unit operated well after restart. 2nd pwr. failure killed unit. 31-day test period 100K Ω.
3	Smooth	.062 Solid	1800	5.0	5.0	Reprimed unit restart. Operated for 1.08 x 10^6 pulses until another pwr. failure shutdown vacuum system. One stop and restart. 7-day test. 100KΩ
4	Smooth	.062 Solid	1800	5.0	5.0	Rebuilt unit with new teflon. 100KΩ primer. Operated for 4.96 x 10^6 pulses with three stops and restarts. 11-day test. Shut-down.

Trigger Life Test

The life tests of the trigger segment are summarized in Table VI.2. Test 2a is a continuation of test 2 with the only change being an increase in voltage from 1800V to 2250 volts.

In test #2, the segment accumulated nearly 14×10^6 pulses over a 34-day period with six intentional shutdowns and restarts. Operation became errotic at 1800 volts, and the applied voltage was increased to 2250 volts.

Increasing the voltage extended the life for an additional 12.25×10^6 pulses over a 31-day period. There were eight intentional stops and restarts during this period. In addition, a building power failure shut down the test inadvertently. When power was restored, the pulse circuit continued to operate but with the vacuum system working only on the roughing pump, the pressure in the chamber was too high resulting in extensive cross component arcing with obvious improper operation of the trigger. When the pressure was reduced in the chamber, the trigger continued to operate satisfactorily until another general power failure one week later early on a Friday evening. The same condition as above developed and this killed the trigger segment.

Life Test #3 ran for seven days with the accumulation of 1.08x10 pulses. The operation then became erratic.

Life Test #4 ran for 11 days with 4.96×10^6 pulses accumulated. Testing was terminated because of engine testing in another area of the plant.

Throughout the trigger segment development and life testing, the same pulse circuit, capacitor and spark gap were used. These accumulated 46.5×10^6 pulses with no problems noted during the seven months of testing (other than uncontrollable power losses).

D. LINJET ENGINE ASSEMBLY TESTS

Summary

The objectives of the LINJET engine assembly tests were threefold.

1. Demonstrate the workability of the concept of a porous member injection mechanism coupled with a radial discharge segmented trigger assembly.
2. Measure the performance of an engine of this design.
3. Meet or exceed the design goals delineated in the Statement of Work.

As will be seen from the discussion that follows, all of the test objectives were met, with two exceptions. In summary, during the 36 hours when the main capacitor was discharged, some of the performance parameters were as follows:

1. Measurable thrust was obtained for 10 hours and 45 minutes.
2. Thrusts levels greater than 2224 μ-newtons (500 μlbf) were obtained for 48 minutes.
3. A peak thrust of 6681 μ-newtons (1502 μlbf) was attained for approximately two minutes.
4. Impulse bits greater than 444.8 μ-newton-seconds (100 μlb-seconds) were achieved for greater than 91 minutes.
5. Impulse bit to energy ratios greater than 22.24 μ-newton second per joule (5 μlbf-second per joule) were attained for 71 minutes.
6. During the last test, an integrated overall efficiency of 24% was attained.

The exceptions to the work statement goals was an inability to test continuously for 48 hours and attaining a specific impulse of 1000 seconds.

Engine assembly tests were planned to be conducted in two phases. The first phase to consist of static tests (no thrust measurement) during which the trigger capacitor voltage, trigger pulse frequency and the main capacitor voltage would be varied to determine the combination of input parameters which would produce consistently satisfactory operation. The tests would also serve to demonstrate the adequacy of the engine - logic control box interface. The second phase was to be operation during which thrust measurements would be made with the input parameters determined in phase one.

The testing was conducted on two basic configurations of the engine. Configuration #1 is shown in Fig. V-1, and configuration #2, is shown in Fig. V-2. Within each basic configuration there were minor variations: in configuration #1 several methods were attempted to seal the propellant injection ring at the interfaces with the support housing and the exhaust nozzle. These are listed in Table VI-3. For configuration #2, different injection rings were used and, in one test series, an attempt was made to thermally insulate the main capacitor from the heat produced by the engine. To achieve an electrically conductive injection ring seal for this configuration, the engine body and nozzle had flat machined surfaces, the injection ring was ground flat on each side and the sealing was accomplished by crushing a 0.5mm (0.020 in.) 24K gold wire between the sealing surfaces. The gold wire was formed to the appropriate diameter with ends overlapped, and was held in place on the support ring and nozzle sealing surfaces with an adhesive to prevent movement during assembly.

TABLE VI-3

SEAL CONFIGURATIONS

	ENGINE BODY AND NOZZLE SEALING SURFACES	INJECTION RING SEALING SURFACES	OTHER SEALING MECHANISMS
(a)	Machined flat	Machined surfaces as cut from bar	None
(b)	Machined flat	Ground flat	None
(c)	Shallow concentric V. Grooves (both parts)	Ground flat	Thin copper gaskets each side of injection ring
(d)	Shallow concentric V Grooves	Ground flat	Electrically conductive epoxy both sides

In addition to the differences in engine configuration, there were differences in the quantity of propellant loaded in the propellant tank and the sealing of the propellant tank during engine operation.

In the test series with configuration #2 (18 Apr. to 9 May 1973), the propellant tank was filled to approximately 70% of its volume to reduce static head, and the propellant and propellant tank were out-gassed to reduce the pressure head. In addition, during engine testing, the propellant tank was vented so that the very small static head of the fuel was the only external driving force other than capillary flow to feed propellant to and through the injection ring.

PROBLEMS:

A number of problems were encountered during the testing of the LINJET engine. The principle problems were excess propellant flow and false triggering. Excess propellant flow was caused by leakage at the injection ring interfaces with the nozzle and the support ring and by high feed rates through the injection ring as the temperature increased above the propellant melting point of 60°C (140°F). Excessive propellant flow resulted in a buildup of propellant in the clearance volume between the injection ring and the pintle. When it was mixed with the carbonaceous deposits from normal firings it caused a short across the normal discharge path of the capacitor leading to a cessation of operation of the engine.

False triggering was a more prevalent problem during all of the testing. It may be caused by too high a pressure in the test chamber which is the result of propellant usage greater than the pumping capacity of the vacuum pumps. With the high pressure in the chamber or a locally high pressure within the engine itself the capacitor will discharge across the gap in the engine without excitation as the charge voltage on the capacitor reaches a value compatible with the local pressure and the distance across the gap.

False triggering was also observed where the pressure in the chamber was in the 1.0×10^{-6} torr range. This type of false triggering was observed just prior to forced engine shutdowns due to apparent shorting of the engine. Post test inspections indicated a carbonaceous buildup on the trigger assembly and on the insulating surfaces. It is hypothesized that the carbon like deposits had some discontinuities. These acted as gaps so that as the charge voltage was building up on the capacitor, a value would be reached where breakdown across the discontinuity would occur. With continued false triggering the discontinuities would be bridged and the engine would short.

The Gallium electrical interface caused some difficulties in obtaining test data. The melting point of Gallium is $\sim 27^{\circ}C$ (85°F) and when the cold walls of the vacuum chamber were turned on the Gallium would freeze in two galleries in the outer ring. A hot plate type heater was placed below the plastic piece containing the galleries and was intended to maintain the temperature above the freezing point of the Gallium. The two galleries which froze were above the bundle of wires leading from the individual galleries to the terminal boards and electrical feed throughs of the vacuum chamber. The wire bundle masked the heat to the galleries directly above them. In retrospect the problem could have been minimized by separating the wires into many small cables rather than having one large cable.

A limited part of the phase 1 tests were conducted in a 0.49 m diameter by 0.67 m high (19 in d x 26 in) oil diffusion pumped vacuum chamber. The engine assembly was built up and a system check out test was conducted on the four trigger segments (with no voltage on the main capacitor) and the logic control box. Severe EMI problems were encountered in that when a fire pulse from the logic control box was sent to one of the four trigger segments, the other three would fire simultaneously. A solution to the problem was obtained by a complete rework of the grounding system including the addition of more shielding in the engine assembly cables and the incorporation of isolation diodes and filter capacitors in the logic control box.

Following the rework of the engine to correct the EMI induced problems a series of four tests were conducted. In the first two tests, with the pintle of the engine at negative polarity, operation was erratic. In the third and fourth tests, after changing polarity to make the pintle positive, a total running time of six hours and six minutes was accumulated. In each run where the temperature exceeded 60°C (140°F) (the melting point of the propellant) there was a rapid change in pressure in the chamber and false triggering of the main capacitor. This required shutdown of the engine to allow the vacuum pumps to reduce pressure. These forced shutdowns occurred twice in each run.

Since the vacuum system was incapable of maintaining the required ambient pressure (less than 1×10^{-6} torr) when the engine was operating at "rated" temperature a move was made to a larger chamber (1.52 m diameter X 1.52 m high) (5 ft x 5 ft) with a greater pumping capacity. In addition the chamber had provisions for cryogenically cooling the walls which would aid in maintaining the required low pressure.

Because of the move to the larger chamber and the necessity to rewire the thrust stand to further supplement the solution of EMI suppression, the decision was made to conduct all subsequent engine tests on the thrust stand at the expense of deleting the two step approach of static tests (no thrust measurements while varying parameters of voltage and temperature) to a one step approach of varying parameters while measuring thrust.

Table VI-4 is a summary of test results obtained in the Phase 2 testing of the LINJET engine. The data presented in the table are extracts from each engine test during which a significant thrust level (greater than 60μ newton [15 μlbf]) was attained. The raw data for each engine test as reduced from the analog record traces are presented in Appendix E.

The numbering of the test in Table VI-4 is somewhat misleading in that it would appear to the casual reader that these are separate tests. In fact, some of these data are from the same test run but at times when there are distinct changes in conditions during the course of the total test run. This was done for clarity of presentation of the significant results obtained during the program.

Later in this section, a portion of the recorder trace and an analysis for each test point is presented for the corresponding points in Table VI-4. In general, where there are variations in the thrust level on the trace, the data in the table represents the lowest steady state value of the thrust. This was done because the time scale of the recorder (3mm/minute) and the non-linearity of the angular deflection vs. recorder deflection calibration does not lend itself to accurate mechanical integration using a planimeter to obtain an impulse bit.

Method of Data Reduction

The derivation of the method for calculation of the thrust and the impulse of the LINJET engine is as follows:

For a wire in torsion

$$(1) \quad \theta = \frac{TL}{JG}$$

where θ = angular displacement (radians)
T = torque - (newton-meter)
L = wire length (meter
J = polar moment of inertia (meter^4)
G = shear modulus of elasticity (newton/meter^2)

Also

$$(2) \quad K = \frac{T}{\theta}$$

where K = torsional spring constant (newton-meter/radian)

combining (1) and (2)

(3) $K = \frac{JG}{L}$

For an oscillating system, the period (T) is:

(4) $T = 2\pi\sqrt{\frac{I}{K}}$

where I = mass moment of inertia of the oscillating body (newton-meter-second^2)

Defining

(5) $k = JG = LcKc = L_tK_t$

where

Lc = wire length at calibration
L_t = wire length at test
Kc = torsional spring constant at calibration
K_t = torsional spring constant at test
k = wire constant dependent upon the physical and mechanical properties of the wire material used (newton-meter^2)

Combining (4) and (5) and rearranging

(6) $k = \frac{4\pi^2 I Lc}{T^2}$

The mass moment of inertia of a cyclindrical mass is

(7) $I = \frac{M r^2}{2}$

where

M = Mass (Kg)
r = radius (meter)

Combining (6) and (7)

(8) $k = \frac{2\pi^2 M r^2 Lc}{T^2}$

A calibration of the wire was performed using the following values

M = 18,275 Kg (40.296 lbs)
r = 0.09947m (3.916 in)

Lc = 0.3421 m (13 15/32 in.)
T = 42 seconds

The diameter of the Beryllium-Copper wire used to suspend the pendulum platform was 0.0635 cm (0.025 in.)

The wire constant "k" determined from the calibration test was 6.923×10^{-4} newton-meter^2 (2.4129×10^{-1} pound-in.^{2})

Noting that

$$(9) \quad T = FD$$

where T = torque (newton-meter)
F = thrust (newton)
D = Distance of thrust action line from pendulum axis (meter)

Combining (2), (5) and (9) and rearranging

$$(10) \quad F = \frac{k\theta}{L+D}$$

For all tests the moment arm D was 0.133m (5.25 in.).

For tests between 13 Feb. 73 and 8 Mar. 73 the wire length was 0.3421 in. (13 15/32 in.)

For the tests of 20 Apr. 73 and 7 May 73 the wire length was 0.3405m (13 13/32 in.)

Therefore for the tests of 13 Feb. to 8 Mar.

F = 265.55 · θ micro-newtons

F = 59.553·θ micro-pounds

and for the tests of 20 Apr, and 7 May

F = 266.8 · θ micro-newtons

F = 59.805·θ micro-pounds

where θ = angular displacement - degrees.

Impulse bit is defined as $F \cdot t$ where "t" is time. But $t = 1/f$ when "f" is the pulse frequency. Therefore, impulse bit is:

$$(11) \quad IB = \frac{F}{f}$$

Because of the excess propellant flow problem an experimental determination of specific impulse could not be made. The excess propellant either ran out of the engine and was unrecoverable or heavily coated the internal parts that were not included in the pre-test weighing. To permit calculation of efficiency, and thus obtain an indication of engine performance a value of 400 seconds was assumed for specific impulse. This was considered to be suitably conservative as it was 2.5 times smaller than the design goal and represents a value that has been readily achieved similar work by GE and other investigators.

The efficiency of the engine at any point in time is the energy output over the energy input, assuming that specific impulse is constant.

$$\eta = \frac{Eout}{Ein} = \frac{Ge}{f} \frac{F}{Ein} \frac{I_{sp}}{} = \frac{go}{2} \cdot \frac{I_b \cdot I_{sp}}{Ein}$$

	go	=	gravitational constant	- 9.808 m/second/second
	I_b	=	impulse bit	- newton - second/pulse
	I_{sp}	=	specific impulse	- second
	Ein	=	capacitor energy	- joules/pulse or newton meters/pulse
	F	=	thrust	- newtons
	f	=	firing rate	- pulses/second
and	Ein	=	$\frac{1}{2} CV^2$	
where	C	=	capacitance - farads	
	V	=	applied potential - volts	

The total energy into the operation of the engine is

$$Ein = \Sigma (E_p \cdot f \cdot t)$$

where	E_p	=	energy per pulse	- joules/pulse
	t	=	time	- seconds

The overall efficiency is then

$$\eta_o = \frac{Ge}{2} \quad \frac{(F \cdot t) \cdot I_{sp}}{(E_p \cdot f \cdot t)}$$

Test points 1 through 16 of Table VI-4 do not reflect the entire time period during which thrust was measured. They do reflect "point data" for a period of time when the test parameters were constant. In a number of the tests, the parameters were not held constant during the total time period of the test. For these tests, a numerical integration was performed to obtain the total impulse delivered by the engine during the test, and an overall efficiency for the test was determined.

Table VI-5 presents the total impulse, input energy and overall efficiency of the 12 runs during which a significant measurable thrust was obtained. These twelve runs encompass the points 1 through 16 presented in Table VI-4.

TABLE VI-4. Engine Test Summary

Test Point	Date	Main Capacitor Voltage Volts	Main Cap Energy (Joules/Pulse) watt-sec / Pulse	Thrust (μnewtons) μ-lb$_f$ / Pulse	Firing Rate Pulse / Sec	Impulse Bit (μnewton-sec / Pulse) (μlb$_f$-sec) / Pulse	Imp-Bit / Energy μnewton-sec / Joule μlb$_f$-sec / watt-sec	Efficiency (%)	Run Time at Thrust Level (min)	Temp (^{o}C)
1	2/13	800	9.02	210.3 (47.3)	1.0	210.3 (47.3)	23.30 (5.24)	4.6	296	42.6
2	2/14	2000	56.40	1011.5 (227.4)	1.0	1011.5 (227.4)	17.93 (4.03)	3.5	4	60
3	2/14	1400	27.64	2150.8 (483.5)	1.0	2150.8 (483.5)	77.83 (17.50)	15.3	14	61.5
4	2/14	1400	27.64	3188.9 (716.9)	1.0	3188.9 (716.9)	115.39 (25.94)	22.7	14	62.2
5	2/26	1200	20.30	425.9 (95.8)	5.0	85.18 (19.16)	4.2 (0.944)	0.8	5	46.2
6	2/26	1200	20.30	638.8 (143.6)	1.0	127.8 (28.7)	6.29 (1.41)	6.1	16	42.1 → 64.2
7a	2/28	500	3.52	1104.7 (248.4)	1.0	1104.7 (248.4)	313.4 (70.45)	61.4	5	55.3 → 48.8
8	2/28	800	9.02	878.4 (197.5)	1.0	878.4 (197.5)	197.34 (21.88)	19.1	4	49.5 → 47.5
9	3/7	1100	17.06	519.1 (116.7)	5.0	103.8 (23.3)	6.08 (1.37)	1.3	67	53.9 → 90
10	3/8	1100	17.06	718.7 (161.6)	5.0	143.7 (32.3)	8.43 (1.89	1.7	42	60
11	3/8	1100	17.06	891.7 (200.5)	5.0	178.3 (40.1)	10.45 (2.35)	2.1	2	60
12	4/20	1000	14.10	1437.4 (323.2)	5.0	287.5 (64.6)	20.39 (4.58)	4.1	25	80
13	4/20	1400	27.64	1437.4 (323.2)	5.0	287.5 (64.6)	10.40 (2.34)	2.1	5	80
14	5/7	800	9.02	6681.3 (1502.1)	5.0	1336.3 (300.4)	148.1 (33.3)	29.1	2	59 → 82
15	5/7	800	9.02	3500.4 (787.0)	1.0	3500.4 (787.0)	387.9 (87.2)	76.1	3	82 → 67
16	5/7	900	11.42	3354.0 (754.0)	1.0	3354.0 (754.0)	293.7 (66.0)	57.5	4	63

TABLE VI-5. Test Summary - Total Impulse and Overall Efficiency

Date	Test No.	Test Time (sec)	Impulse (Newton-sec)	Impulse (lb-sec)	Input Energy (Joules)	Efficiency (%)	Comments
2-13-73	1	17760	2.458	5.51×10^{-1}	1.60×10^{5}	3.0	Test Point 1
2-14-73	2	360	3.707×10^{-1}	8.34×10^{-2}	2.03×10^{4}	3.5	Test Point 2
2-14-73	3	2640	2.951	6.63×10^{-1}	5.65×10^{4}	10.3	Includes Test Point 3
2-14-73	4	1300	2.971	6.68×10^{-1}	3.59×10^{4}	16.2	Includes Test Point 4
2-26-73	5	360	1.056	2.375×10^{-1}	3.65×10^{4}	5.7	Test Point 5
2-26-73	6	890	4.849×10^{-1}	1.090×10^{-1}	1.81×10^{4}	5.3	Test Point 6
2-28-73	7	1630	1.473×10^{-1}	3.311×10^{-2}	1.20×10^{4}	.2	Test Point 7
2-28-73	8	700	1.067	2.399×10^{-1}	5.04×10^{3}	41.6	Includes Test Points 7a and 8
2-28-73	8	600	6.395×10^{-1}	1.438×10^{-1}	1.27×10^{4}	9.9	Test Point 8a
3-7-73	9	5820	14.479	3.255	4.56×10^{5}	6.3	Test Point 9
3-8-73	10	2610	9.640	2.167	2.23×10^{5}	8.5	Includes Test Points 10 and 11
4-20-73	11	1980	8.767	1.971	1.93×10^{5}	9.0	Includes Test Points 12 and 13
5-7-73	12	2040	6.838	1.535	5.36×10^{4}	25.0	Includes Test Points 14 through 16

DETAILED TEST DATA AND ANALYSIS

This subsection presents in detail the various tests conducted on LINJET. A section of the recorder trace is reproduced and presented to augument the text which generally describes the test conditions, test objectives, results, and a cross-reference to the data in Tables VI-4 and VI-5.

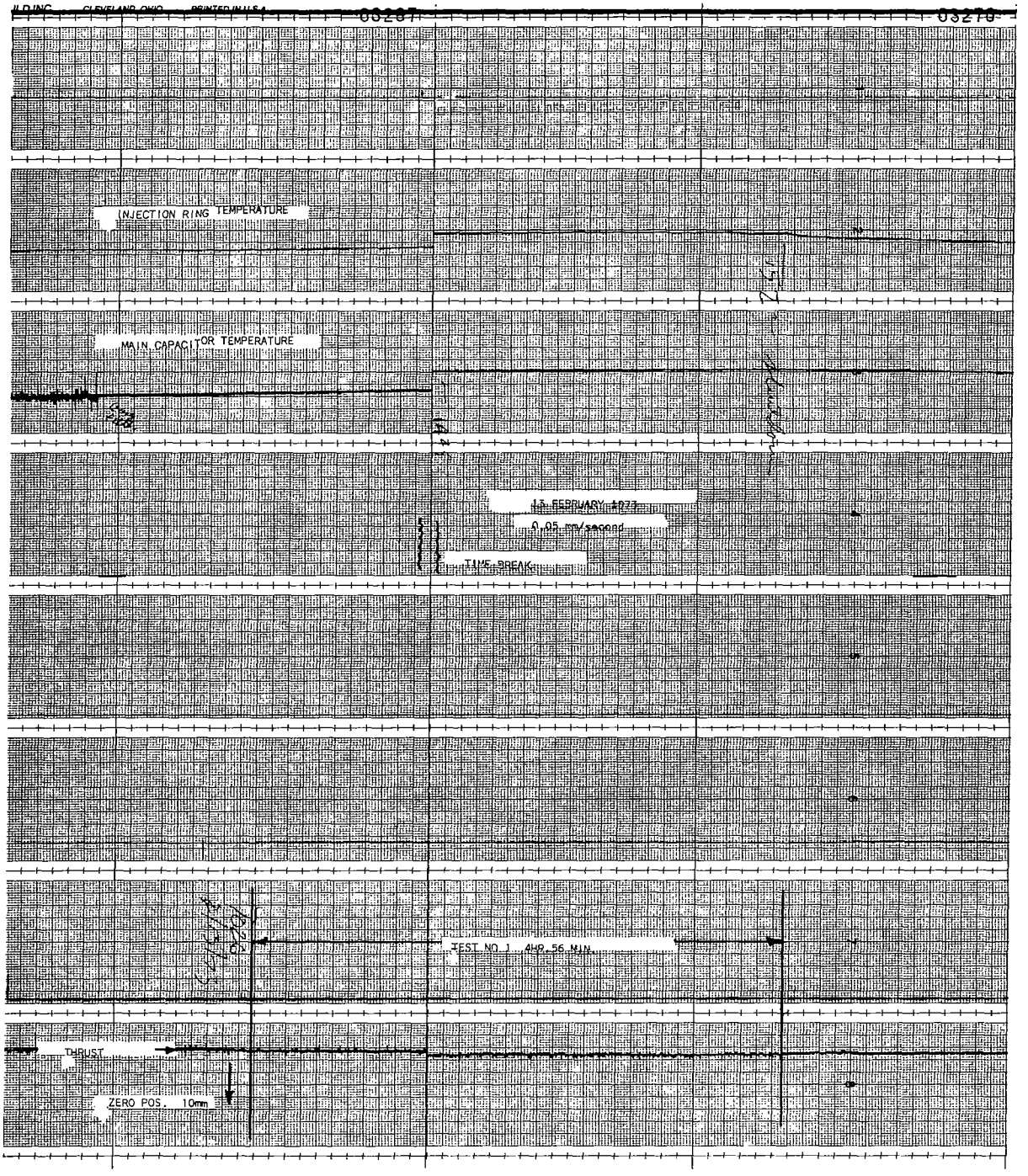

FIGURE VI-9 - TEST POINT #1

Test Point #1 (see Figure VI-9-6) is the first run in the large vacuum chamber. The engine was operated at constant frequency (1 Hz) and with constant voltages on the trigger capacitors (1800v) and the main capacitor (800v). A steady gradual increase in thrust from 67 micro-newtons (15 μlb_f) to 210 μ-newtons (47 μlb_f) occurred over four hours 56 minutes of running time. The temperature of the injection ring increased from 27°C (80.6°F) to 42.6°C (109°F) over the same interval. The test was a check out run to provide assurance that the engine and instrumentation system would operate satisfactorily.

The total impulse delivered during the test was 2.458 newton-seconds (0.551 lb-seconds) for an input of 1.60×10^5 joules. The overall efficiency was 3.0%.

These data are shown as test 1 in Tables VI-4 and VI-5.

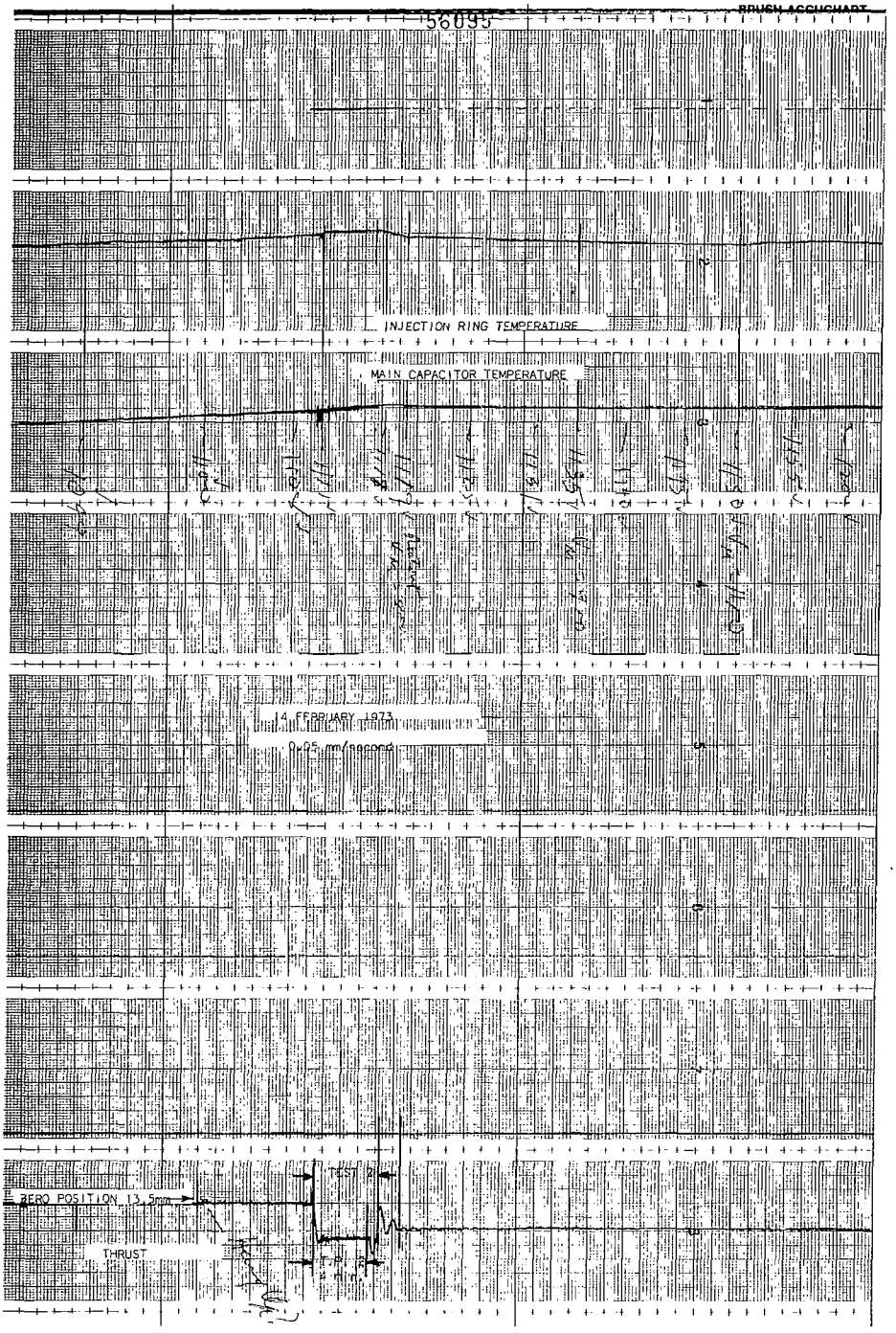

FIGURE VI-10 - TEST POINT #2

Test Point #2 is four minutes of operation at a steady state thrust level of 1011.5 μnewtons (227.4 μ-lb_f) which occurred at the end of two hours 31 minutes of operation on 24 Feb. 1973. The recorder trace for this test is shown as Fig. VI.10. As will be noted from the trace, the thrust increased sharply as the temperature reached 60°C (140°F) (the melting point of the propellant). The thrust trace was essentially smooth for four minutes then increased sharply. The temperature also shows a slight rise. This coincided with false triggering (firing rate greater than the trigger pulse rate) which was noted by the operator. The power supply to the main capacitor charging circuit was then shut off to stop the false triggering.

For a total energy input of 2.03×10^4 joules the engine produced 3.707×10^{-1} newton-seconds impulse for an overall efficiency of 3.5%.

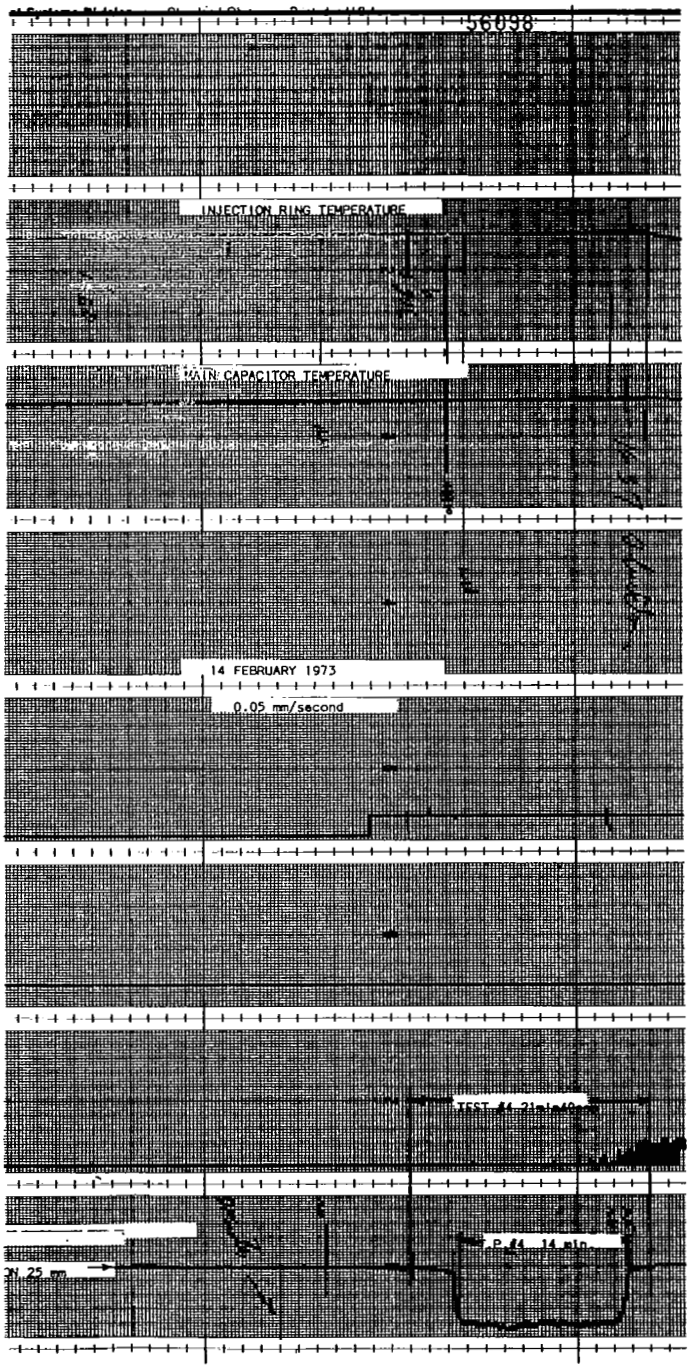

FIGURE VI-12 - TEST POINT #4

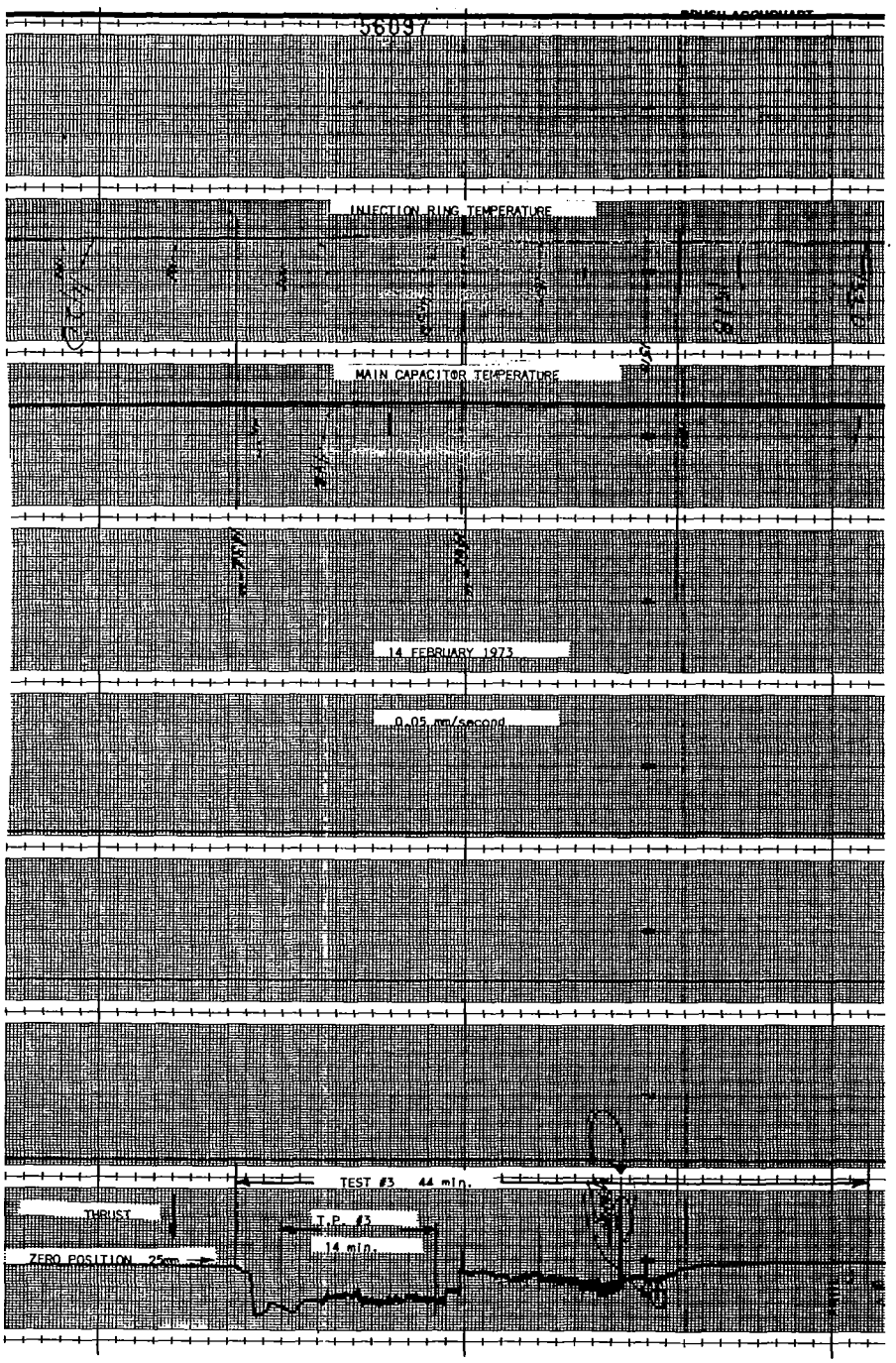

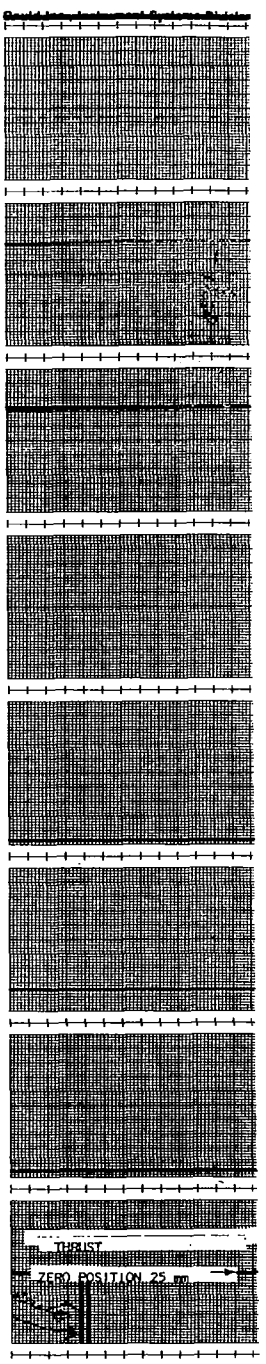

PIGURE VI-11 - TEST POINT #3

Tests #3 and #4 are two parts of a continuous engine test run of 2 hours 37 minutes conducted on 14 Feb. 73. Test #3 shown on Figure VI.11 includes 18 minutes at 1400 volts and 26 minutes at 1100 volts. Test Point #3 of Table VI.4 was 14 minutes of operation at a thrust greater than 2150 μ-newton (483.5 μlb_f) at 1400 volts. The voltage was then reduced to 1100 volts to keep the temperature from getting too high. The total impulse of the entire 44 minutes was 2.951 newton-seconds (0.633 lb_f-seconds). The overall efficiency was 10.3%.

Test #4 shown on Figure VI.12 is the second part of the engine test run. Following Test #3 the voltage was increased in two steps to 1400 volts. When the temperature reached 60°C (140°F) there was a slight increase in thrust. When the temperature reached 62.2°C (144°F) there was a sharp increase in thrust which reached a steady state level of 3189 μ-newtons (717 μlb_f). Thrust peaked at 3515 μ-newtons (790 μ-lb_f). The overall efficiency for the 21 minutes 40 seconds of thrust was 16.2% for the 2.971 newton-seconds (0.668 lb-seconds) of impulse produced.

The thrust dropped off at the end of Test #4 due to a short in the engine. The short was caused by a buildup of propellant which bridged the gap between the injection ring and the center electrode. No post test weight was obtained since the engine leaked propellant.

The leakage appeared to be caused by poor sealing between the injection ring and the machined surfaces of the engine support ring and the nozzle. The support ring and the nozzle were reworked to configuration Ic of Table VI-3. Non-operational tests demonstrated that this was not a satisfactory solution to the propellant leakage problem, so the engine was rebuilt to configuration Id of Table VI-3.

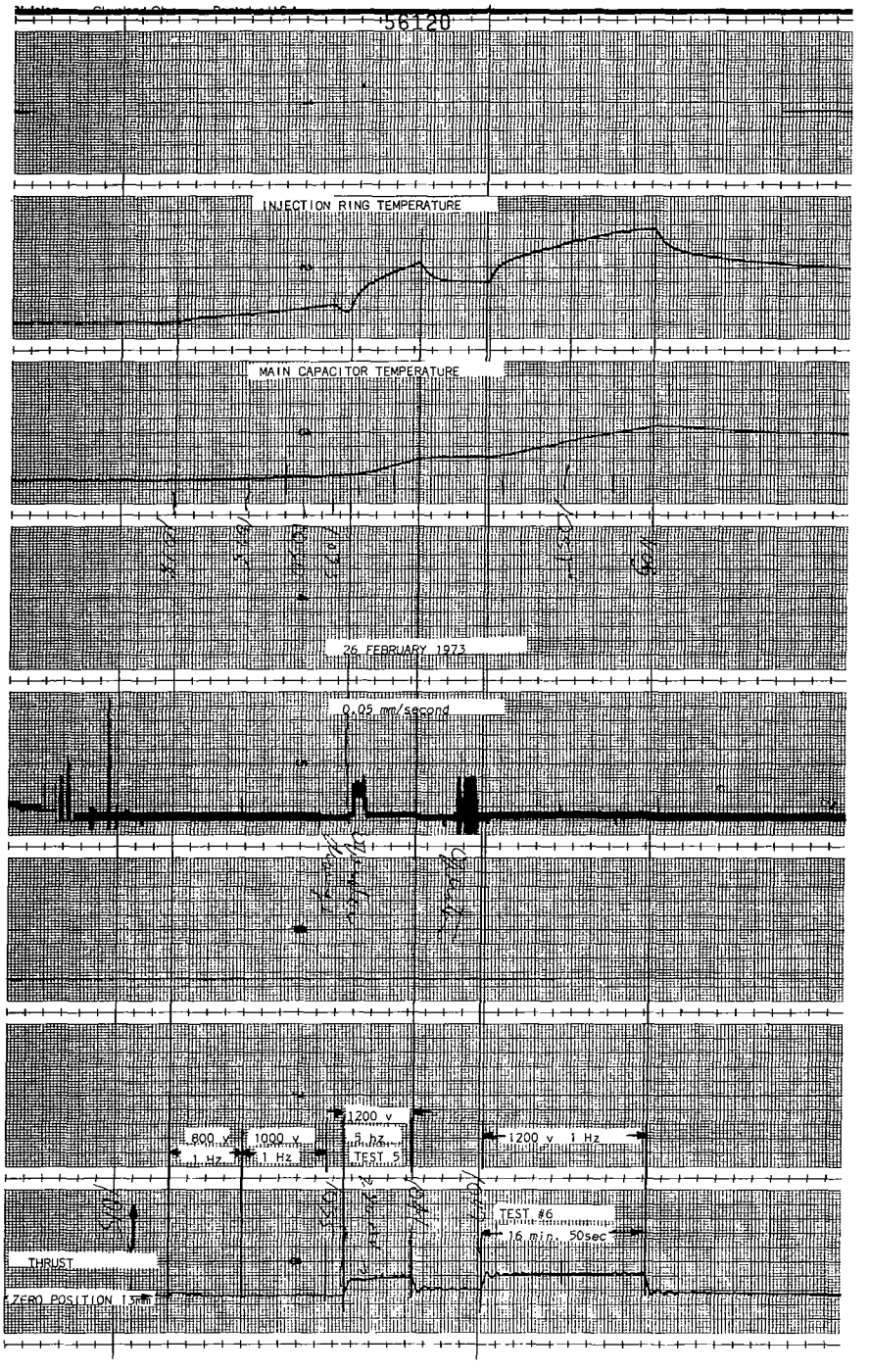

FIGURE VI- 13 - TEST POINTS #5 AND #6

Tests #5 and #6 shown on Figures VI-13 are two parts of the same engine test run of 38 minutes duration on 26 Feb. 73. Test #5 was conducted with the engine operating of 1200 volts on the main capacitor and the triggers operating at 1800 volts and at 5 Hz rate. The plateau of the thrust curve shows a steady increase from 304.5 μ newtons (68.5 μ lb_f) to 426 μ newtons (95.8 μ lb_f) for five minutes 20 seconds as the temperature increased from 36.5 C (97.7F) to 46.2 C (115.2 F). The engine was shutdown to change the trigger pulse rate and the charging resistor in the main capacitor circuit. The engine operated at an overall efficiency of 5.7% per the total running time of six minutes.

Test #6 produced a steady state thrust of 638.8 μ newtons (143.6 μ lb_f) for 16 minutes as the propellant temperature rose from 42.8 C (109 F) to 64.2 C (147.8 F). The main capacitor voltage was 1200 volts with the triggers operating at 1800 volts and a 1 Hz pulse rate. The overall efficiency for the total operating time of 16 minutes 50 seconds was 5.3%. The test was terminated when the triggers failed to fire because the output buffer IC of the logic control box failed.

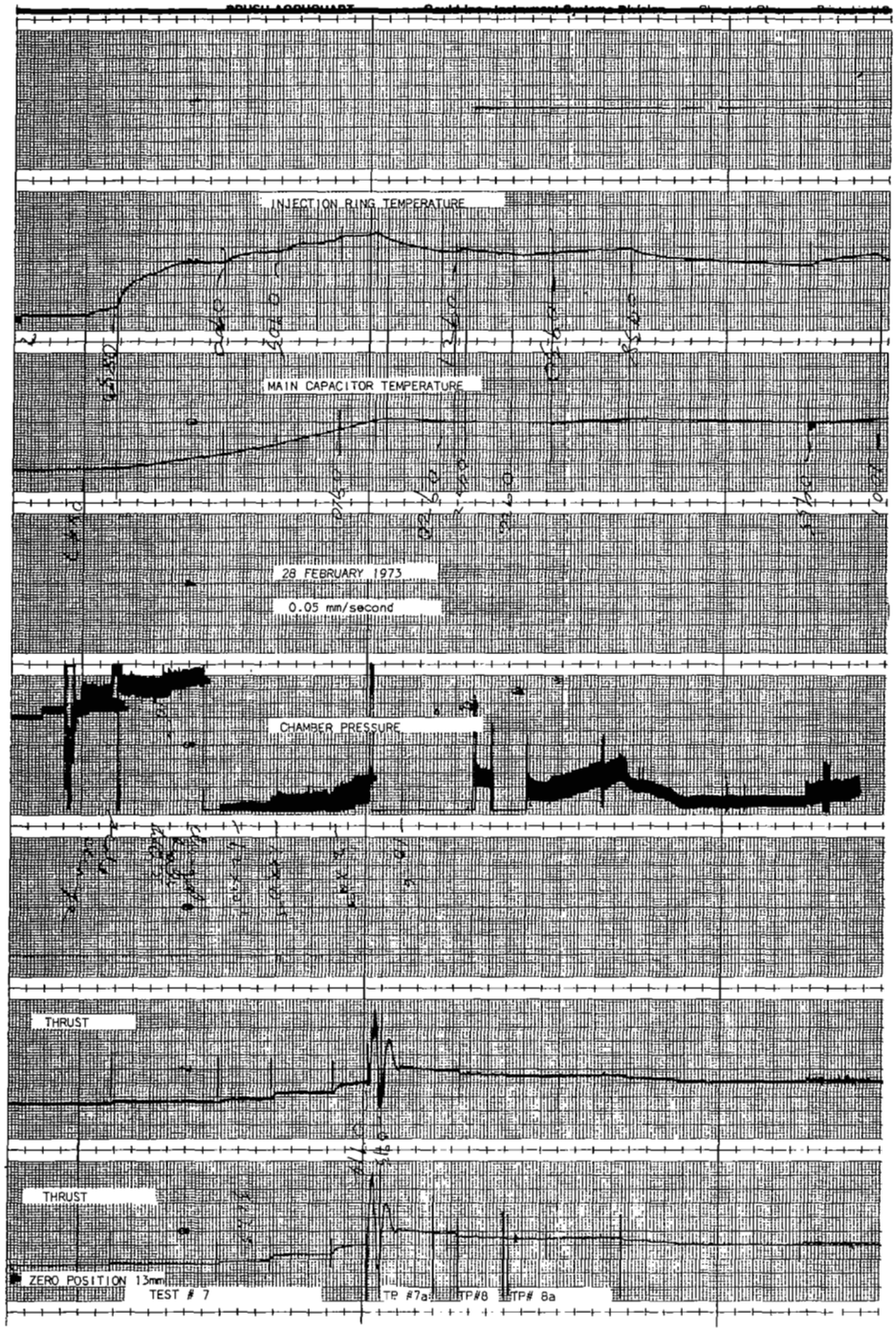

FIGURE VI-14 - TEST POINTS #7, #7a, #8, AND #8a

Test Points #7, #7a, #8 and #8a (Figure VI.14) are segments of the same engine test conducted on 28 Feb. 73. The triggers were operated at 1800 volts and 5 Hz during test #7 and at 1800 volts and 1 Hz for the remaining test points.

Test Point #7 contained 27 minutes 10 seconds of running at 800, 1000, 1200 and 1400 volts on the main capacitor. Maximum thrust of 795 μnewtons (179 μlb_f) occurred at 27 minutes, 10 seconds where the temperature had reached 55.3°C (131.5°F). The overall efficiency was 0.2%. The engine was shutdown when false triggering occurred. The engine was restarted when the false triggering had stopped.

Test points #7a and #8 were two segments of a continuous engine test sequence. T. P. #7a shows a start at 500 volts on the main capacitor with the engine at 55.3°C (131.5°F) slightly below the normal operating temperature of the fuel injection ring of 60°C (140°F). The thrust overshoot peaked at 3150 μ-newtons (708 μlb_f) then dropped to 1104.7 μ-newtons (248 μlb_f) and then gradually decreased to 1040 μ-newtons (234 μlb_f) as the temperature decreased from 55.3°C (131°F) to 48.8°C. The voltage was increased from 500 to 800 and then 1100 volts at which point false triggering occurred. The voltage was reduced to 800 volts (the start of Test Point #8) and the thrust remained constant at 878 μ-newtons (197 μlb_f) as the temperature decreased from 49.5°C (121°F) to 47.5°C (117.6°F) through Test Point #8. The engine was shutdown to charge the charging resistance.

The peak overshoot at the start of test point #7a may have been the natural oscillation of the torsional pendulum which had been excited by the thrust engendered by the false triggering which caused the shutdown at 0914 hours. Although there was no voltage applied to the triggers the engine did not extinguish immediately.

The overall efficiency of this engine test which included test points #7a and #8 was 41.6%.

The engine was restarted after the charging resistor change with 1200 volts on the main capacitor and the triggers operating at 1 Hz. The thrust was essentially constant at 1110. μ newtons (250 μlb_f) although the voltage was increased to 1500 volts and then reduced to 1000 volts. The test was run for 10 minutes with an overall efficiency of 9.9%.

Further attempts to run resulted in a short in the engine which appeared to be the result of leakage at the injection ring interfaces.

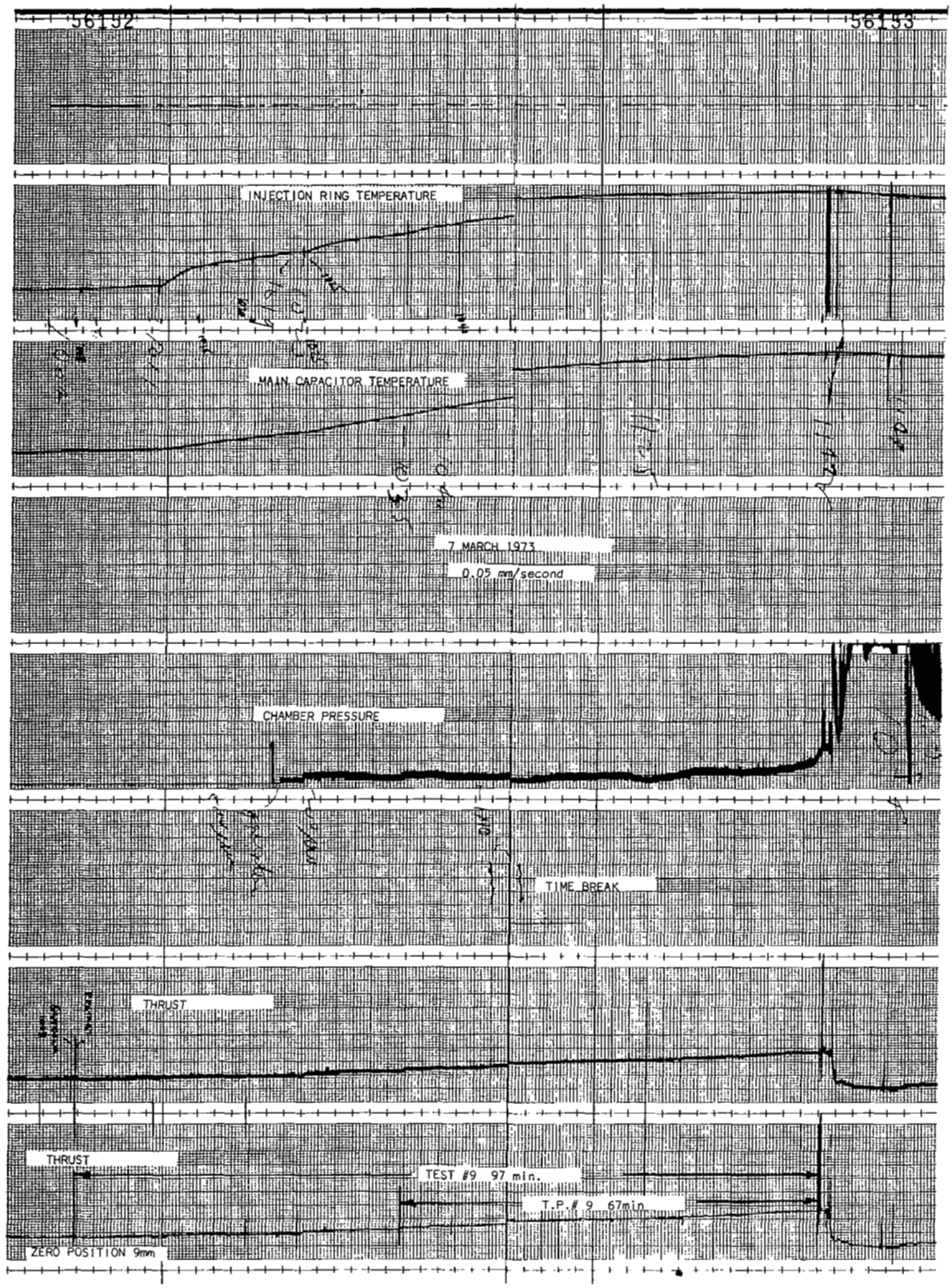

FIGURE VI-15 - TEST POINT #9

The engine was reassembled with the injection ring embedded in the electrically conductive epoxy at the interface surfaces of the support ring and nozzle.

Test Point #9 (Fig. VI.15) shows a run conducted on 7 Mar. 73 with a steadily increasing thrust and injection ring temperature. The applied voltage to the main capacitor was 1100 volts and the triggers were pulsed at 5 Hz at 1800 volts. Thrust increased over the final 67 minutes from 264 μ newtons (59.3 μ lb_f) to 772 μ -newtons (173 μ lb_f) with an average value of 519 μ -newtons (116.7 μ lb_f). Shutdown was caused by the engine false triggering and a high pressure (1×10^{-4} torr) in the vacuum chamber. The overall efficiency was 6.3% over the running time at measurable thrust of 97 minutes. The injection ring temperature increased from 53.9°C (129°F) to over 90°C (194°F) during the test interval.

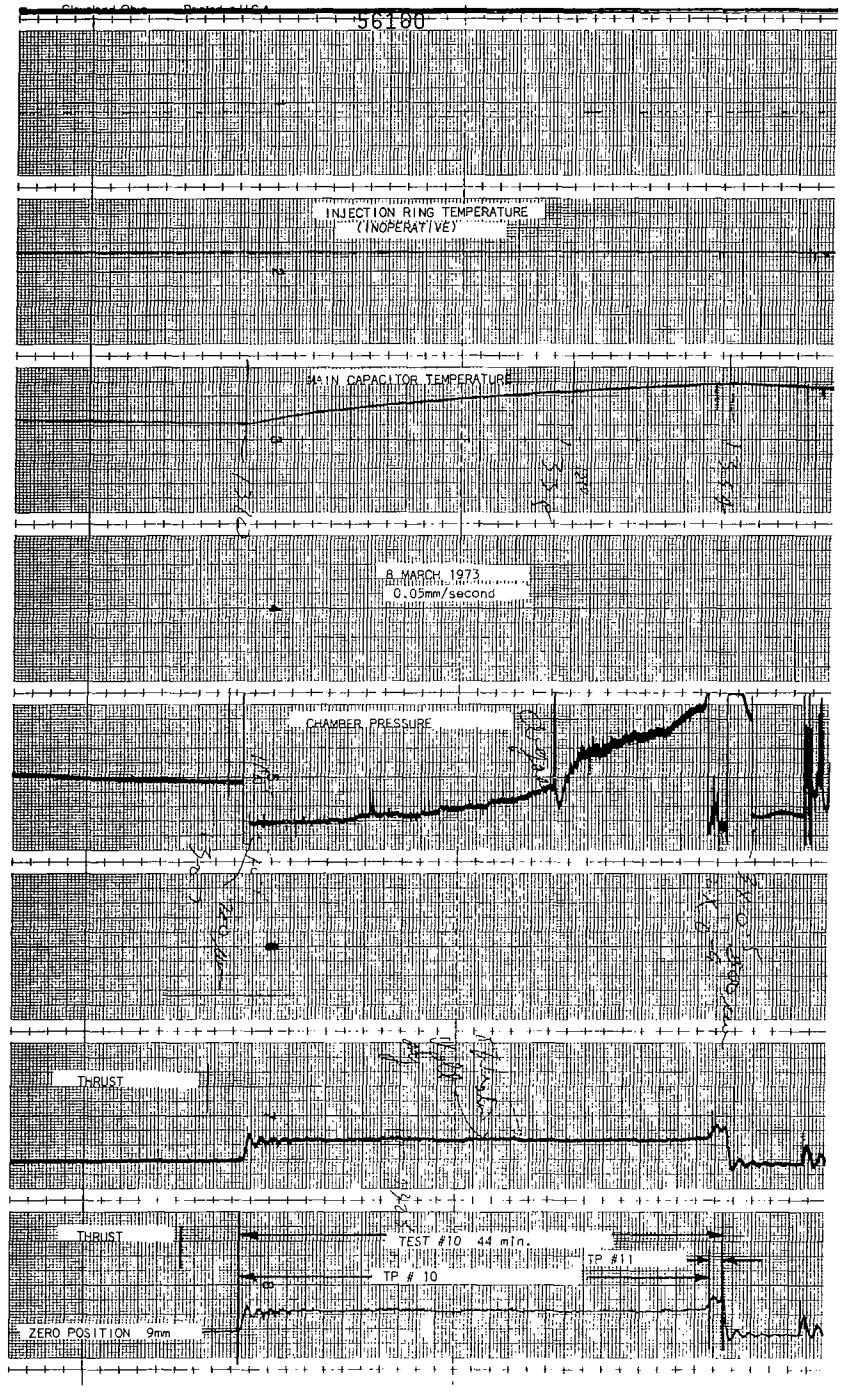

FIGURE VI-16 - TEST POINTS #10 AND #11

Test Points #10 and #11 (Fig. VI.16) are two parts of 44 minutes of operation. Test Point #10 is the first 42 minutes during which the thrust level was essentially constant at 718.7 μ newtons (161.6 μlb_f) for 38 minutes. The thrust then began to increase slightly up to the 42 minute mark when there was an abrupt increase to 891.7 μ newtons (200.5 μ lb_f). The engine was shutdown at the 44 minute mark because the chamber pressure had increased to 2×10^{-4} torr. During this test the injection ring thermistor was inoperative but the capacitor temperature indicated a peak value of 65.6°C at 44 minutes. In general the capacitor temperature would lag the injection ring temperature by 10°C.

Repeated attempts to restart the engine resulted in false triggering of the engine and arcing at the Gallium electrical interface. The overall efficiency for the total of 44 minutes of testing was 8.5%.

Post test inspection revealed a continuous carbonaceous deposit over the center electrode ceramic insulator, the main capacitor insulator and the trigger ring assembly. The conductive path thus formed caused the thruster to short out.

The engine was redesigned in this area to provide a baffle arrangement to control the carbonaceous deposit. (See Fig. V-2 and discussion in section V). In addition an attempt to thermally isolate the thruster from the main capacitor was made by incorporating a ring of C-10 epoxy filled fibre glass material between the engine and the capacitor. The electrically conductive path was maintained by copper rings positioned between the capacitor and the G10 insulator and on the engine mounting surface. The copper rings were joined by four 12.7mm (0.50 in.) flat braided wire straps soldered to each ring.

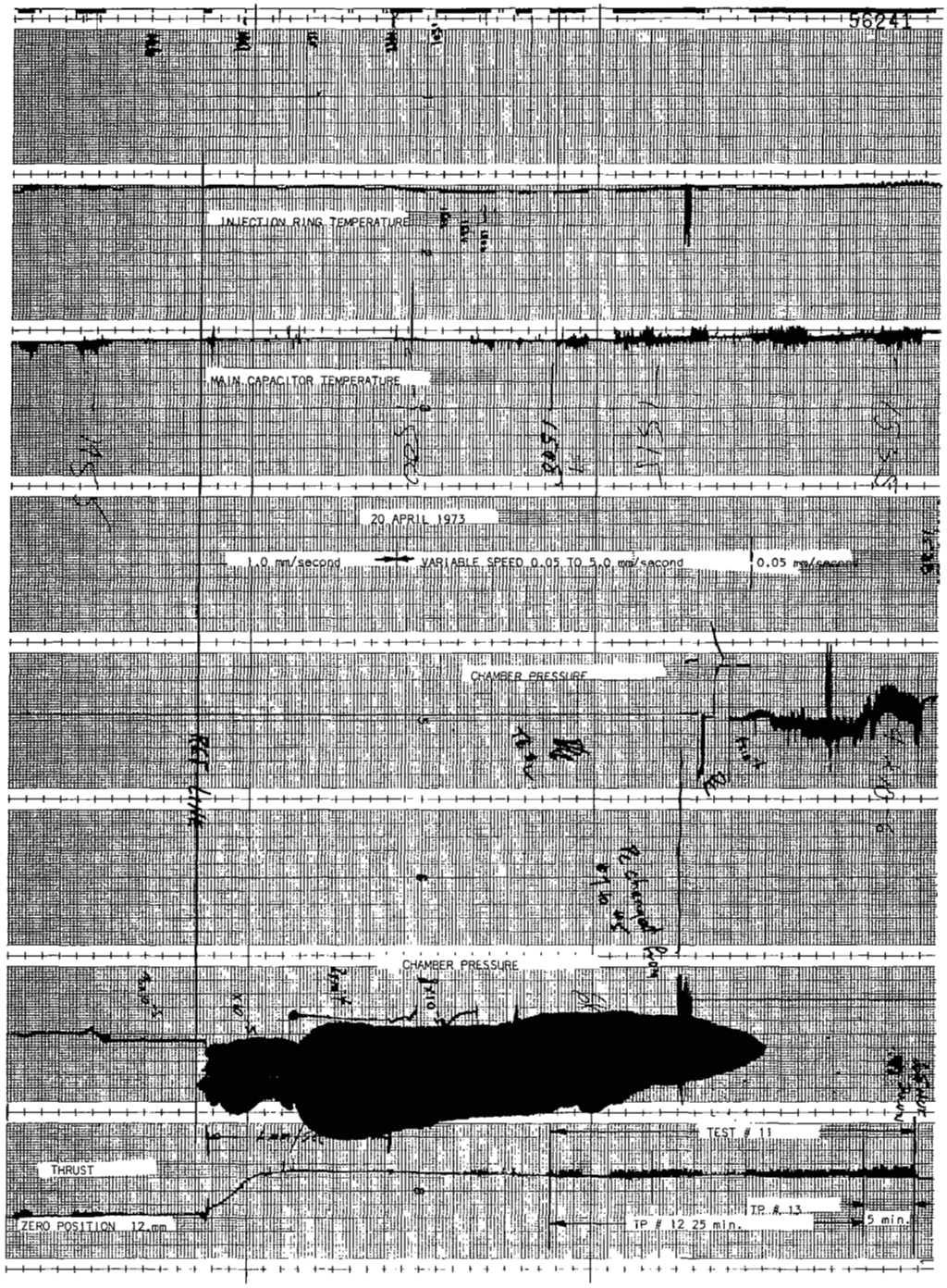

PIGURE VI-17 - TEST POINTS #12 AND #13

The injection ring for test point 12 and 13 (Figure VI.16) consisted of 10 micron wire mesh screen which had been wrapped on a mandrel to the proper outside diameter and welded at the inner and outer ends. The screen assembly was ground flat on each side. The screen material used to form the injection ring was the same material used to feed propellant in the support ring.

The V grooves were machined from the support ring and the nozzle to leave a flat sealing surface and the 0.5mm diameter (0.020 in) gold wire seal described in Section V was used.

Eight more troughs were added at the Gallium interface to provide electrical connection for engine heater leads, heater control temperature sensor, an additional main capacitor temperature sensor and two additional main capacitor high voltage return leads. The latter were necessary in that the previously noted arcing at the Gallium interface resulted in "blowing" the Gallium out of the gallery that transferred the main capacitor high voltage return. With this change no further problems were experienced with arcing at the Gallium interface.

Test Points #12 and #13 are two segments of the final 30 minutes of continuous operation of a total of 42 minutes at a relatively high thrust level during which the main capacitor charging voltage was 1000 volts for 25 minutes resulting in a thrust of 1437.4 μnewtons (323.3 μlb_f), and 1400 volts for five minutes, with no change in thrust level due to a malfunction of the thrust stand. The apparent cause of the malfunction was the freezing of the Gallium in two of the outer troughs.

During the entire 42 minutes the injection ring temperature was above 77.5°C with the peak temperature above 90°C for the last five minutes. The main capacitor temperature exceeded 90°C during the test. During the first 12 minutes of operation with the engine operating at various voltages between 400 and 1400 volts and frequencies of 0.1 Hz and 5.0 Hz the thrust peaked at 1505 μnewtons (338 μlb_f).

The test was terminated when the main capacitor shorted. The efficiency was 9.0%
Post test inspection revealed two probable causes for the short in the engine: the wire mesh screen had delaminated over a segment of the inside diameter and had bulged radially inward so that it closed the normal gap between injection ring and center electrode (pintle) of the engine. Also during operation, the engine mounted on the torsional pendulum, had a slight backward tilt; thus the axial center line of the engine was higher at the nozzle end than at the aft end of the main capacitor. The melted fuel ran down to the lowest level and bridged a portion of the gap between the two pieces forming the baffle. This effectively shortened the path between the main capacitor cathode and anode so that the carbonaceous deposits on the center post insulator and trigger ring assembly again offered a relatively low resistance path to the main capacitor voltage.

In addition the temperature readings indicated that the attempt at the thermal isolation of the engine and the capacitor was ineffective. Therefore it was not used in the next test.

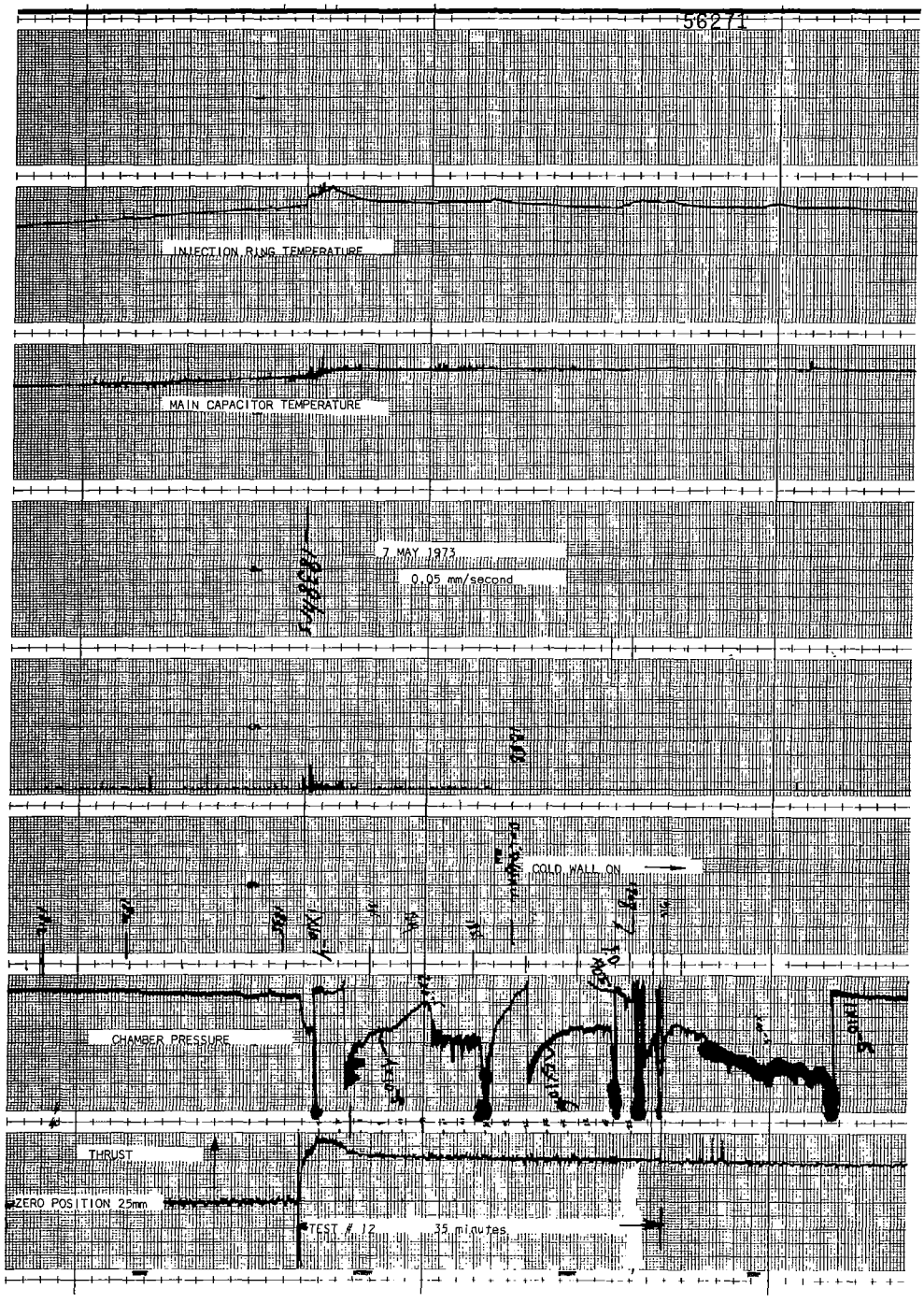

FIGURE VI-18 - TEST POINTS #14, #15 AND #16

The engine configuration for the final test had a 40 micron pore size, sintered stainless steel injection ring sealed with 0.5mm (.020 in) diameter gold wire as previously described. The thermal isolation ring and the electrical conductor assembly were replaced by a single copper ring equal in thickness to the combined thickness of the two pieces. The only purpose of the copper ring was to maintain the engine configuration and electrical continuity without extensive re-machining of the pintle, center post insulator and the trigger stand-off/baffle.

Test Points #14 through #16 (Figure VI.18) are segments of a continuous run of 34 minutes duration made on 5 May 73. During this run the highest thrust level, 6681 μnewtons (1502 μlb_f), was achieved and a thrust level above 2741 μnewtons (616 μlb_f) was sustained for the 34 minutes.

It is noted that after approximately five minutes of testing thrust is constant even though the applied energy is significantly changed. It is speculated that this is because the torsional pendulum was prevented from moving.

The peak propellant injection ring temperature of 82°C coincided with the peak thrust. For the final 27 minutes of the run the injection ring temperature varied between 55.5°C (132°F) and 63°C (166°F). The run was shutdown because the pressure in the chamber increased to the 1×10^{-4} torr range inducing continuous false triggering. During the final 14 minutes of the run the cryogenic cooling to the chamber walls had been turned on but had not had time to be effective.

The effect of the cold walls was noted in the measurement of thrust in that the Gallium apparently froze in one or more of the cavities and the thrust trace did not return to the "zero" position at shutdown. Approximately 12 hours after the cold walls were turned off and the vacuum chamber had warmed up, the thrust trace returned to "zero".

Following this run the engine was operated for approximately three hours 15 minutes without any measurable success. Attempts to operate at main capacitor voltages above 600 volts would induce false triggering with injection ring temperatures between 35°C (95°F) and 53°C (128°F).

During the test the engine was mounted on the torsion balance so that the axial center line through the engine and main capacitor had a slight downward tilt toward the nozzle end. This was to prevent a repeat of the previous run during which melted fuel had run back into the engine and bridged the gap in the baffle arrangement.

Post test inspection of the engine showed a fuel buildup which bridged the diametral gap between the propellant injection ring and the pintle in an arc from the six o'clock to the eight o'clock position (top is twelve o'clock). As noted before the G-10 spacer ring had charred, but there was only a slight discoloration of the center post insulator and the support ring/baffle, and none was present beyond the first trigger electrode ring.

VII. CONCLUSIONS AND RECOMMENDATIONS

As noted at the onset of this report, this program was to demonstrate a concept of a new type of electric thruster. For a program wherein only one set of hardware was used and which was based on a point design and with little opportunity to investigate some basic elements of the design concept, the results have been most encouraging. Admittedly, at the engine, or system, test level, the data is not as complete or as well documented as one would like, but all efforts were made to make the results as realistic and creditable as possible. This was carried to the point that as far as is known, worse case values were taken in reporting the results. All this notwithstanding, the results in the main are still most encouraging. As thrusts greater than 4450 micro-newtons(1000 μlbf) and efficiencies greater than 24% were achieved.

As has been noted, several areas need attention. Some of the most significant will be discussed.

Main Capacitor

In the testing that was accomplished, there has been no evidence that the electrical characteristics properties change as the result of the testing. The problems encountered were mechanical in nature as manifested by oil leakage at the center terminal and lack of parallelism of the ceramic insulator referenced to the ring terminal. The center terminal is a lead soldered joint that is susceptible to failure from torquing during assembly or heating during engine operation. Lincoln Laboratories has developed a high temperature brazed configuration which should be used in all future thruster applications.

In the engine design, the capacitor ceramic insulator was used as a bearing surface for the trigger in the engine assembly. Because of the non-parallelism of this surface (as much as 1.6 mm), special tapered shims had to be carefully fitted for each engine assembly with a different capacitor. This is a problem that is readily solved by proper purchase specifications and manufacturing process control. Alternatively, but not as desirable, is engine redesign to eliminate the used of this surface.

Trigger Circuit

The principal problem in this area was obtaining a reliable discharge across the Teflon propellant ring. By an iterative procedure, it was established that a priming paste of carbon powder and fluorocarbon grease was necessary to produce a discharge. As will be noted from the test data, this worked for several million pulses but did become erratic in operation. With an increase in applied voltage,

the operation was stable. This condition leads to three courses of action that appear promising and should be pursued. First, the mechanism of the discharge and the composition of the primer should be fully investigated and characterized so that it could be optimally applied in future designs, if desired. Second, the use of a "standard" semi-conductor ignitor, perhaps as made by Bendix, should be considered. These are devices that have proven effective in other designs. Third, the increase in voltage to correct erratic operation suggests the use of a high energy inductive loop as opposed to the existing capacitive discharge. In addition to seeking its own discharge voltage level at which to fire across the terminals, the electronics used in the circuit would be greatly simplified.

In this engine, the trigger terminals are cast in RTV silicone rubber. This is a simple, low cost, readily modified approach that is adequate for a laboratory device. However, evidence of charring has been noted after several hundred thousand pulses. For extended life testing or flight operations, ceramics should be used as the binder/support material.

Feed System

This area constituted the major problem area in the entire program. It is recommended that future designs incorporate means of positively sealing the injection ring into the assembly. Explicitly, this means a welded or similar type of joint. Early in the program, during the design phase, it was not realized that the propellant, in the liquid state, had such penetrating flow characteristics. Consequently, metal to metal sealing surfaces were deemed adequate, and the design was based on that approach. With the later revelation of the apparent high capillary flow, a positive seal could not be designed into the system within the resources of the program. Thus, the perturbation of seal design noted in Section VI. It is felt that the gold ring design works but there is an element of lingering doubt that can be dispelled with a welded joint.

A second area to consider is the porosity and exposed area relationship to flow of propellant in the injection ring. In all testing, sooner or later, an excess flow of propellant was noted in the discharge chamber. In the early testing, seal leakage was the major contributor. In the later testing, it appears that flow through the ring itself was the source. The propellant flow tests and development of an emperical tool for calculating the flow mechanics (see Appendix A) have to be re-analyzed based on a test program that more nearly duplicates the actual application. It is

felt that the work done is applicable to a flow process to saturate a wick. However, no experiments or resultant analyses were conducted to determine the effects on flow when the flowing material is intermittently removed from an exposed surface of the wick. It appears that the 40 micron pore sizes used in the tests were so large that, during main capacitor discharge, the surface became wetted and, therefore, free flowing, rather than restrained by surface tension forces at the exposed surface.

It is recommended that a subscale test program be conducted to determine the effects on flow of an electrical discharge at the end of a wick with pore size, temperature and exposed area as the controlled variables.

Specific impulse was to be determined by pre and post test engine weighing to determine weight loss. Due to unfortunate and unforeseen circumstances, a determination could not be made for test. Since the propellant is a liquid for normal engine operation, it is recommended that a graduated capillary type sight gage be installed during short-term development tests so that propellant use rate can be monitored during tests without the need for engine disassembly.

The LINJET is believed to be a reasonably efficient thrust device when operated at or near the melting point of the perflourocarbon fuel and with input energies in the range of 9 to 20 joules per pulse. When operated at temperatures well below or well above (greater than 10°C) the melting point of the fuel, the performance is poor i.e. efficiencies are probably less than 10%. It is postulated that the efficiencies are poor for the case where the temperature is below the melting point because there is insufficient fuel available at the inner diameter of the fuel injection ring for ablation and hence thrust. For the other extreme, when the fuel temperature is well above the melting point, there is too much fuel available with the injection ring pore size used in the majority of these tests. The excess fuel masks off the injection ring which is one electrode in the discharge circuit and the arc is forced to find an alternate path to complete the circuit. This path is relatively remote from the fuel source and little ablation or thrust generation takes place.

In a concluding summary, it is felt that the engine essentially has met or exceeded the program goals. Further, the concept of a liquid propellant injection system has been successfully demonstrated, and that what remains is a refinement of the design, particularly in the sizing of the injection ring. The high thrust and high efficiency indicated, coupled with the potential of remote propellant tankage offers an attractive propulsion possibility for long life spacecraft.

APPENDIX "A"

PROPELLANT FEED ANALYSIS FOR THE LINJET ENGINE

by

Dr. C. H. Marston

1. Introduction

A key factor in the LINJET concept for electric propulsion is the use of a waxy perflourocarbon propellant which is fed to the thrust chamber by surface tension forces acting in a porous material. The concept has been investigated experimentally (Ref. 1) in a thruster but, at the time the experiments were conducted, neither analysis or propellant property data were available to provide a basis for rational design.

Two types of experimental data are now available (see Appendix "B" herein) that permit an analysis to be made. Propellant surface tension and viscosity as well as wetting angle with stainless steel have been measured directly (Fig.A1,A2,A3). Also "wick" experiments have been performed in which the mass gain and propellant rise have been measured as a function of time for rectangular cross-section bars of porous stainless steel suspended vertically at constant temperature in a reservoir of propellant. Since the viscous effect is proportional to capillary flow length, flow rate will decrease with time even in the regime where gravity head can be neglected. The analysis has therefore been extended to this unsteady flow case and a general equation for column height as a function of time derived, using a bundle of parallel capillary tubes as basic flow model. A simple direct method of evaluating mass flow rate for design purposes has also been developed.

2. Analysis - Non-steady Flow in a Wick

2.1 Nomenclature

A	cross-sectional area
d	capillary diameter
g	acceleration of gravity
h	column height
h^*	column height at $t = t^*$
k_ℓ	ratio of viscous path length to column height
ℓ	viscous path length
m	propellant mass in porous material

$\dot{m}$	propellant mass flow rate in porous material
n_h, n_m	exponents defined by equations 2.15 and 2.16
t	time
t^*	reference time for empirical data reduction (t^* = 1 hr.)
u	propellant velocity
η	ratio of true flow cross-section area to gross cross-section of porous material
θ	contact angle between propellant and porous material
λ	dimensionless height defined by equations 2.3 and 2.5
μ	viscosity
ρ	density
σ	surface tension
τ	dimensionless time defined by equations 2.6 and 2.7

2.2 Analytical Model

A simple flow model which assumes flow in a bundle of small diameter capillary tubes in the presence of gravity, surface tension and viscous forces only (no dynamics and no pressure gradient) yields the following equations

gravity + viscosity = surface tension

$$\rho g h + \frac{8 \mu u \ell}{d^{2}/4} = \frac{4\sigma}{d} \cos\theta \qquad (2.1)$$

$$\dot{m} = \rho u \eta A \qquad (2.2)$$

When the fluid sufficiently "wets" the solid surface, θ is small and Cos $\theta \simeq 1$.

The maximum possible height of fluid in the tube results when the gravity term is equal to the surface tension term and the velocity goes to zero.

$$h_{max} = \frac{4\sigma}{\rho g d} \qquad (2.3)$$

we note that $u = d\ell/dt$ and make the following definitions

$$\ell = k_\ell h \qquad (2.4)$$

$$\lambda = h/h_{max} \qquad (2.5)$$

$$\tau = t/t_{ref} \tag{2.6}$$

$$t_{ref} = \frac{128\mu\,\sigma\,k_\ell^2}{\rho^2 g^2 d^3} \tag{2.7}$$

The constant k_ℓ is introduced to allow for a path length through the porous material which is longer than the direct vertical rise. Equation (2.1) then reduced to the following expression for column height as a function of time in dimensionless form

$$\lambda + \lambda \frac{d\lambda}{d\tau} = 1 \qquad 0 \leq \lambda \leq 1 \tag{2.8}$$

*with the initial condition**

$$\tau = 0, \quad \lambda = 0 \tag{2.9}$$

This first order differential equation may be solved by separation of variables. The solution, Fig. 4, is most conveniently written with τ as a function of λ.

$$\tau = -\lambda + \ell n \left[\frac{1}{1-\lambda}\right] ; \quad 0 \leq \lambda \leq 1 \tag{2.10}$$

Two limiting forms are of interest.

For $\lambda << 1$,

$$\lambda \simeq (2\tau)^{1/2} \tag{2.11}$$

and column height is thus proportional to the square root of time when the gravity head effect is negligible. At the other extreme, when $(1 - \lambda) << 1$,

$$\lambda \simeq 1 - e^{-\tau} \tag{2.12}$$

---

*Strictly speaking, the initial condition should be written $\tau = 0$, $\lambda = \lambda_o$ since, at zero height, dynamics may be important and Equation (2.1) would not apply. For $\lambda_o << 1$ however, the solution is the same as that given by Equation (2.10).

so, as might be expected, maximum column height is approached asymptotically. A rearrangement of equation 2.8, combined with equation 2.2 also shows that

$$\frac{\dot{m}}{A} \propto \frac{d\lambda}{d\tau} = \frac{1-\lambda}{\lambda} \tag{2.13}$$

For $\lambda \ll 1$, on substitution of the reference quantities

$$\frac{\dot{m}}{A} = \left[\frac{m}{k_\ell^2}\right] \frac{\rho\, d\, \sigma}{8\, \mu\, h} \tag{2.14}$$

2.3 Empirical Model

For design application an empirical data reduction scheme was also developed. The analysis suggests that, in the regime of $\lambda \ll 1$, where gravity head is negligible, equations of the following form should hold.

$$h = h^* \left(\frac{t}{t^*}\right)^{n_h} \tag{2.15}$$

$$m = m^* \left(\frac{t}{t^*}\right)^{n_m} \tag{2.16}$$

Here t^* is some convenient reference time, chosen arbitrarily as 1 hour, and h^* and m^* are values of h and m at $t = t^*$. Solving for $\dot{m}/A$ and using equation 2.15 to eliminate t/t^* yields

$$\frac{\dot{m}}{A} = \frac{m^* n_m}{A t^*} \left(\frac{h}{h^*}\right)^{\frac{n_m - 1}{n_h}} \tag{2.17}$$

When the data for h and m as a function of time are plotted on log-log paper they do tend to fall on straight lines, experimentally justifying the form of equations 2.15 and 2.16.

The values for n can be determined as the slopes of the lines and the values of h^* and m^* read directly at $t = 1$ hour. For m^* measured in grams, $t^* = 1$ hour and using a sample cross-section

area of .028 $in.^2$, equation 2.17 becomes

$$\frac{\dot{m}}{A}\left[\frac{\mu\ 1\ b\ m}{in^2 - sec}\right] = 58.4\ m^* n_m \left(\frac{h}{h^*}\right)^{\frac{n_m - 1}{n_h}} \qquad (2.18)$$

Reasoning that height should be directly proportional to mass gain, one would expect both n_m and n_h to be equal. Furthermore, on the basis of equation 2.11 one would expect a value of 1/2. Data at hand do not fully bear out this expectation.

3. Results

Samples of a propellant material (Halocarbon Products Corporation wax 6-00*) have been tested at 170°F, 140°F, and 120°F using wick columns with nominal pore sizes of 40μ, 20μ, and 10μ. Property data has also been determined (Appendix B) and is reproduced here as Fig. A1, A2 and A3.

As can be seen from these figures, reliable measurements were not obtained below 150°F and extrapolation was necessary to evaluate properties at 140°F. Extrapolation below 140°F was not considered justified.

Correlation of dimensionless height with dimensionless time is shown on a semilog plot, Fig. A4. Most of the data are for $\tau << 1$, where the slope of the curve is small, but the correlation is an encouraging indication that the analytical model has some validity. Small τ and large τ limiting forms are also shown and it is clear that they apply for $\tau < .01$ and $\lambda > 5.0$ respectively.

*Density 1.89 g/cm^3, Ref. 2

HALOCARBON WAX SERIES 6-00
BATCH #3772

HALOCARBON PRODUCTS CORP.
HACKENSACK, N.J.

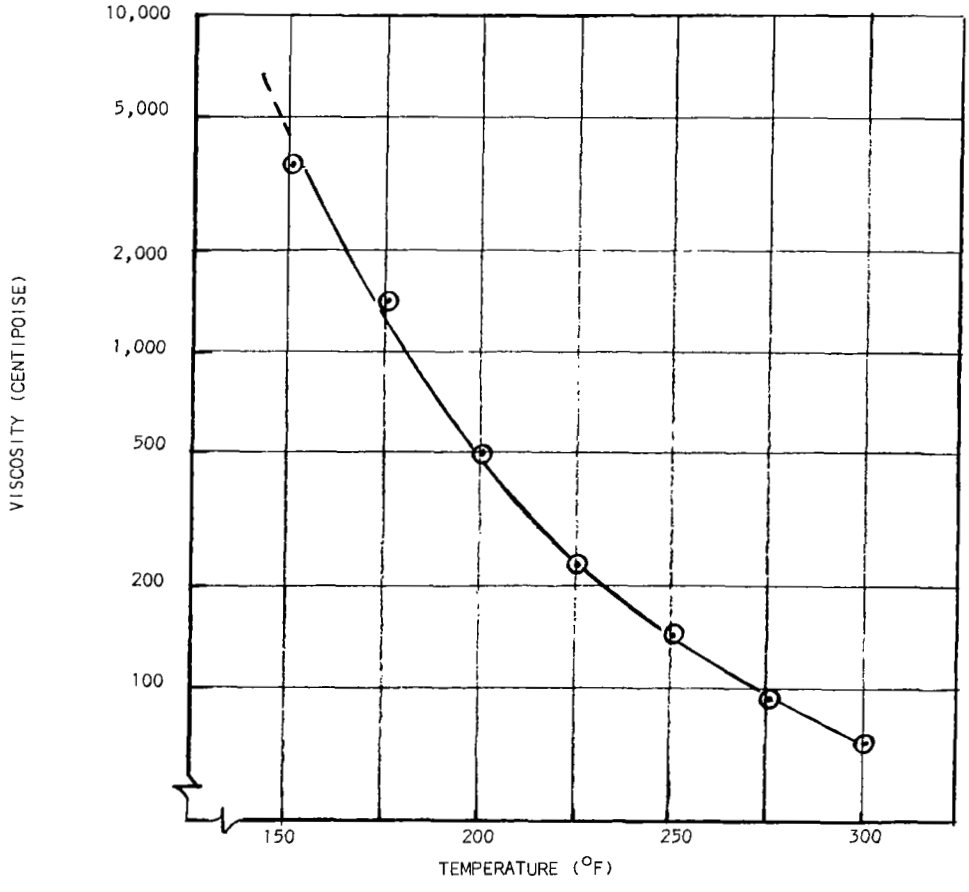

FIGURE A-1 VISCOSITY vs TEMPERATURE

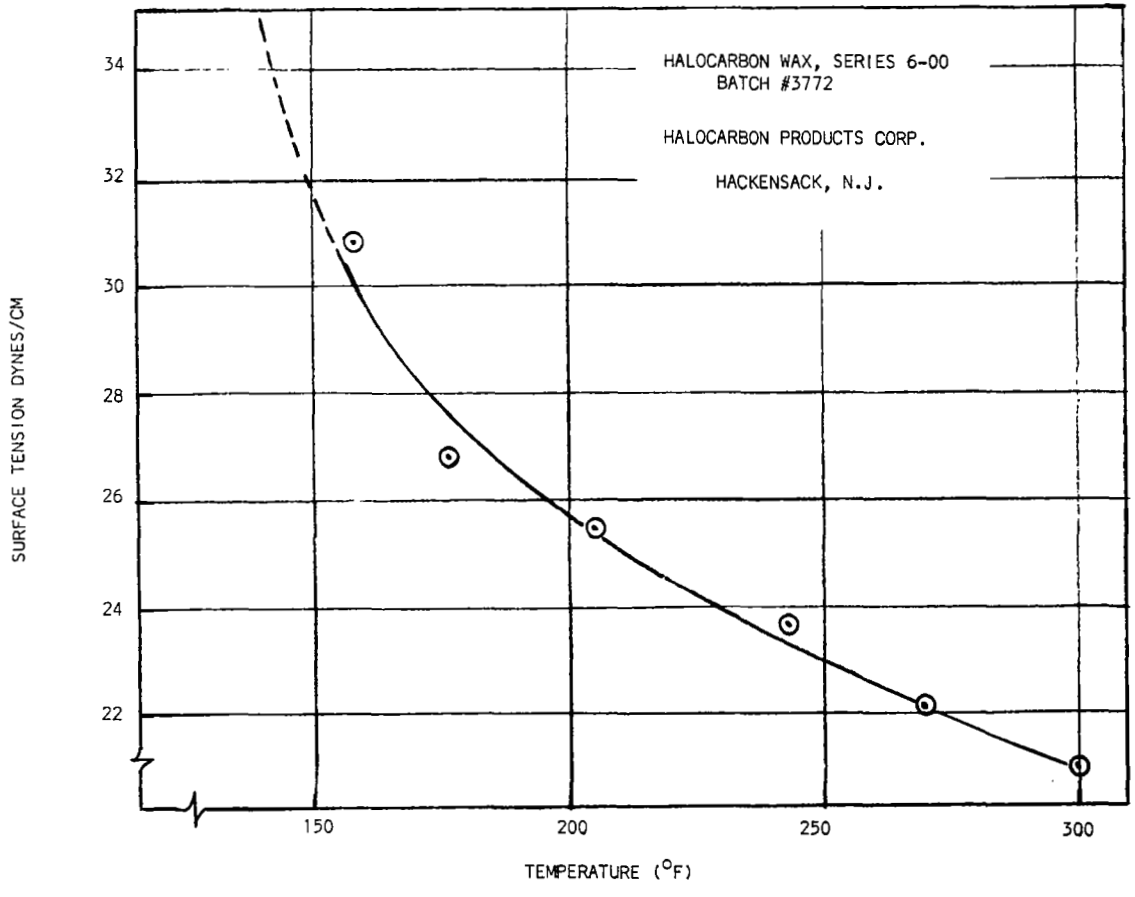

FIGURE A-2 SURFACE TENSION vs. TEMPERATURE

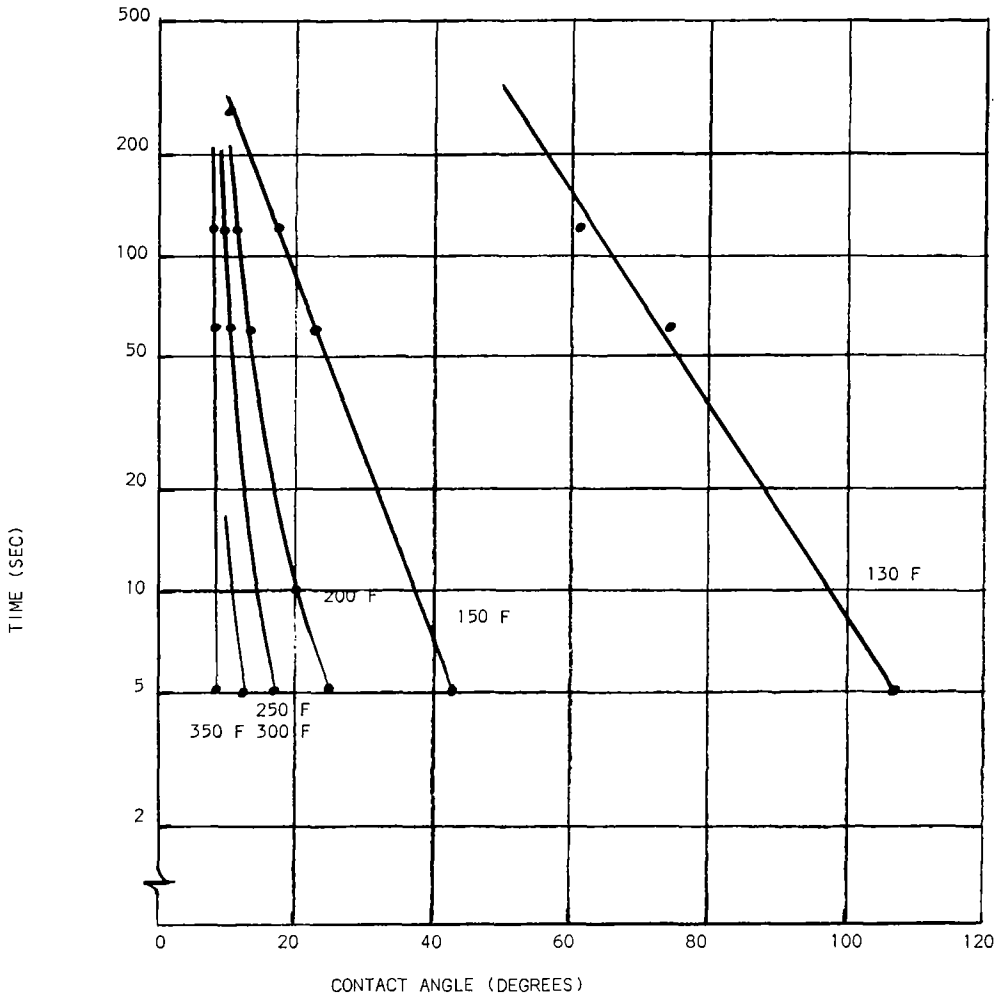

FIGURE A-3 - ANGLE OF CONTACT AS A FUNCTION OF TIME FOR VARIOUS TEMPERATURES

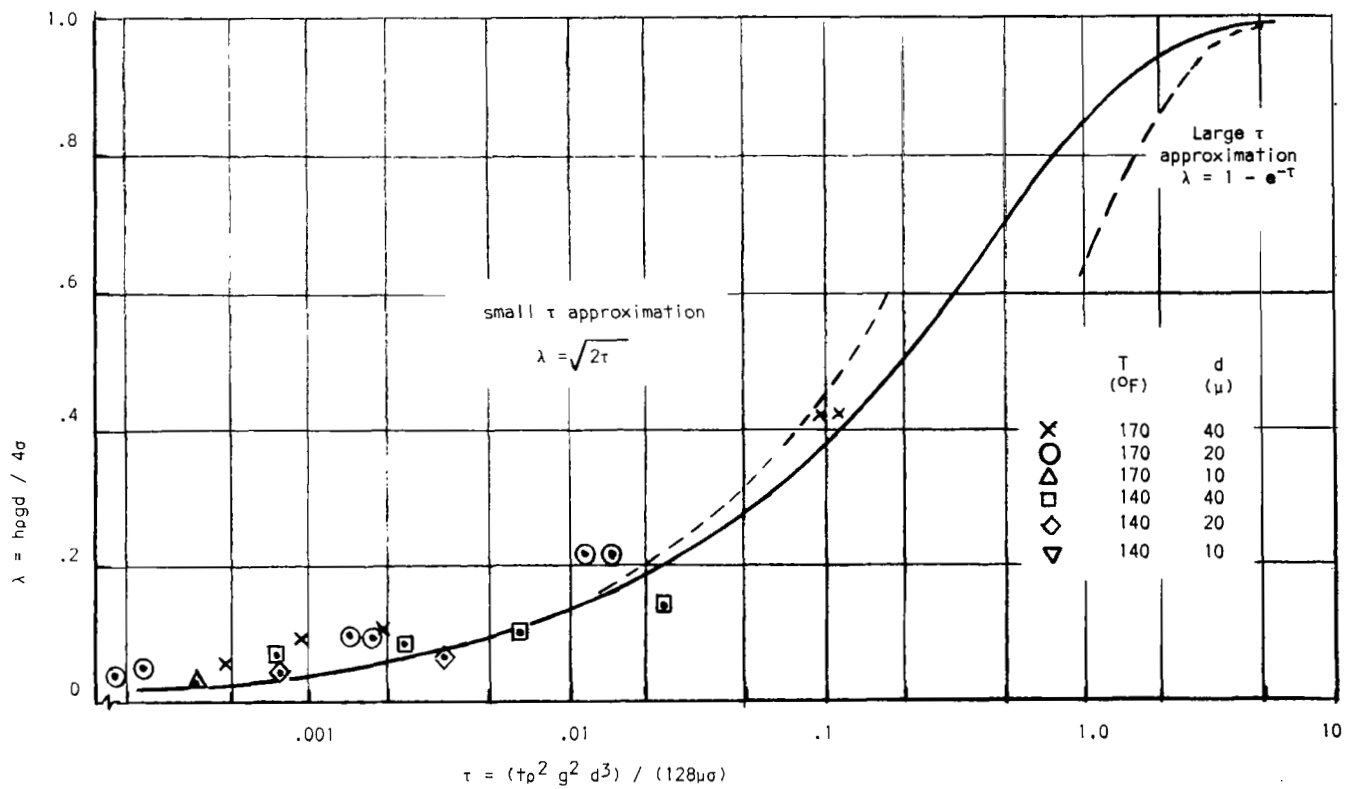

FIGURE A-4 - PROPELLANT RISE IN A CAPILLARY WICK

Test data were also reduced using the empirical relation, equation 2.18. Measurements (Appendix B) of both weight gain and propellant rise were made only on the 170°F series of tests. These were plotted, Fig. A5, to provide a correlation of propellant rise with the weight gain measurements made at the other temperatures. An inconsistency between values obtained over the first hour or so and measurements 65 hours and longer was not resolved.

Results of the empirical data reduction are shown in Fig. A6, along with calculated values using property data and equation 2.14. The empirical constants are listed in Table A1. The empirical data are lines showing mass flow rate per unit area as a function of height. The analysis results and design requirement are based on a specific path length and are therefore shown as points on the plot.

While the data do tend to fall on straight lines on a log-log plot of height or weight gains vs time as predicted by equations 2.15 and 2.16, the slopes are less than the expected value of 1/2 (see Section 2.3) and weight and height exponents for the 170°F case differ significantly.

TABLE A1

Empirical Constants For Propellant Rise Tests at 170°F and 140°F ($t^* = 1$ hr)

T (°F)	Pore Size (μ)	h^* (in.)	n_m	m^* (gm)	n_m
170	10	.52	.357	.30	.253
	20	.66	.326	.36	.230
	40	,63	.329	.42	.203
140	10	---	----	.20	.23
	20	---	----	.23	.21
	40	---	----	.31	.20

However both direct empiricism and analysis show a substantial margin of safety in the propellant delivering capability of the porous material.

REFERENCES

1. LaRocca, A. V. and Perkins, G.S., "Development of Solid Propellant Electric Thruster Systems for Attitude Control and Station Keeping of Spacecraft", AIAA Electric Propulsion and Plasmadynamics Conference, Colorado Springs, Colo., September 11-13, 1967, AIAA Paper No. 67-661.

2. Brochure, Halocarbon Products Corporation, 82 Burlews Court, Hackensack, NJ.

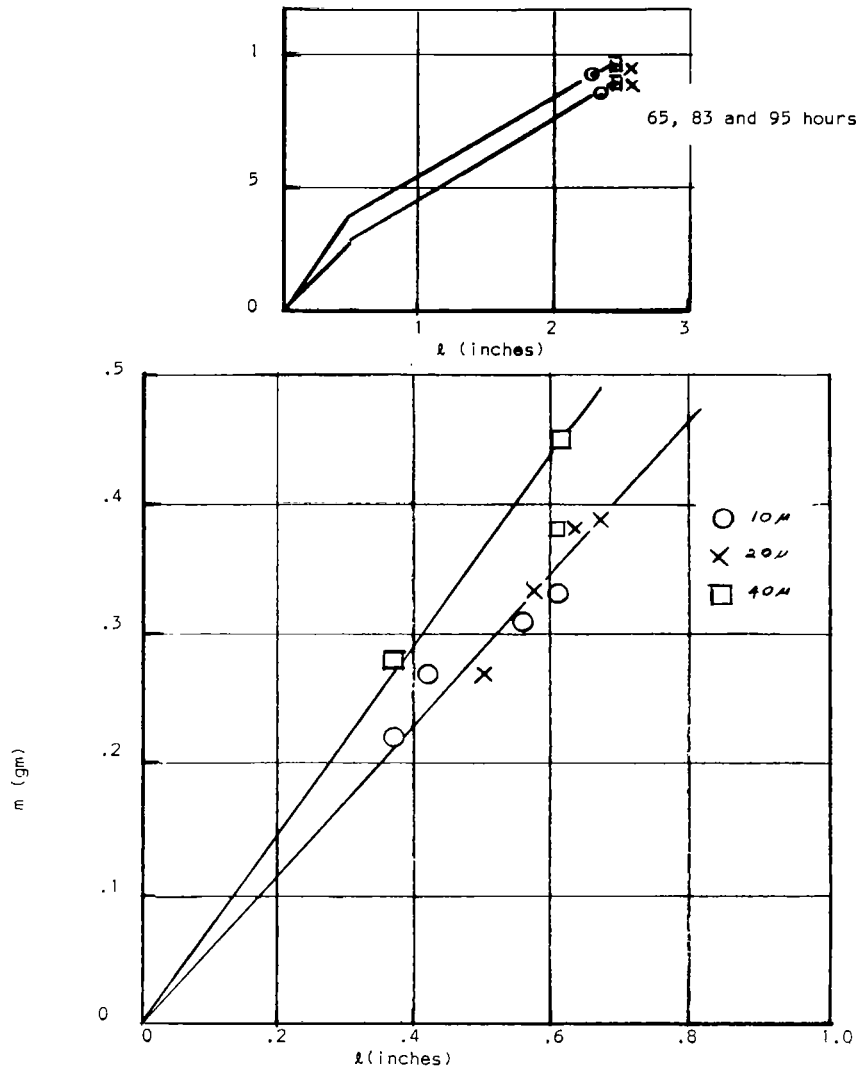

FIGURE A5 - CORRELATION OF MASS CHANGE WITH PROPELLANT HEIGHT BASED ON 170°F DATA

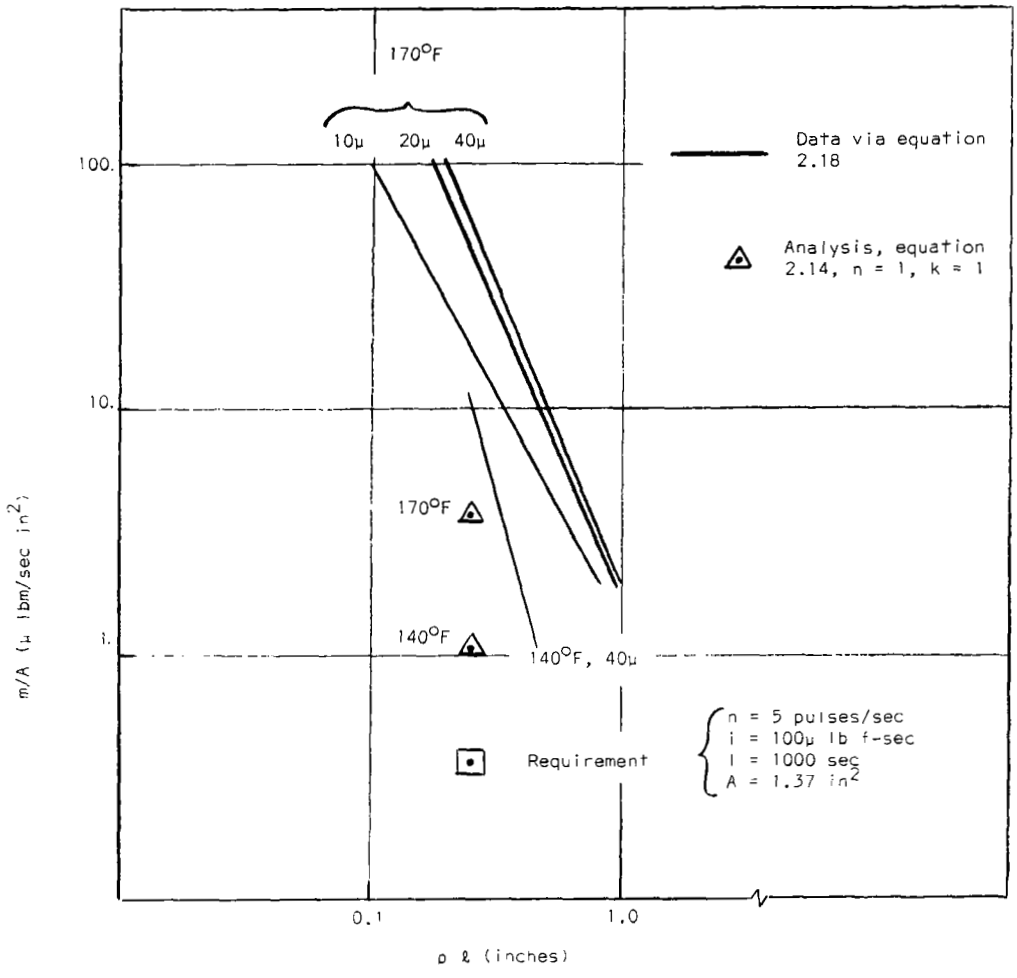

FIGURE A6 - MASS FLOW vs HEIGHT IN SINTERED POROUS MATERIAL

APPENDIX "B"

LINJET PROPELLANT CHARACTERIZATION

by

R. Law
G. McKinley
B. Nelson
W. Saylor

(Materials Engineering - GE/SSO)

This section summarizes the measurement techniques used and the data obtained for characterization of Halocarbon Wax, Series 6-00, Batch #3772, Halocarbon Products Corporation, 82 Burlews Court, Hackensack, N.J. Halocarbon Wax, Series 6-00 is the compound currently used as a LINJET propellant.

This appendix contains these sections:

1. Viscosity, Melting Range and Surface Tension Measurements.
2. Surface Wettability of Stainless Steel by Halocarbon Wax, Series 6-00, Batch #3772.
3. Rate of Weight Loss in Vacuum as a Function of Temperature.
4. Wicking Characteristics of Porous Metals and Metal Screens.
5. Infrared Analysis.

SECTION 1. VISCOSITY, MELTING RANGE AND SURFACE TENSION MEASUREMENTS

Viscosity

Viscosity was measured in the manner described in ASTM Test Method D2669-67 using a Brookfield Synchro-Lectric Viscometer, Model RVT.

TABLE B1 - VISCOSITY DATA

Temp. °F	Spindle	RPM	Readings	Multiplying Factor	Viscosity, CP
300	4	100	3.6,3.4,3.5	20	70
275	4	100	4.7,4.7,4.7	20	94
250	4	100	7.2,7.3,7.1	20	144
225	4	100	11.3,11.5,11.7	20	230
200	4	100	24.5,25.0,25.5	20	500
175	4	100	70.0,71.5,73.0	20	1430
150	4	50	91.8,92.4,93.2	40	3700
150	4	20	37.8,38.0,38.2	100	3800

Viscosity as a function of temperature is shown in Figure B.1

HALOCARBON WAX SERIES 6-00
BATCH #3772

HALOCARBON PRODUCTS CORP.
HACKENSACK, N.J.

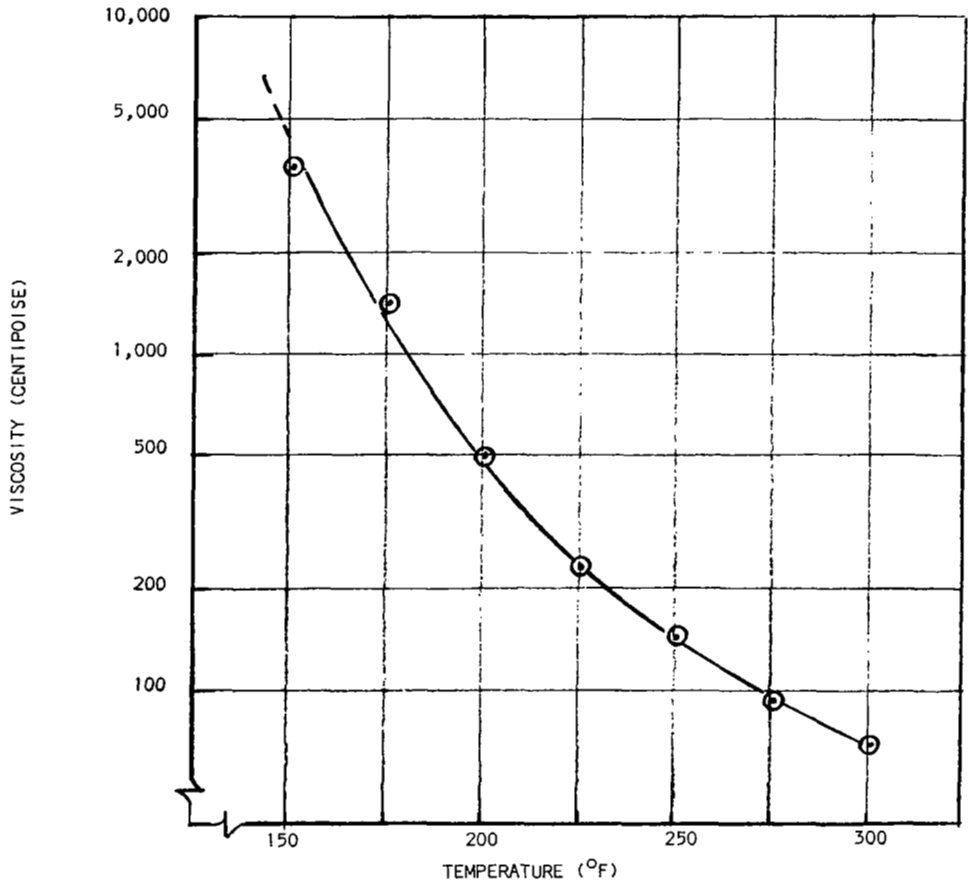

FIGURE B-1 - VISCOSITY VS TEMPERATURE

Melting Range

A melting range of 100 to 140°F was determined by use of the Fisher Johns Melting Point Apparatus.

Surface Tension

Surface tension was measured by the Ring Method [1] using a six centimeter circumference platinum iridium ring and the Cahn RG Electrobalance as mounted in the Fischer TGA apparatus. Densities at the test temperatures were extrapolated from data obtained from Halocarbon Products Corp. Correction factors were extrapolated from the Tables in Reference #1. Data are shown in Table B-2.

Surface tension as a function of temperature is plotted in Figure B-2.

TABLE B2 - SURFACE TENSION DATA

Temp.°F	D	M	$V = \frac{M}{D-d}$	R^3	R^3/V	R/r	F	L	Surface Tension, Dynex Per Cm $\frac{MGF}{2L}$
300	1.72	.312	.181	.8707	4.81	53.75	.831	6.00	$\frac{.312 \times 980.2 \times .831}{2 \times 6.00} = 21.2$
270	1.79	.328	.183	.8707	4.76	53.75	.832	6.00	$\frac{.328 \times 980.2 \times .832}{2 \times 6.00} = 22.3$
243	1.84	.349	.190	.8707	4.58	53.75	.835	6.00	$\frac{.349 \times 980.2 \times .835}{2 \times 6.00} = 23.8$
205	1.90	.375	.197	.8707	4.42	53.75	.836	6.00	$\frac{.375 \times 980.2 \times .836}{2 \times 6.00} = 25.6$
176	1.93	.392	.203	.8707	4.29	53.75	.839	6.00	$\frac{.392 \times 980.2 \times .839}{2 \times 6.00} = 26.9$
158	1.95	.447	.229	.8707	3.80	53.75	.846	6.00	$\frac{.447 \times 980.2 \times .846}{2 \times 6.00} = 30.9$

D = Density of Liquid, Grams/cc

d = Density of Air Saturated With Vapor of the Liquid (Assumed Negligible)

M = Weight of Liquid Raised Above Free Surface of the Liquid, Grams

V = Volume of Liquid Raised Above Free Surface of the Liquid, cc

R = Mean Radius of the Ring, cm

r = Radius of the Wire from Which Ring is Made, cm

F = Correlation Factor

L = Mean Circumference of the Ring, cm

G = Gravity Constant in CGS Units

1. W. D. Harkins and H. F. Jordan, "A Method for Determination of Surface and Interfacial Tension from the Maximum Pull on a Ring". Journal Am. Chemical Soc., Vol. 52, p 1751 (1930).

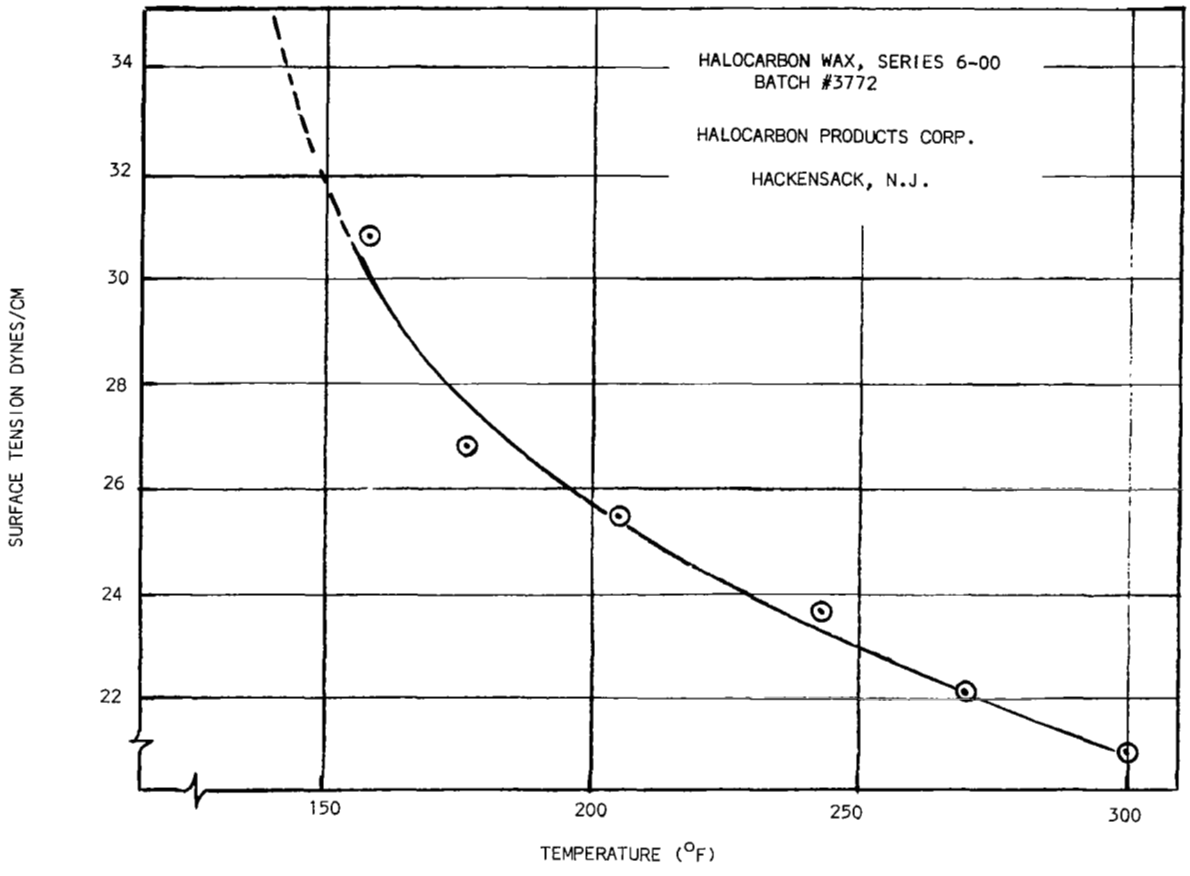

FIGURE B-2 – SURFACE TENSION VS TEMPERATURE

SECTION 2. SURFACE WETTABILITY OF STAINLESS STEEL BY HALOCARBON WAX
(Angle - of - Contact Method)

This method deals with the behavior of a drop of liquified halocarbon wax at a specific temperature when applied directly to the surface of a stainless steel sample held at the same temperature. The procedure involves the measurement of the angle-of-contact of the drop with the metal surface. The angle-of contact is defined as that interior angle formed by the baseline and the tangent to the curve (formed by the drop) at the point of contact with the baseline. The advancing angle-of-contact between a liquid and a solid surface is a measure of the wettability of the latter by the former.

Theoretically when a drop of a liquid rests on the surface of a solid, and a gas is in contact with both, the surface energies acting in the direction the surfaces at the interfaces must balance. Referring to Figure B3(a), one can write,

$$\sigma sa = \sigma SL + \sigma La \cos \theta \qquad (1)$$

where:

σsa = surface tension of substrate

σsL = interfacial tension of solid-liquid

σLa = surface tension of liquid

θ = angle-of-contact

Rearranging equation (1) one obtains

$$\cos \theta = \frac{(\sigma sa - \sigma sL)}{\sigma La} \qquad (2)$$

where $(\sigma sa - \sigma sL)$ is defined as the "wetting tension" of the solid. When $\theta = 0^{\circ}$, the liquid is said to just wet the surface of the solid, and the wetting tension of the solid will be equal to the surface tension of the liquid. This is true for the perfect case, however, in the practical sense one can not achieve a perfect system and therefore one can only approach an angle-of-contact of 0°. A perfect system would be one in which the solid would be completely flat, smooth, free of any blemishes as well as contaminates. The liquid would be uniform and pure and the gas would behave as an "ideal gas" and would be saturated with the liquid vapors. Geometrically then, referring to Figure B3(b) the liquid drop resting on the solid surface can be considered a segment of a sphere. And from geometrical relationships then

$$\phi = 2 \sin^{-1} \ell/2R$$

and

$$\theta = \phi/2$$

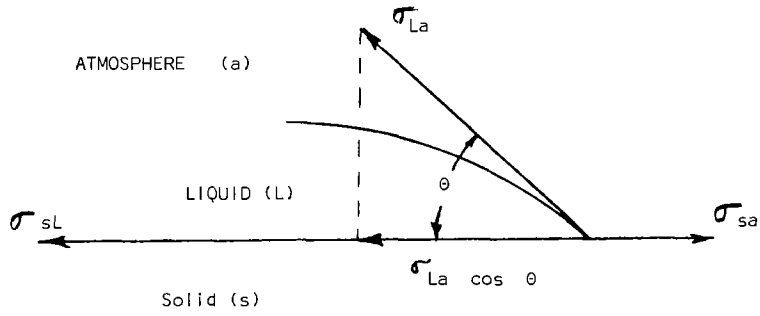

(a)

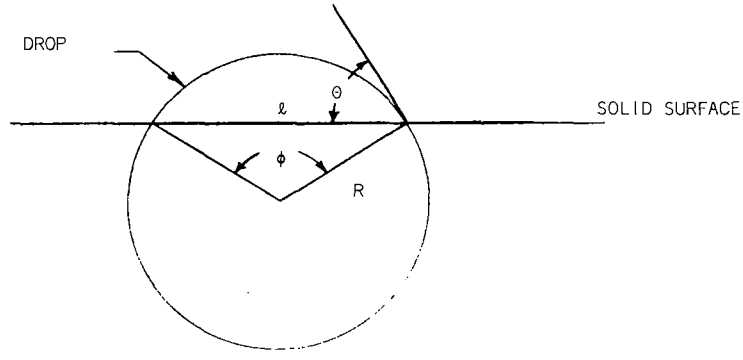

(b)

FIGURE B-3 - GEOMETRIC DEFINITION

Therefore

$\theta = \sin^{-1} \ell/2R$ (angle -of-contact)

The angle-of-contact is a function of the length of the spherical segment formed by the drop and the effective radius of the drop spherical surface.

Apparatus

The apparatus used to make the angle-of-contact measurement, shown in Figure B4, consists of the following:

(1) Camera - Bausch & Lamb Macrocamera with a 158mm f/11 lens. The exposure time is 0.5 seconds using Polaroid 4x5 film.

(2) Lamp - 75 watt flood lamp.

(3) Hot Plate - A hot plate with a temperature controller capable of at least 400°F.

(4) Thermocouple and Controller - Capable of reading and maintaining the temperature to ±2°F over the range of 100-400°F.

(5) Medicine Dropper

(6) Oven (not shown) - A temperature controlled oven capable of maintaining the temperature to ±2°F over the range of 100-400°F.

(7) Timer (not shown)

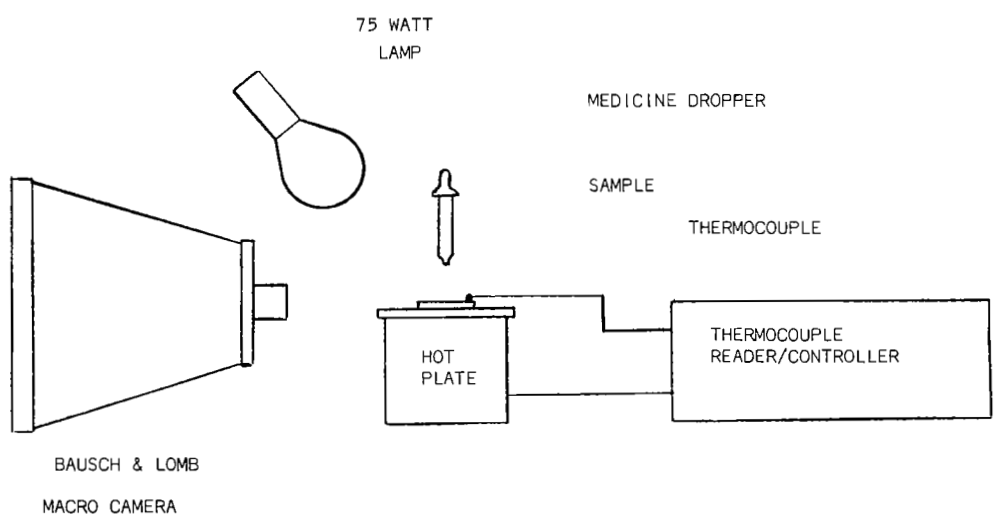

FIGURE B-4 - DIAGRAM OF MEASUREMENT APPARATUS

Procedure

Place the stainless steel plate sample or the #5014 micron porous stainless steel sample on the hot plate. Attach the thermocouple and set to the desired temperature. Place halocarbon wax sample in oven at the same temperature. Allow the temperature to reach equilibrium (10-15 minutes). Quickly extract a sample of the liquid halocarbon wax with the medicine dropper and with the tip of the dropper at about 1/4 to 1/2 in from the metal surface deposit a drop of the test liquid. Project the image of the drop, enlarged to approximately 3 times, on to the Polaroid film. The camera is focused on the metal sample beforehand. Make an exposure after the drop has been in contact with the metal surface for 5 seconds. Make a second exposure after 60 seconds and a third exposure after 120 seconds. The angle-of-contact is then determined as previously explained.

Results

The photographic results of the angle-of-contact measurements for halocarbon wax on both smooth and porous stainless steel samples at various temperatures are shown in Figures B5, B6, B7 and B8. Figure B9 shows a plot of the angle-of-contact for halocarbon wax on a smooth stainless steel sample as a function of time after a drop of the liquid wax sample is placed on the metal sample for various temperatures. The figure shows that as the temperature is increased the angle-of-contact decreases; as expected, approaching some minimum angle of about 8^{o}. The figure also shows that at a given temperature the angle-of-contact continues to change (decreases) as a function of time. The change becomes small with the higher temperatures. This is probably due to surface imperfections and contaminations and therefore probably one can consider the surface wetted by the liquid at that temperature where the angle-of-contact is small and also changes minimally with time. In this case, approximately 250^{o}F. Figure B10 is a replot of the data contained in Figure B9.

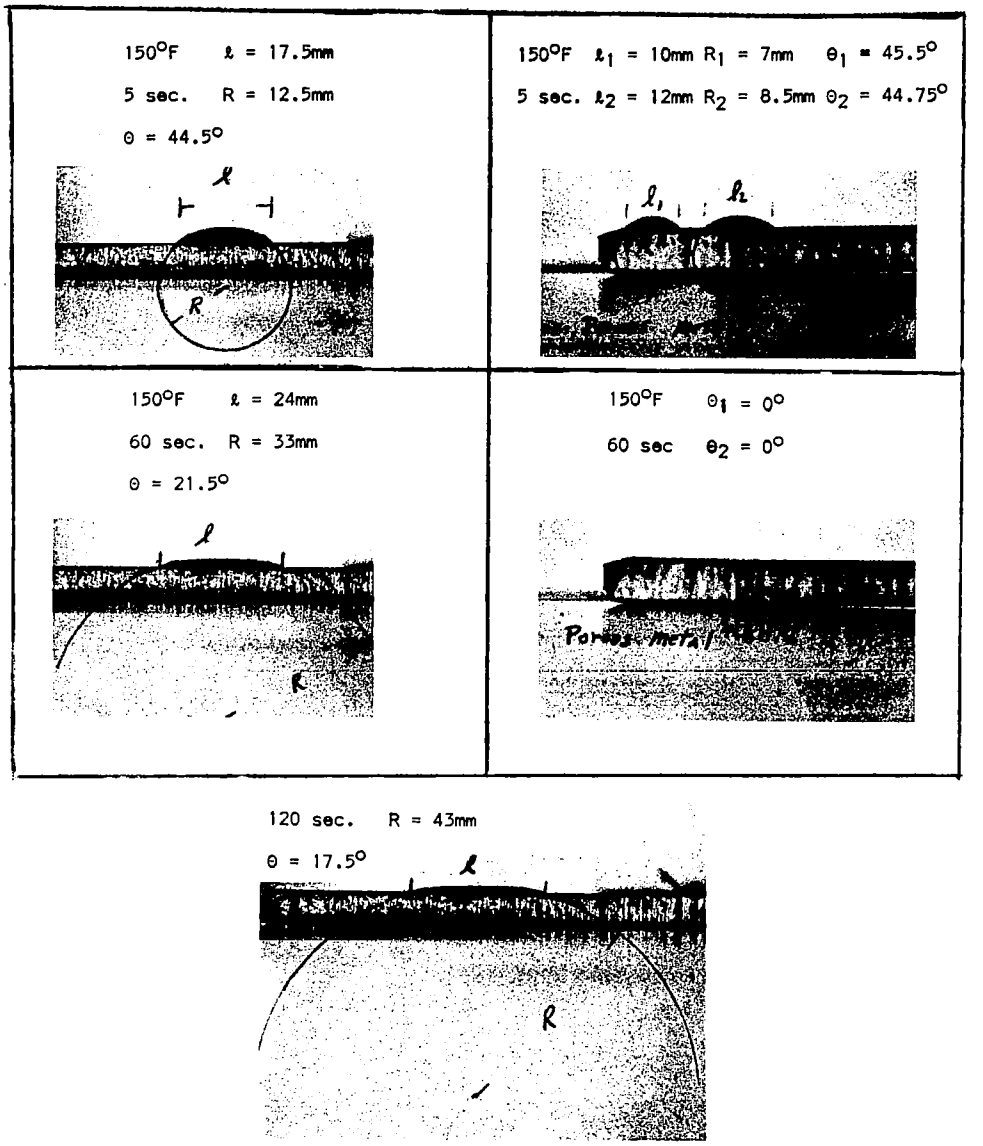

FIGURE B-5 - ANGLE OF CONTACT ON SMOOTH AND POROUS STAINLESS STEEL AT 150 °F

200°F ℓ = 19mm θ = 25°

5 sec. R = 22.5mm

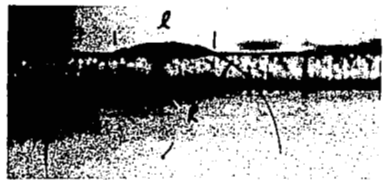

200°F ℓ = 14mm θ = 24.3°

5 sec. R = 17mm

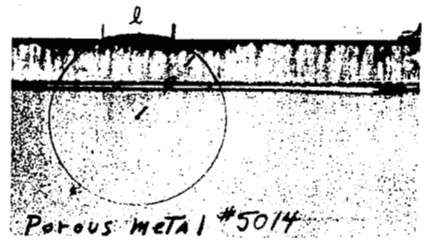

200°F ℓ = 33mm θ = 13°

60 sec. R = 73.5mm

200°F θ = 0°

60 sec.

200°F ℓ = 33mm θ = 11°

120 sec R = 86mm

250°F θ = 0°

5 sec.

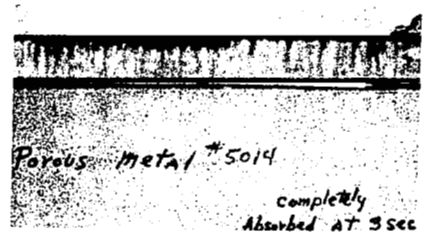

FIGURE B-6 - ANGLE OF CONTACT ON SMOOTH AND POROUS STAINLESS STEEL AT 200 °F

250°F ℓ = 20mm θ = 16°

5 sec R = 34mm

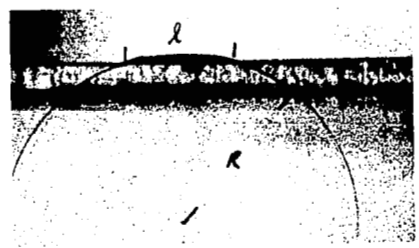

300°F ℓ = 22mm θ = 11.75°

5 sec. R = 54mm

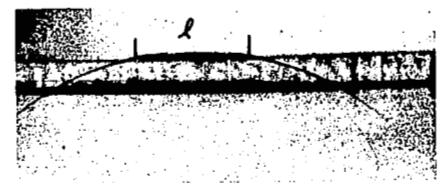

250°F ℓ = 26.5mm θ = 10°

60 sec. R = 76mm

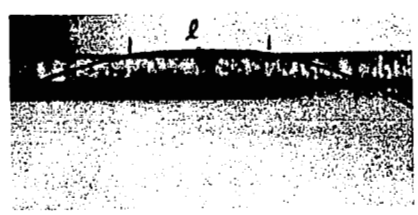

300°F ℓ = 25mm θ = 8.7°

60 sec. R = 83mm

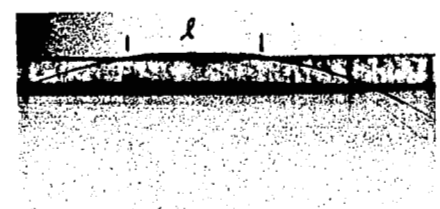

250°F ℓ = 27mm θ = 9.25°

120 sec. R = 84mm

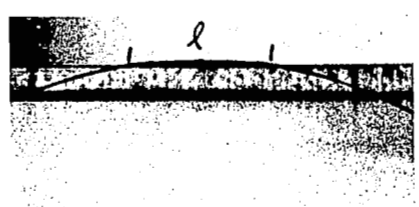

300°F ℓ = 25.5mm θ = 8°

120 sec. R = 91mm

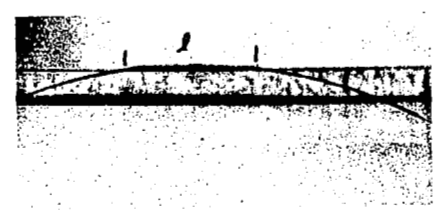

FIGURE B-7 - ANGLE OF CONTACT ON SMOOTH STAINLESS STEEL AT 250 °F AND AT 300 °F

130°F ℓ = 11.5mm θ = 107°

5 sec. R = 6mm

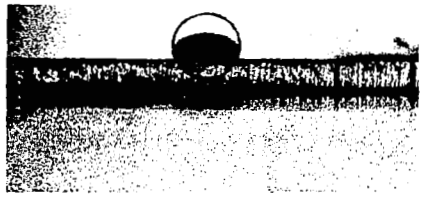

350°F ℓ = 25mm θ = 9°

5 sec R = 80mm

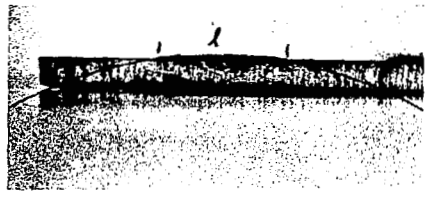

130°F ℓ = 14.5mm θ = 76°

60 sec. R = 7.5mm

350°F ℓ = 29mm θ = 8°

60 sec. R = 104mm

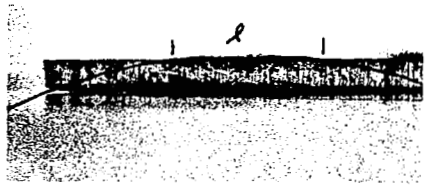

130°F ℓ = 15.75mm θ = 56°

120 sec. R = 9.5mm

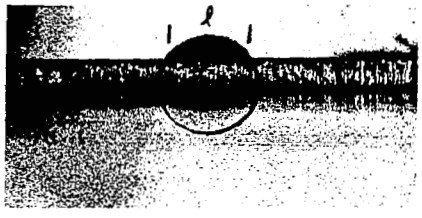

350°F ℓ = 29mm θ = 8°

120 sec. R = 104mm

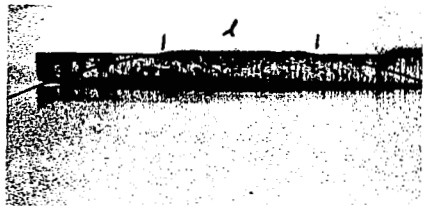

FIGURE B-8 - ANGLE OF CONTACT ON SMOOTH STAINLESS STEEL AT 130 °F AND AT 350 °F

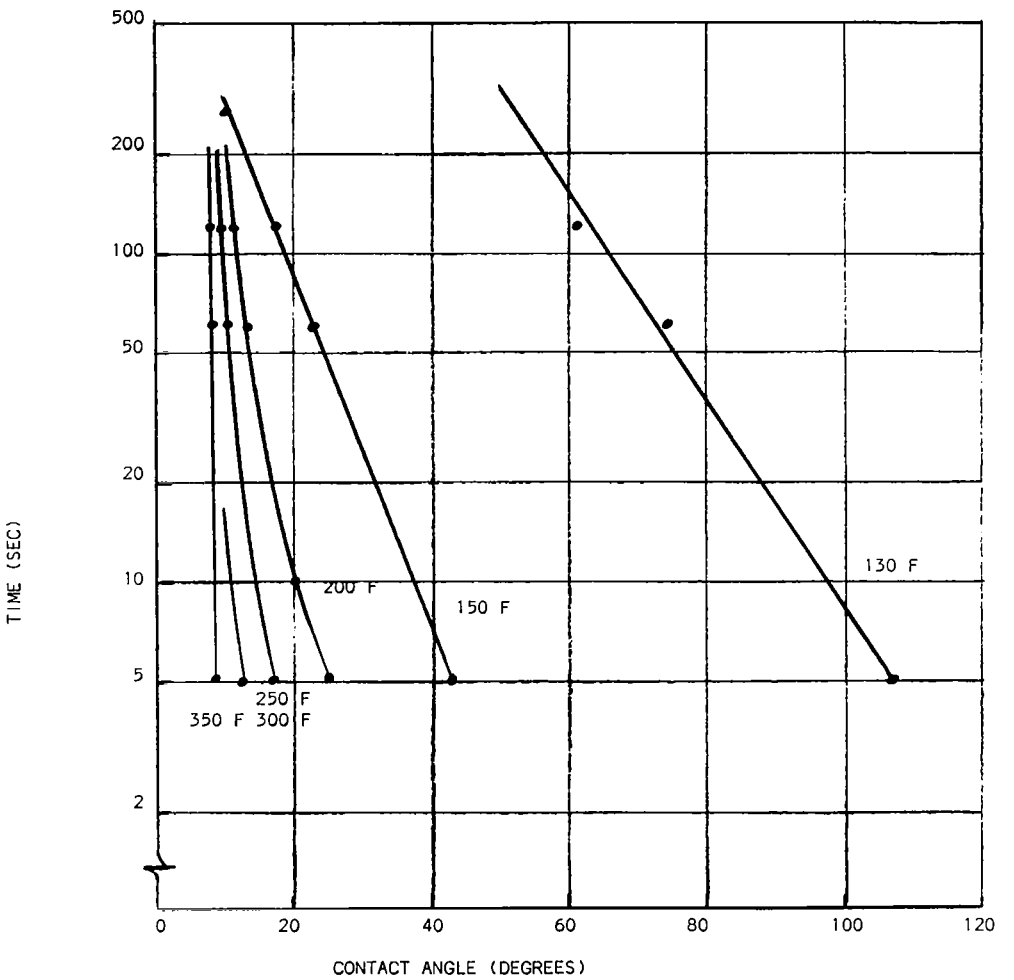

FIGURE B-9 - ANGLE OF CONTACT AS A FUNCTION OF TIME FOR VARIOUS TEMPERATURES

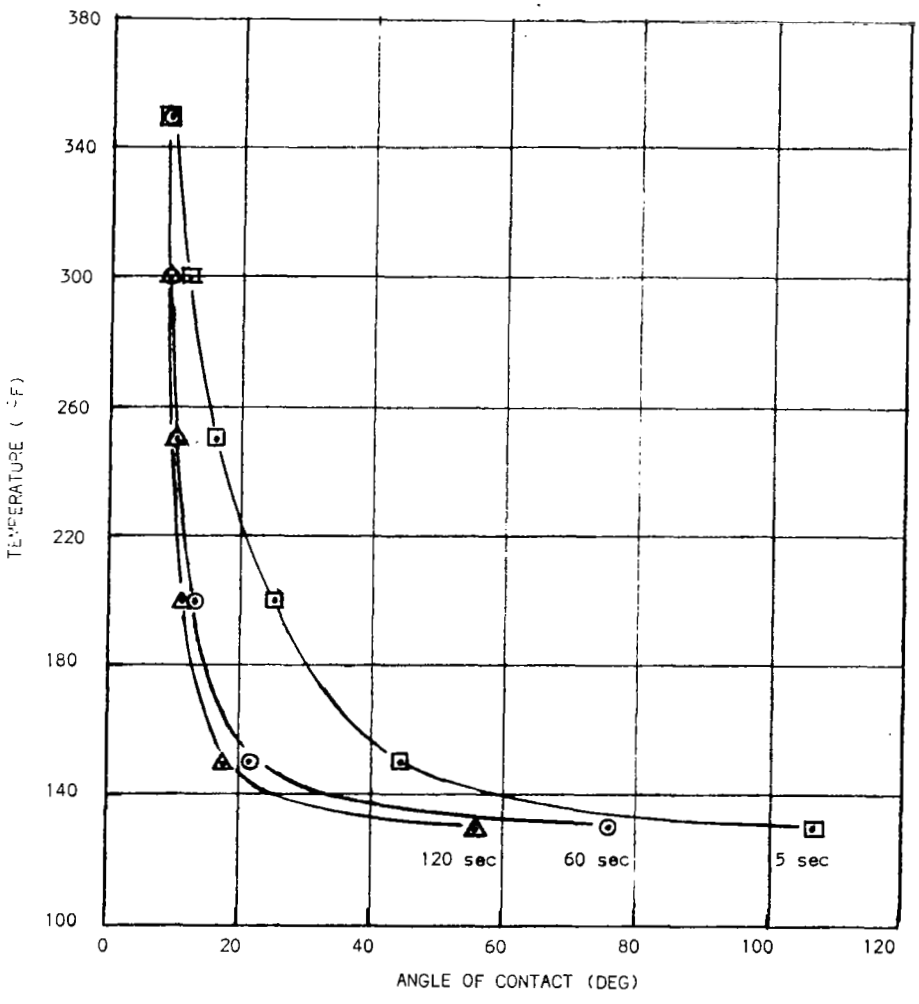

FIGURE B-10 - ANGLE OF CONTACT AS A FUNCTION OF TEMPERATURE FOR VARIOUS TIMES

SECTION 3. RATE OF WEIGHT LOSS IN VACUUM AS A FUNCTION OF TEMPERATURE

Experimental Method

The Fisher Model 120 Thermogravimetric Analysis Accessory with an oil diffusion pump-mechanical pump vacuum system was used for this test.

The sample was placed on the balance pan and enclosed within a hang-down tube which in turn was suspended from underneath and fitted to the weighing chamber port. After the system was evacuated, an oil bath (preheated and maintained at desired temperature) was raised into position around the hang-down tube to surround the sample area. Sample weight loss was continuously recorded on a strip-chart recorder.

Experimental Conditions

A. Sample Parameters
   1. ∿11 mm diameter
   2. ∿1 mm thick
   3. 126.5 mg - initial weight

B. Sample Environment
   1. <1 micron vacuum
   2. Weight loss rates were obtained at temperatures of 150°, 200°, 250°, and 300°F.

Results and Discussion

Results of the weight loss analysis are shown in Figure B11. Evaporation rates were followed for a sufficient length of time to ascertain the steady state diffusion rate of volatile materials through the bulk of the sample.

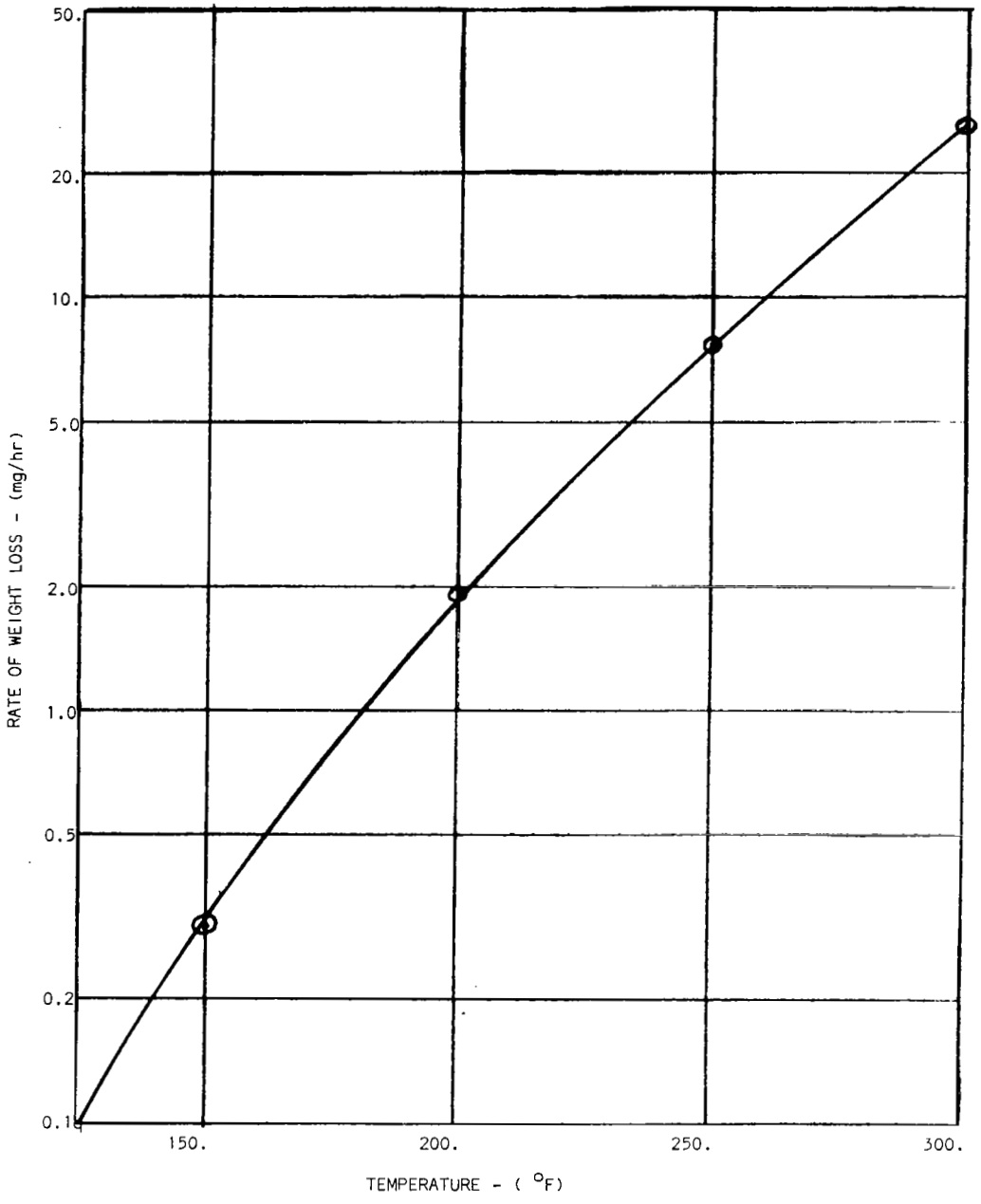

FIGURE B-11 - WEIGHT LOSS IN VACUUM VS TEMPERATURE

SECTION 4. WICKING CHARACTERISTICS OF POROUS METALS AND METAL SCREENS

Experimental Method

In circulating ovens maintained at a specified temperature, samples were positioned so that one end of each sample was immersed (approximately 1/8 to 3/16 inches) in Halocarbon Wax, Series 6-00, Batch #3772. At designated times the samples were taken out of the oven and weighed (after scraping off excess wax clinging to end of sample). For some samples the vertical distance the wax had penetrated was measured.

Results

Results are tabulated in Table B3 through B11.

TABLE B.3 - 102°F WICKING OF POROUS STAINLESS STEEL STRIPS - 1/8" x 1/4" x 4 to 4 3/4" LONG (AVERAGE FOR THREE SPECIMENS)

	10μ - #6281		20μ - #6519		40μ - #5014	
Elapsed Time Hours	Total Weight Gained Grams	Wet Height Inches	Total Weight Gained Grams	Wet Height Inches	Total Weight Gained Grams	Wet Height Inches
72	0.3655		0.3436		0.5039	
95	0.3931		0.3507		0.5260	
114	0.4388	13/16	0.4112	3/4	0.5641	13/16
162	0.4613	1 1/2	0.4249	1 3/8	0.5898	1 9/16
234	0.5034	1 9/16	0.4395	1 1/2	0.6147	1 9/16
594	0.6380	1 7/8	0.5417	1 3/4	0.7393	1 7/8

TABLE B.4 - 140°F WICKING OF POROUS STAINLESS STEEL STRIPS - 1/8" x 1/4" x 4 to 4 3/4" LONG (AVERAGE FOR THREE SPECIMENS)

	10μ - #6281		20μ - #6519		40μ - #5014	
Elapsed Time Hours	Total Weight Gained Grams	Wet Height Inches	Total Weight Gained Grams	Wet Height Inches	Total Weight Gained Grams	Wet Height Inches
1	0.1989		0.2230		0.3298	
2	0.2384		0.2529		0.3709	
3	0.2493		0.2596		0.3722	
5	0.2924		0.3045		0.4500	
9	0.3243		0.3569		0.4907	
26	0.3976		0.4346		0.5609	
98	0.5795		0.5931		0.7408	
194	0.7858		0.5931		0.9024	
266	0.9010		0.8506		0.9912	
626	1.0588		0.9657		1.0827	

TABLE B.5 - 170 - 180°F WICKING OF POROUS STAINLESS STEEL STRIPS - 1/8" x 1/4" x 4 TO 4 3/4" LONG (AVERAGE FOR THREE SPECIMENS)

	10μ - #6281		20μ - #6519		40μ - #5014	
Elapsed Time Hours	Total Weight Gained Grams	Wet Height Inches	Total Weight Gained Grams	Wet Height Inches	Total Weight Gained Grams	Wet Height Inches
1/3	0.2217	3/8	0.2751	1/2	0.3055	3/8
2/3	0.2744	7/16	0.3391	9/16	0.3832	5/8
1	0.3120	9/16	0.3766	5/8	0.4292	5/8
1 1/3	0.3287	5/8	0.3963	11/16	0.4524	5/8
65	0.8843	2 7/16	0.9249	2 9/16	0.9027	2 1/2

TABLE B.6 - 140°F WICKING OF STAINLESS STEEL SCREENS - AIRCRAFT POROUS MEDIA (R/M, T304), PALL, GLEN COVE, NEW YORK

	10 MICRONS (J)		40 MICRONS (R)		70 MICRONS (S)	
Elapsed Time Hours	Weight Gained After Wetting Grams	Wet Height Inches	Weight Gained After Wetting Grams	Wet Height Inches	Weight Gained After Wetting Grams	Wet Height Inches
Initial Wetting	-----	3/16		5/16		1/4
2	0.0086	9/32	0.0210	13/32	0.0176	11/32
7	0.0149	3/8	0.0277	7/16	0.0316	13/32
80	0.0532	13/16	0.0322	15/32	0.0298	3/8
250	0.0902	1 7/32	0.0331	15/32	0.0271	3/8
561	0.1274	1 9/16	0.0307	15/32	0.0255	3/8

TABLE B.7 - 170°F WICKING OF STAINLESS STEEL SCREENS - AIRCRAFT POROUS MEDIA (R/M, T304), PALL, GLEN COVE, NEW YORK

	10 MICRONS (J)		40 MICRONS (R)		70 MICRONS (S)	
Elapsed Time Hours	Weight Gained After Wetting Grams	Wet Height Inches	Weight Gained After Wetting Grams	Wet Height Inches	Weight Gained After Wetting Grams	Wet Height Inches
Initial Wetting	----	3/16	------	1/4	------	3/16
1/2	0.0044	3/16	0.0160	5/16	0.0023	7/32
2	0.0115	11/32	0.0146	11/32	0.0094	1/4
7	0.0271	1/2	0.0245	3/8	0.0114	9/32
33	0.0602	7/8	0.0296	13/32	0.0070	9/32
80	0.0945	1 7/32	0.0254	13/32	0.0094	9/32
200	0.1216	1 1/2	0.0260	13/32	0.0054	9/32
399	0.1457	1 13/16	0.0240	13/32	0.0047	9/32

TABLE B.8 - 170°F WICKING OF ROLLED STAINLESS STEEL SCREENS - AIRCRAFT POROUS MEDIA (R/M, T304), PALL, GLEN COVE, NEW YORK

	10 MICRONS (J)		40 MICRONS (R)		70 MICRONS (S)	
Elapsed Time Hours	Weight Gained After Wetting Grams	Wet Height Inches	Weight Gained After Wetting Grams	Wet Height Inches	Weight Gained After Wetting Grams	Wet Height Inches
Initial Wetting	----	9/16	-----	1/2	-----	3/8
1 1/2	0.0541	15/16	0.0254	9/16	0.0156	13/32
7	0.1167	1 7/16	0.0201	9/16	0.0193	13/32
14 1/2	0.1614	1 3/4	-----	----	------	-----
201 1/2	------	-----	0.0313	9/16	0.0333	7/16

TABLE B.9 - 170°F WICKING OF POROUS STAINLESS STEEL BUSHING - 1 3/8" O.D. x 7/8" I.D. x 3/4" LONG

Elapsed Time - Hours	Total Weight Gained - Grams
16	8.2895
40	8.6870
137	8.7415
305	8.9357
478	9.0138
642	9.1133

TABLE B.10 - 170°F WICKING OF POROUS BRONZE BUSHING 1 3/8" O.D. x 7/8" I.C. x 3/4" LONG

Elapsed Time - Hours	Total Weight Gained - Grams
24	5.6479
54	5.7327
168	5.8297
340	5.8642
504	5.9442

TABLE B.11 - 170°F WICKING OF STAINLESS STEEL SCREEN DISC - 4 3/4" O.D., 1 11/32" DIA. HOLE IN CENTER, WITH 14 SCATTERED 1/4" DIA. HOLES

Elapsed Time Hours	Total Weight Gained-Grams	Wet Height Inches
1/2	0.0268	7/32
24	0.0846	3/4
54 1/2	0.1300	1
168	0.2289	1 5/8
340	0.3358	2 1/4
504	0.3938	2 9/16

SECTION 5. INFRARED ANALYSIS

Experimental Method

A Perkin-Elmer Model 457 infrared spectrophotometer was used to obtain the infrared spectrum in the 2-15 micron range of Halocarbon Wax, Series 6-00, Batch #3772 (Figure B12.)

A sample of wax was dissolved in chloroform and cast as a film on a sodium chloride crystal.

Discussion

Chemically, halocarbon oils are saturated low molecular weight polymers of chlorotrifluoroethylene and have the general formula - $(CF_2CFCl)_n$ -. They are made by a controlled polymerization technique and are then stabilized so that the terminal groups are completely halogenated and inert. The product is then separated into various fractions from light oils to waxes by vacuum distillation.

The main features of the infrared spectrum of Halocarbon Wax, Figure B12, include the absence of C-H structure at 3.4μ, the presence of a pair of strong bands between 8-9μ attributed to the CF_2 group and a strong band at 10.3μ resulting from the single CF group present as CClF. The infrared spectrum indicates the Halocarbon Wax to be completely saturated (no double bonds) and free of hydrogen. The presence of unsaturation or hydrogen severely compromises the inertness of the chlorofluorocarbon. Unsaturated polychlorotrifluoroethylenes combined with air and moisture can become acidic and be corrosive toward metals, particularly steel, while any hydrogen in a molecule can be a point of attack by oxygen or other strong oxidizers.

Infrared spectrometry will determine the completeness of saturation and the absence of hydrogen in Halocarbon Wax.

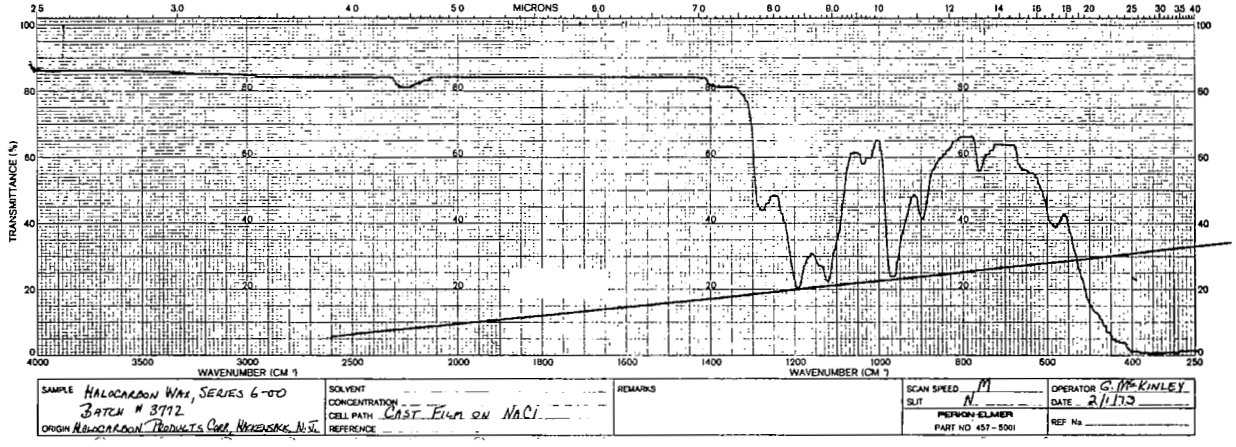

FIGURE B-12 - INFRARED SPECTRUM IN THE 2 - 15 MICRON RANGE

APPENDIX C

FIRE CONTROL LOGIC BOX
OF THE LIQUID INJECTION ELECTRIC THRUSTER (LINJET)

by E. Hansen

INTRODUCTION AND PURPOSE

The LINJET Logic Box provides a means of controlling the firing rate of the LINJET engine while assuring that the trigger segment that initiates main capacitor firing is changed by advancing the leading fire control pulse each time the engine fires. Figure C1 provides a timing diagram which defines the control of pulses applied to each trigger segment. There are four trigger segments in the LINJET engine, and the trigger pulses in Figure C1 are identified as to which of these trigger segments are being driven at any point in time.

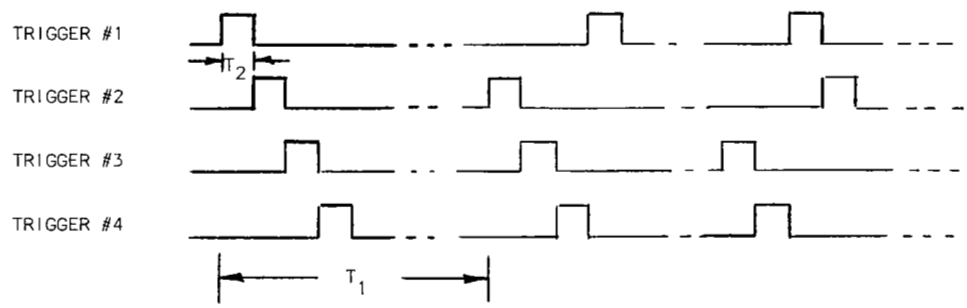

Figure C1 Timing diagram of the pulse output to the trigger segment driver circuits.

As indicated in Figure C1, the fire control circuit changes the trigger segment to which the first fire pulse is applied each time a four-pulse group is applied to the LINJET. The rate of applying the four pulses of each train to the four trigger segment is 2KHz or at a repetition rate of 0.5 msec (T_2 in Figure C1) between the leading edge of each pulse. The interfacing circuitry between the logic control box and the actual trigger segment gap located in the engine differentiates the pulse such that only the leading edge of each pulse precipitates individual trigger segment sparks. The period between the four pulse groups (T_1 in Figure C1) represents the desired firing rate of the LINJET engine. The overall automatic firing rate is selectable to be 5 Hz, 1 Hz, .1 Hz, or .01 Hz. Provisions have also been incorporated to provide a single four-pulse group control via a manual momentary switch closure.

CIRCUIT OPERATION DESCRIPTION

The following paragraph describes how the circuit operates via logic, schematics and diagrams. Figure C2 represents a schematic of the logic wiring in the Logic Control Box.

FIRING RATE CONTROL

The automatic firing rate has been made selectable from 5 pps to .01 pps in four steps. All timing is based on a single 64KHz clock as shown in Figure C2. The 64KHz clock rate is divided by a factor of 1.28×10^4 to achieve the 5 pps rate. Rates of 1 pps, .1 pps, and .01 pps are then derived by dividing further by factors of 5, 50, and 500, respectively. The four possible firing rates are made manually selectable via a 4-pole, 4-position switch which controls which repetition rate is applied to the input of a monostable multi-vibrator or one-shot, A18 in Figure C2. The one shot then puts out a series of narrow duration reset and sequence start pulses at the selected repetition rate. The time division (1.28×10^4) referred to above is performed by a series of eight 4-bit digital counters, A2 thru A9 in Figure 2. An And/Or select gate, A14 in Figure C2, provides the logic interface for selecting the desired automatic firing rate.

The firing rate information from the one shot is provided as an input for controlling the start of the four pulse sequence which ultimately, via interface circuitry in the engine, drives the four segment trigger. The firing rate pulses are also used to advance the trigger segment which is the lead pulse in each four pulse group.

TRIGGER SEGMENT DRIVE CONTROL

The trigger segment drive control is provided by shift register A54, timer A3, and associated gates, flip flops, and digital buffer circuits.

The logic diagram in Figure C3 describes how a four-pulse sequence is developed after each reset and start pulse is put out by A23-3. The A23-3 output is, of course, occurring at the selected firing rate. The sequence of events are:

1. Start timer A3, by opening gate A-11, by resetting flip flop A10.
2. Enter parallel data stored at A54-3, -2, -15 and -14 inputs with shift and load controls provided by A12-6 and A12-4 outputs, respectively.
3. Shift parallel data to the right in the shift register four steps while providing a sequence of four pulses at the buffer outputs of A22.

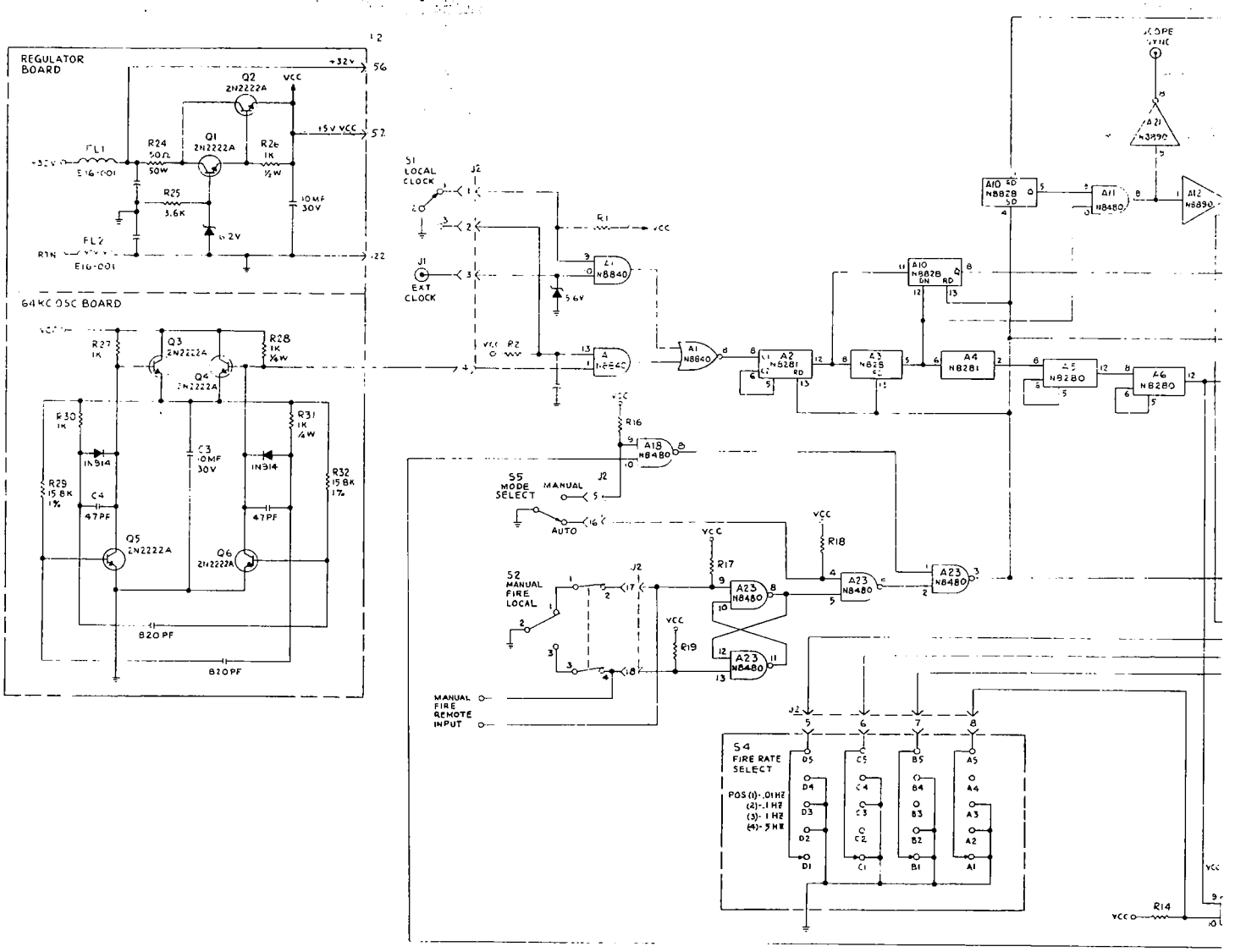
REGULATOR BOARD
+32V
56
Q2
2N2222A
VCC
+5V VCC
57
Q1
2N2222A
FL1
E16-001
R24
50Ω
50W
R26
1K
½W
R25
3.6K
6.2V
10MF
30V
FL2
E16-001
22
64KC OSC BOARD
R27
1K
Q3
2N2222A
Q4
2N2222A
R28
1K
½W
R30
1K
R31
1K
4W
IN914
IN914
C3
10MF
30V
R29
15.8K
1%
C4
47PF
47PF
R32
15.8K
1%
Q5
2N2222A
Q6
2N2222A
820PF
820PF
S1
LOCAL
CLOCK
J2
J1
EXT
CLOCK
R1
VCC
5.6V
A1
N8840
A2
N8281
A3
N8281
A4
N8281
A5
N8280
A6
N8280
A10
N8828
A11
N8480
A12
N8890
A21
N3490
SCOPE
SYNC
R16
A18
N8480
S5
MODE
SELECT
MANUAL
AUTO
S2
MANUAL
FIRE
LOCAL
R17
R18
R19
A23
N8480
MANUAL
FIRE
REMOTE
INPUT
S4
FIRE RATE
SELECT
POS (1)-.01HZ
(2)-.1HZ
(3)-1HZ
(4)-5HZ
R14

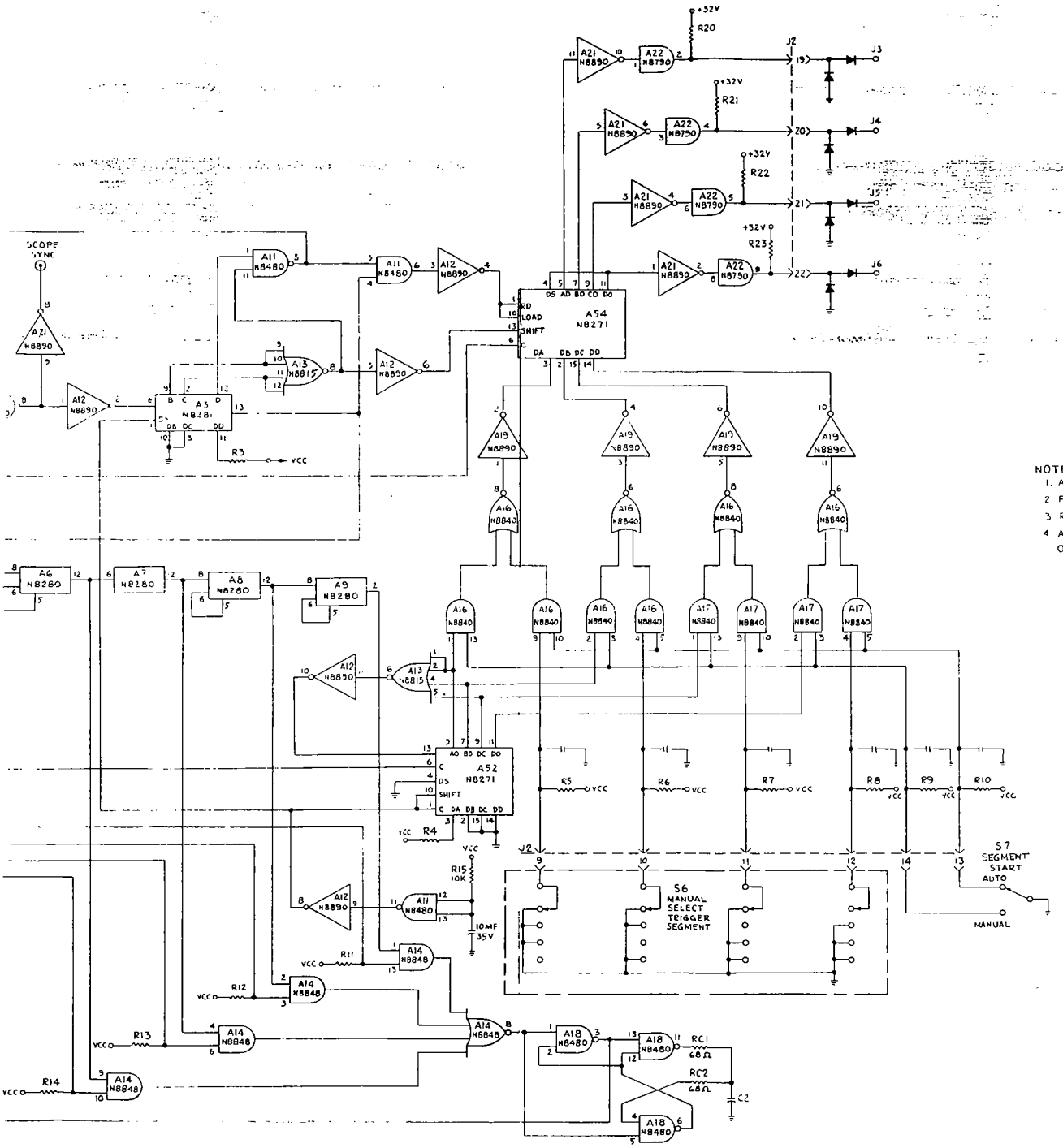

FIGURE C-2 - FIRE CONTROL LOGIC BOX SCHEMATIC

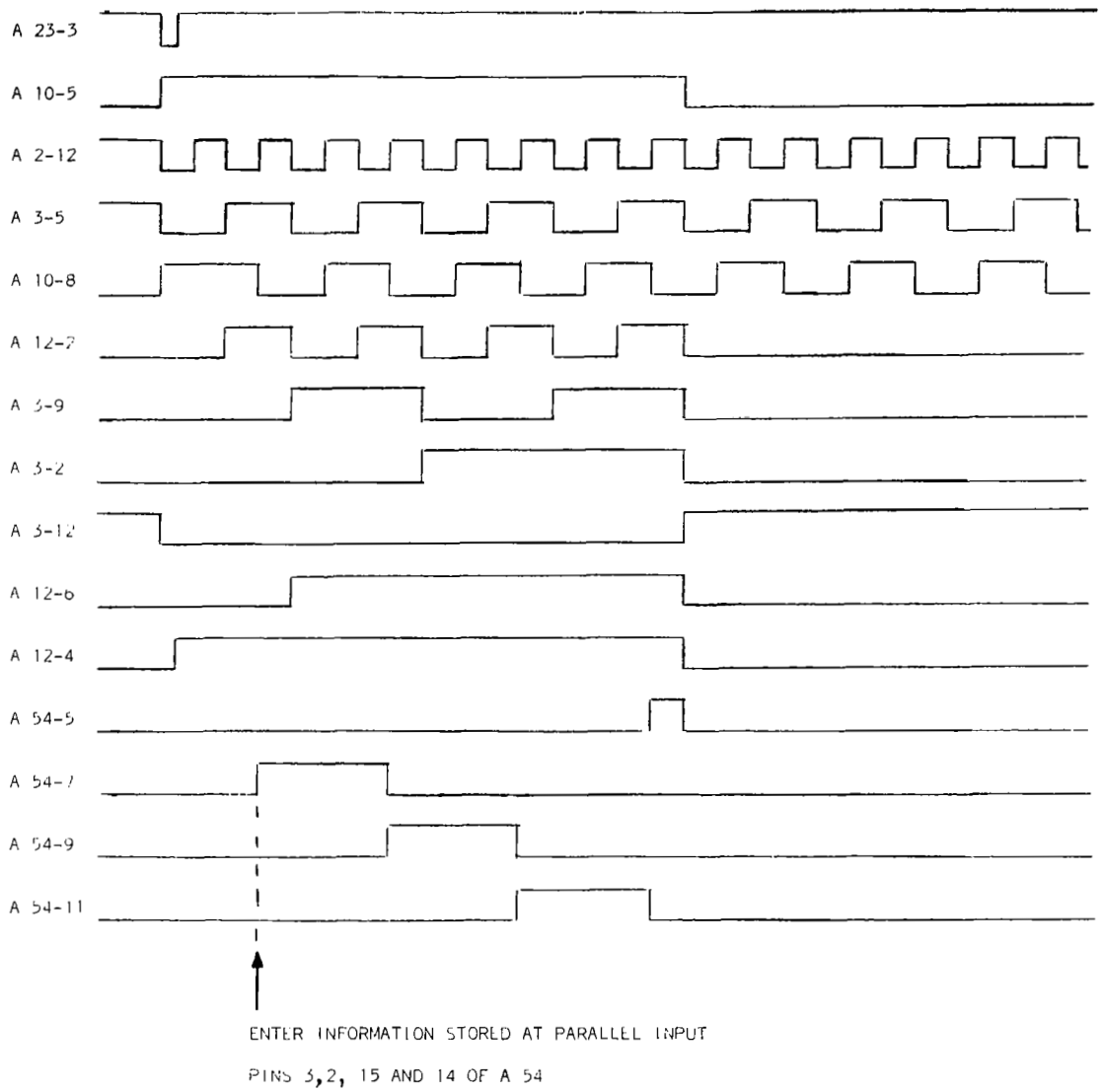

FIGURE C-3 - LOGIC DIAGRAM FOR CONTROL OF FOUR PULSE SEQUENCE

4. At the count of four, the timer A23 closes gate A-11 by resetting flip flop A10 and provides the proper logic signal to reset all A54 shift register outputs to a zero logic level and keep the shift register in this state until the next reset and start pulse from A23-3 is generated.

TRIGGER SEGMENT SEQUENCE ADVANCE CONTROL

The trigger sequence advance control is provided by shift register A52, and associated gates A16, A19, A13, A12, A11 per the schematic in Figure C2. The purpose is to advance the position of the starting pulse of the 4-pulse sequence described above. The A52 shift register in Figure C2 is hooked up as a ring counter whose clock is provided by the reset and start pulse train from A23-3. As each reset pulse arrives, a data state is shifted to the right in A52. Initially, at the power turn on, the outputs from A52 are reset to logic zero by a charging time constant provided by a 10 uf capacitor and 10KΩ resistor network present at the input of gate A11-13. The arrival of the first reset pulse from A-23 after power turn-on then loads the data present at the A52-3, -2, -15, and -14 inputs. The data now present at the A52 outputs, is on each subsequent reset pulse, shifted to the right by one step at a time until the logic levels present at A52-5, -7, -4, and -11 outputs cause the parallel data input to again be loaded into the shift register A54. In this way, the logic levels present at the pulse sequencing shift register A54 are changed between generation of each four-pulse sequence. Therefore, the first trigger pulse in the sequence never occurs more than once for four reset and start pulses at, for example, the J3 output terminal in Figure C2. The initial engine firing pulse on the four-segment trigger in the LINJET is, therefore, advanced one segment each time the trigger assembly is fired.

OPTIONAL MANUAL CONTROLS IN THE SPET LOGIC BOX

A manual firing control can be initiated which bypasses the automatic sequences via switches SW-5 and SW-2. A single four-pulse sequence as described above may be generated manually by putting SW-5 in the manual position and momentarily closing SW-2. The resulting manually-generated reset and start pulse at A23-3, in addition to generating four-pulse trigger sequence, will advance the first pulse position in the sequence each time SW-2 is closed.

A four-pole, four-position switch is also provided by SW-6 and SW-7 to bypass the four-pulse sequence start pulse advance if desired in either manual or automatic firing mode. In this way, the starting pulse can be made to dwell at any single trigger segment in the LINJET Engine.

A means is also provided for applying an external clock to obtain a rate different from the 64K Hz internal clock if desired. In this, the four-pulse sequence repetition rate and the firing repetition rate can be changed to some other timing than those based on the 64K Hz clock.

OPERATING PROBLEMS

Some incidents of burn-out of the output buffer IC A22 have been encountered in spite of diode isolation from the circuitry in the LINJET Engine. Apparently, when the vacuum system in which the LINJET is operating fails to keep the gas pressure below critical levels, corona arc-overs take place fro... the high voltage to the trigger lines which short-out the A22 integrated circuit output bypassing the protective diodes via the shunt capacity of these elements. No other operating problems have been encountered in the logic box.

APPENDIX D

Main Capacitor Life Testing

Present herein are three packets of data relative to the life test of the main capacitor.

The first is extracts from the test log taken during the course of the testing. It has been edited only to put the data in a standard format for readability. The figure numbers referred to in the log are the oscillograph photographs that are the second data packet.

The third data packet is Table D-1 showing a tabulation of various parameters referenced by the figure number on the table to the photographs noted above.

The calculation of the parameters in Table D-1 use the standard formulas for a damped sine wave, as follows:

The current is expressed as:

(1) $$I_t = \frac{V_c}{W_n L} e^{-(R/2L)t} \text{ SIN } W_n t$$

where: W_n = natural frequency

(2) $$W_n = 2\pi/T_p$$

T_p = is the time between successive amplitude peaks as taken from the oscilloscope picture

R = Calculated loop resistance

(3) $$R = \frac{\ln\left[A_m/A_{(m+1)}\right] T_p}{2\pi^2 C}$$

A_m = Amplitude of a pulse

$A_{(m+1)}$ = Amplitude of the next pulse

C = Capacitance (for this test was 28 microfarads as measured by the manufacturer)

L = Loop inductance

$$(4) \quad L \cong \frac{1}{W_n^2 C}$$

The maximum current occurs when

$$(5) \quad \tan W_n t = \frac{W_N}{R/2L}$$

From measured or given data, this can be solved for time as:

$$(6) \quad t = \frac{\tan^{-1}\left[W_n/(R/2L)\right]}{W_n}$$

which can be used in the solution of equation (1) for current.

It should be noted in Table D-1 that a 10 volt reading on input data is used to signify a parameter test on the capacitor and has no other meaning. (During the parameter test the capacitor is acting as an oscillator that is given a single pulse and the output wave shape is a measure of the internal inductance and resistance.) Similarly, the calculated values of current and time for these points have no significance other than to satisfy the computer routine used in making the calculations.

Three other things will be noted in Table D-1. First, that starting with Figure D24 there is a significant increase in peak current, reflecting the change in external loop resistance/inductance. Second, after Figure D26 the parameter tests (10 volt points) shows a significant decrease in internal resistance and inductance. While the reason is not clear, a possible solution is contained in the loss of capacitor oil. Third, Figures D34-D36 were taken during engine firing tests and are indicative of the low inductive/resistive path attained in the engine design.

EXTRACTS OF MAIN CAPACITOR LIFE TEST LOG

Date/Time	Count	Figure #	Remarks
9/26/72		1 to 11	Spark gap operated intermittingly from 9/26 thru 9/28. Scope pictures were taken during this time showing voltage reversal wave forms and parameter measurements.
9/29/72			After several attempts were made to cure the intermittent problem without success, the voltage across the spark gap was reversed, which was contrary to the vendor's suggested mode of operation. The results were positive and the life test proceeded as planned at a 5Hz rate.
1530	460,179	12	Oil leak was observed around the top of capacitor. This oil was cleaned off.
10/2/72			Capacitor life test resumed after week end.
0800	477,200		
1635	603,824	13	Oil again present at top of capacitor.
10/3/72 1630	1,020,900	15	Voltage wave forms observed with scope indicated a decrease in loop current impedance. The test was allowed to continue operating for next 24 hours.
10/4/72 0925	1,302,800	16	The test was interrupted to decrease loop resistance in the discharge loop. Current measurements made from photo above.
1500	1,403,200	17	Capacitor was removed from test circuit for parameter measurements. A slight build up of oil observed on top of capacitor.
10/5/72 1600	1,825,000	19	Only voltage reversal photo taken.
10/6/72 1325	2,164,700		
1500	2,191,200	20, 21	Voltage reversal measurements made. Parameter measurements made.
10/9/72 1540	3,435,900	23	Voltage reversal.
10/10/72 0840	3,714,000		The life test was interrupted to verify current level data. Calculations made on previous wave forms revealed an error of 13,000 amps. The life test to this date has been operated at approximately 9,000 amp levels. At this point, the loop circuit was changed to eliminate all lead wires. The circuit consisted of a 25 milliohm resistor with aluminum bars for connecting to capacitor and spark gap. The loop current increased to 16,000 amps.
1500		24	Parameter measurement.
10/11/72 1500	4,121,358	24, 26	An attempt was made at this point to eliminate all loop inductance by replacing the wire would resistance with shim stock.

Date/Time	Count	Figure #	Remarks
10/12/72			Power dissipation was too great for the shim, which became red hot and melted. The original .025Ω resistor was replaced in the circuit.
1100	4,128,549	27	Test resumed.
			A malfunction in the test circuit caused a power interruption to the test fixture. Cause was not determined.
		27, 28	The series charging resistor was changed from 900 ohms to 700 ohms due to excessive heat generated in the circuit. Test continued from 0800 to 1600.
			Power was interrupted because of counter monitoring circuit. An attempt to restart test failed when the spark gap failed to fire. All attempts to restart gap failed. Capacitor leaking oil.
10/16/72		29	The failed spark gap was replaced with a new unit. The new unit would not operate with less than 3KV applied until after several minutes of operation. Then operated at 2.4KV levels (presumably needed a burn in time).
1300			Test resumed at a 4.5 Hz rate at V = 2400V.
10/17/72	4,651,382	30	Count = 4,651,382 Test circuit - V ≈ 2400 volts R_C ≈ 700 ohms RL ≈ .025 ohms Voltage reversal measurements made for circuit parameters. The 700 ohm charging resistance was increased to 900 ohm to reduce peak charging current. The gap failed to start when voltage was reapplied. At this point, the voltage was reversed again (to suggested vendor mode) and the gap started firing again.
unknown	4,754,500		
10/18/72	4,850,000	31, 32	No measurements taken. Test lead became disengaged during night time interrupting test.
			Spark gap temperature reached 200°F although a fan was blowing continuingly on it.
10/18/72			The amount of oil escaping from the capacitor exceeded the amount in previous increments of testing. The entire cavity within the top of the capacitor was full to overflowing with oil. The oil spill was wiped clean and test continued.
10/19/72	5,229,765		V = 2800 volts Cap. Temp. = 103°F Spark Gap Temp. = 250°F
			Top ring of capacitor again filled with oil.

At this point the spark gap failed and with the concurrence of the customer technical director, this phase of the program was terminated.

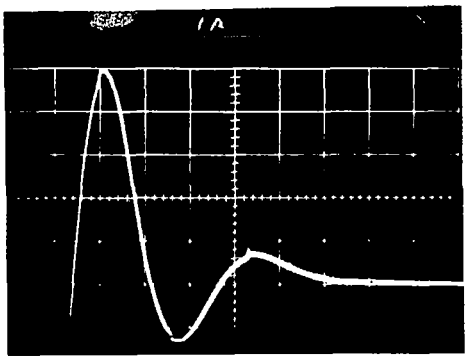

Fig. No.	1
Date:	9/26/72
Time:	1320
Count:	3900
VP:	2500 V
Hor. Sw:	10 μs/cm
S/N:	15118
C:	28 μf

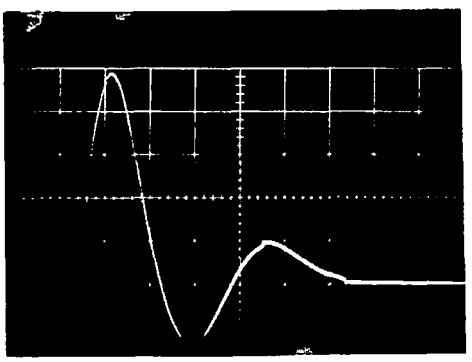

Fig. No.	2
Date:	9/26/72
Time:	1630
Count:	28,200
VP:	2500 V
Hor. Sw:	10 μs/cm
S/N:	15118
C:	28 μf

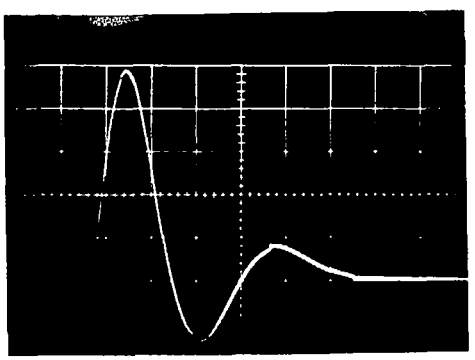

Fig. No.	3
Date:	9/26/72
Time:	1640
Count:	29,000
VP:	2500 V
Hor. Sw:	10 μs/cm
S/N:	15118
C:	28 μf

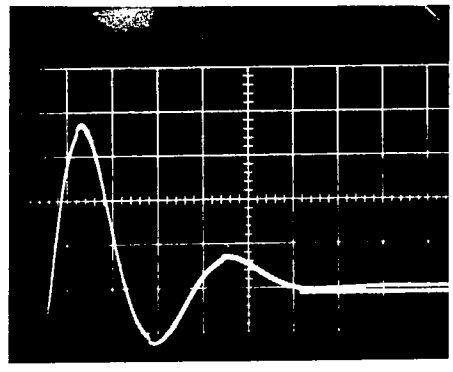

Fig. No. 4
Date: 9/27/72
Time: 0850
Count: 150,100
VP: 2500V
Hor. Sw: 10 μs/cm
S/N: 15118
C: 28 μf

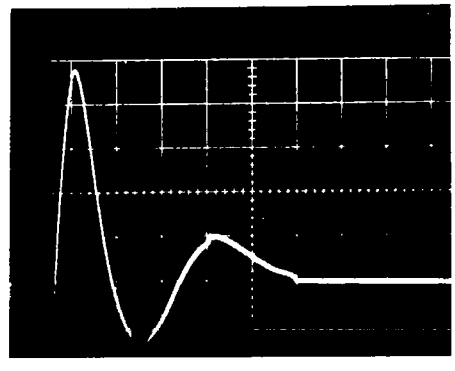

Fig. No. 5
Date: 9/27/72
Time: 1600
Count: 194,900
VP: 2500V
Hor. Sw: 10 μs/cm
S/N: 15118
C: 28 μf

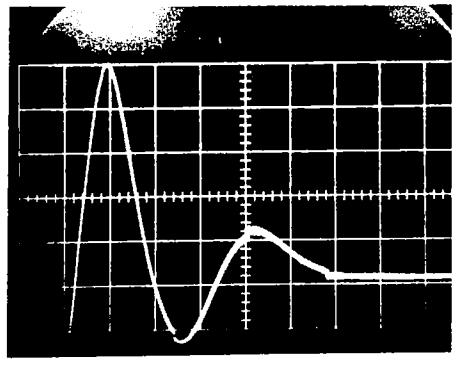

Fig. No. 6
Date: 9/27/72
Time: 1645
Count: 201,600
VP: 2300V
Hor. Sw: 10 μs/cm
S/N: 15118
C: 28 μf
V Reversal: 600V

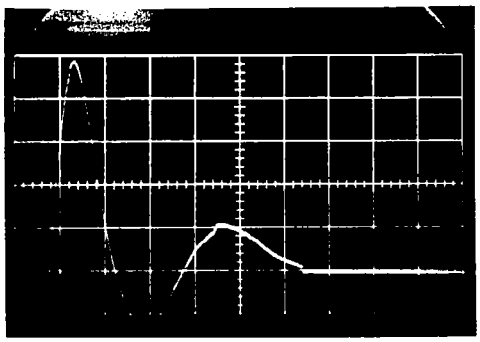

Fig. No. 7
Date: 9/28/72
Time: 0840
Count: 333,700
VP:
Hor. Sw: 10 μs/cm
S/N: 15118
C: 28μf
V Reversal: 600V

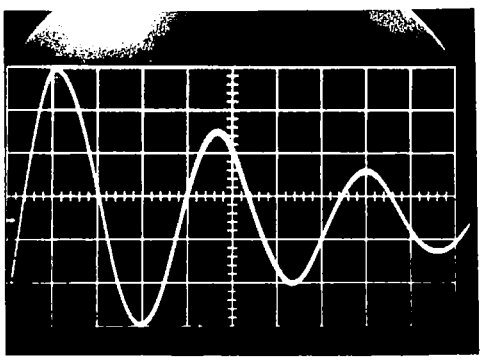

Fig. No. 8
Date: 9/28/72
Time: 1020
Count: 334,991
VP:
Hor. Sw: 2 μs/cm
S/N: 15118
C: 28μf
Parameter Test

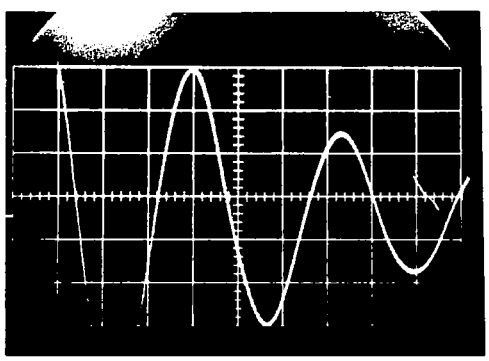

Fig. No. 9
Date: 9/28/72
Time: 1005
Count: 334,991
VP:
Hor. Sw: 2 μs/cm
S/N 15118
C: 28μf

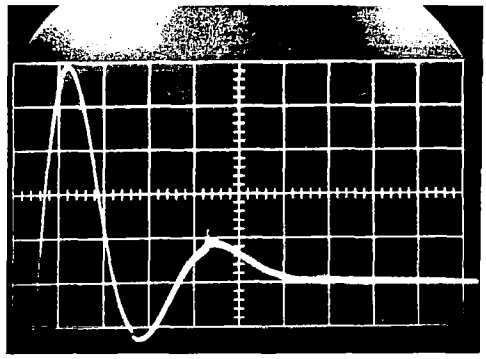

Fig. No.	10
Date:	9/28/72
Time:	1145
Count:	336,690
VP:	2450V
Hor. Sw:	10 μs/cm
S/N:	15118
C:	28μf
V Reversal:	700V

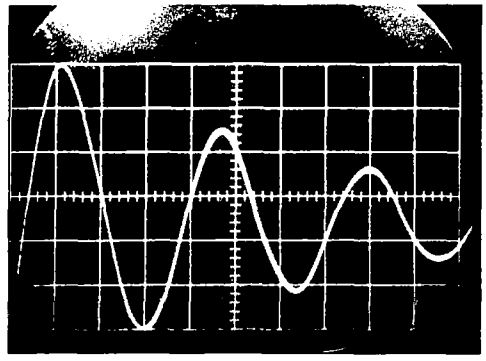

Fig. No.	11
Date:	9/28/72
Time:	1630
Count:	387,174
VP:	
Hor. Sw:	2 μs/cm
S/N:	15118
C:	28μf

Parameter Test

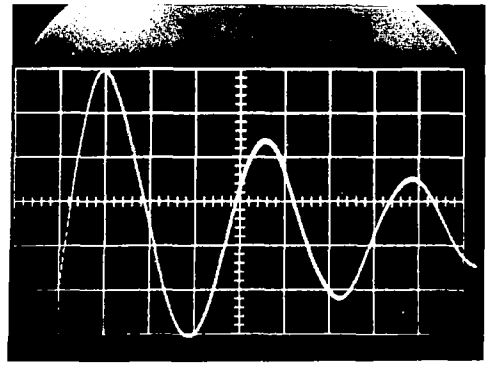

Fig. No.	12
Date:	9/29/72
Time:	1530
Count:	460,179
VP:	
Hor. Sw.	2 μs/cm
S/N:	15118
C:	28μf

Parameter Test

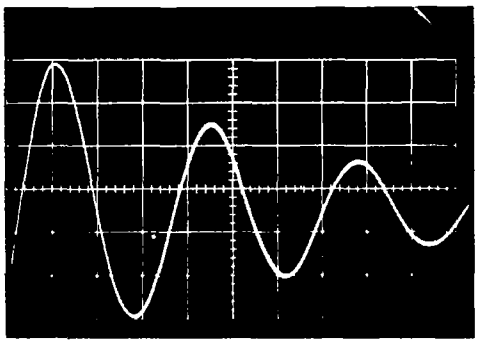

Fig. No. 13
Date: 10/02/72
Time: 1635
Count: 603,820
VP:
Hor. Sw: 2 μs/cm
S/N: 15118
C: 28μf
Parameter Test

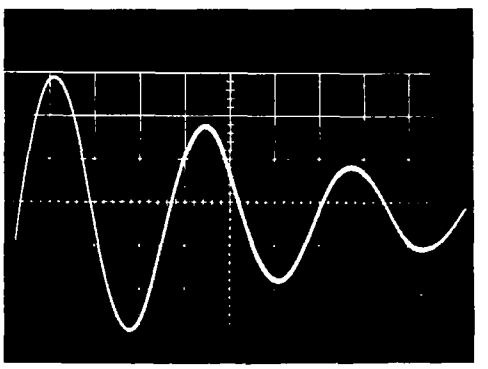

Fig. No. 14
Date: 10/04/72
Time:
Count: 1,405,065
VP: 2400V
Hor. Sw: 2 μs/cm
S/N: 15118
C: 28μf
Parameter Test

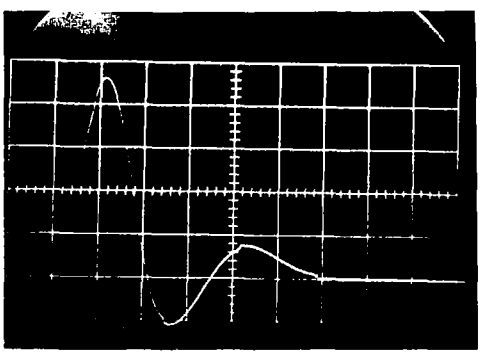

Fig. No. 15
Date: 10/03/72
Time: 1630
Count: 1,020,900
VP: 2500V
Hor. Sw: 10 μs/cm
S/N: 15118
C: 28μf

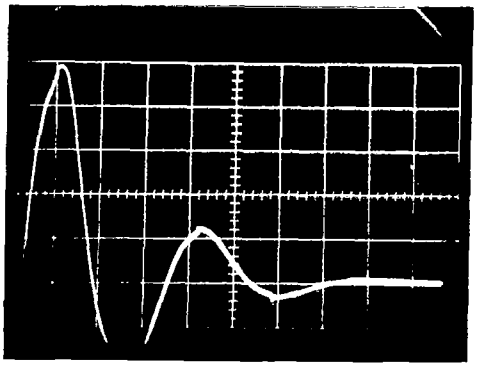

Fig. No.	16
Date:	10/04/72
Time:	0925
Count:	1,302,800
VP:	2400V
Hor. Sw:	10 μs/cm
S/N:	15118
C:	28μf
V Reversal:	760V

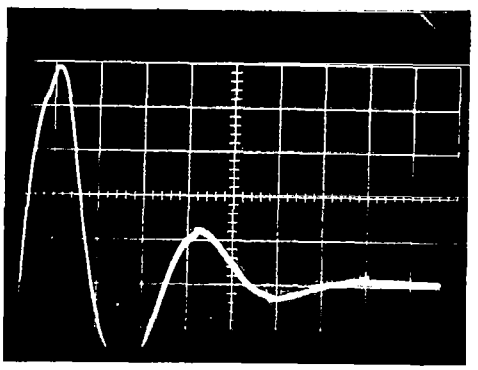

Fig. No.	17
Date:	10/04/72
Time:	1510
Count:	1,403,200
VP:	2400V
Hor. Sw:	10 μs/cm
S/N:	15118
C:	28μf

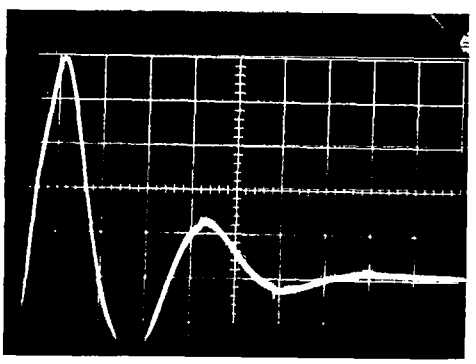

Fig. No.	18
Date:	10/04/72
Time:	1615
Count:	1,406,400
VP:	2400V
Hor. Sw:	10 μs/cm
S/N:	15118
C:	28μf

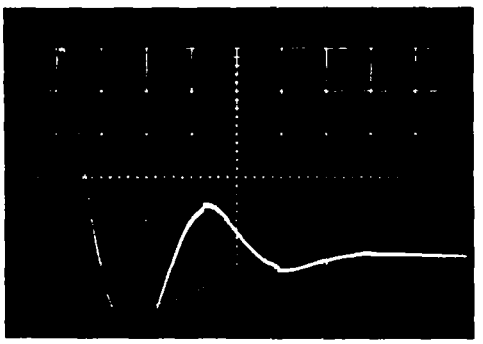

Fig. No.	19
Date:	10/05/72
Time:	1600
Count:	1,825,790
VP:	
Hor. Sw:	10 μs/cm
S/N:	15118
C:	28μf
V Reversal:	700V

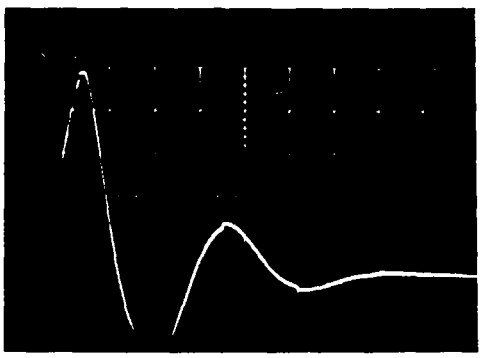

Fig. No.	20
Date:	10/06/72
Time:	1500
Count:	2,191,200
VP:	2400V
Hor. Sw:	10 μs/cm
S/N:	15118
C:	28μf

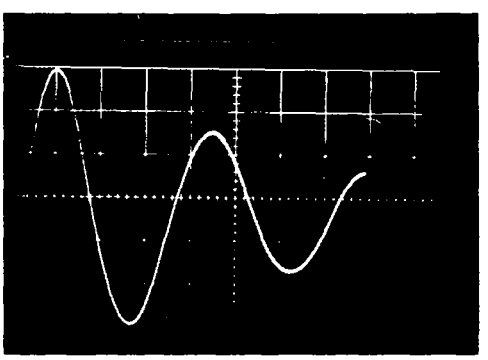

Fig. No.	21
Date:	10/06/72
Time:	1620
Count:	2,191,200
VP:	
Hor. Sw:	
S/N:	15118
C:	28μf

Parameter Test

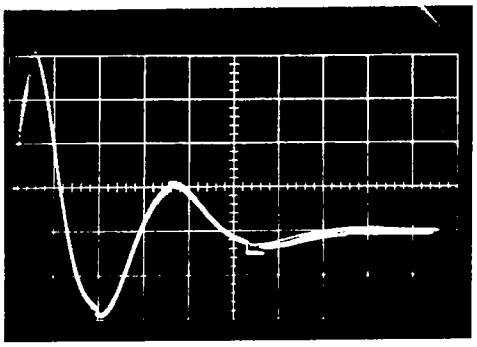

Fig. No.	22
Date:	10/09/72
Time:	
Count:	3,435,900
VP:	
Hor. Sw:	10 μs/cm
S/N:	15118
C:	28 μf
V Reversal:	700 V

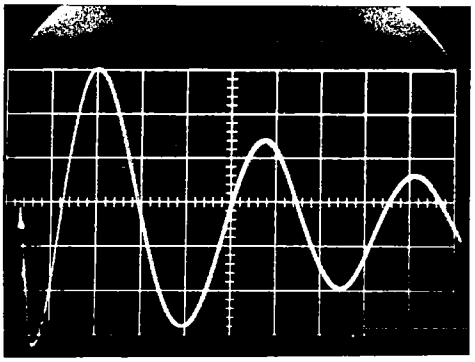

Fig. No.	23
Date:	10/09/72
Time:	
Count:	3,435,900
VP:	2400V
Hor. Sw:	2 μs/cm
S/N:	15118
C:	28 μf
Parameter Test	

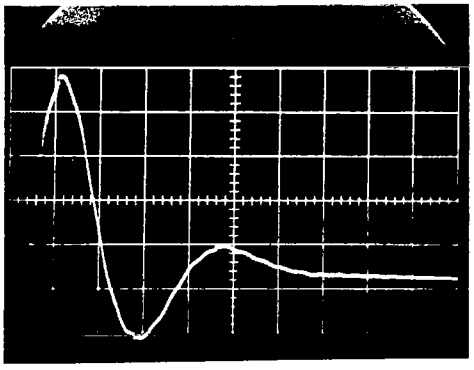

Fig. No.	24
Date:	10/10/72
Time:	1645
Count:	3,758,300
VP:	
Hor. Sw:	
S/N:	15118
C:	28 μf

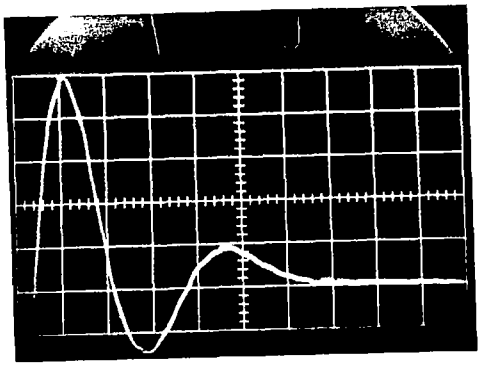

Fig. No.	25
Date:	10/11/72
Time:	1500
Count:	4,121,358
VP:	2400 V
Hor. Sw:	
S/N:	15118
C:	28 μf

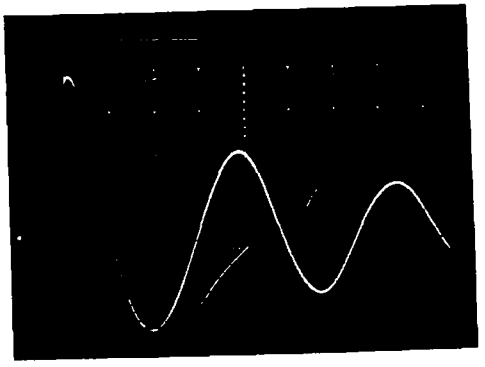

Fig. No.	26
Date:	10/11/72
Time:	1500
Count:	4,121,358
VP:	
Hor. Sw:	2 μs/cm
S/N:	15118
C:	28 μf

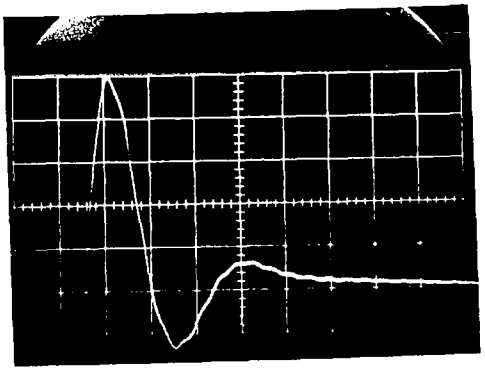

Fig. No.	27
Date:	10/12/72
Time:	
Count:	4,128,549
VP:	
Hor. Sw:	5 μs/cm
S/N:	15118
C:	28 μf

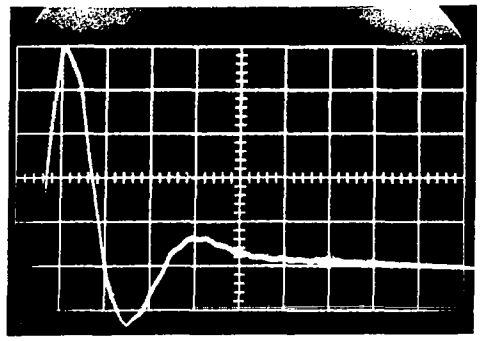

Fig. No. 28
Date: 10/13/72
Time: 0900
Count: 4,251,000
VP:
Hor. Sw: 5 μs/cm
S/N: 15118
C: 28μf
V-Reversal

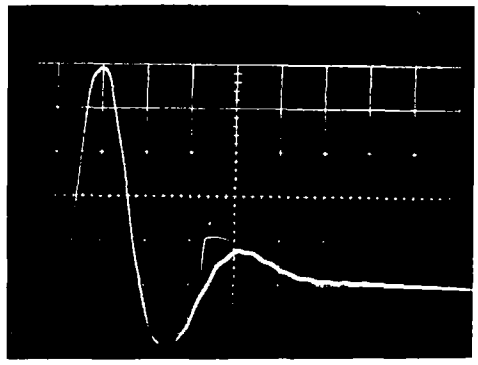

Fig. No. 29
Date: 10/16/72
Time: 1330
Count: 4,355,000
VP: 2400 V
Hor. Sw: 5 μs/cm
S/N: 15118
C: 28μf
New Spark Gap

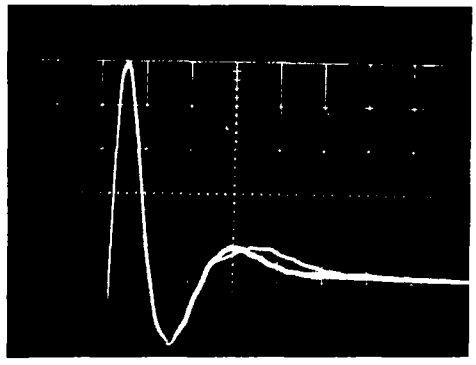

Fig. No. 30
Date: 10/17/72
Time: 0850
Count: 4,651,382
VP: 2400V
Hor. Sw: 5 μs/cm
S/N: 15118
C: 28μf

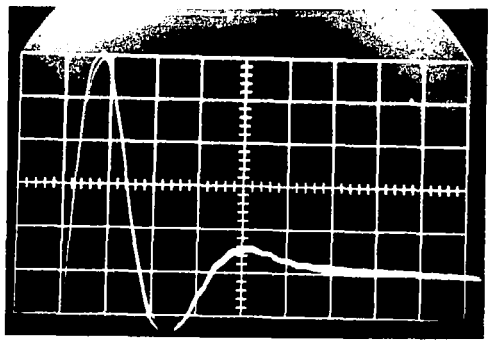

Fig. No. 31
Date: 10/18/72
Time:
Count: 4,882,850
VP: 2500 V
Hor. Sw: 5 μs/cm
S/N: 15118
C: 28μf

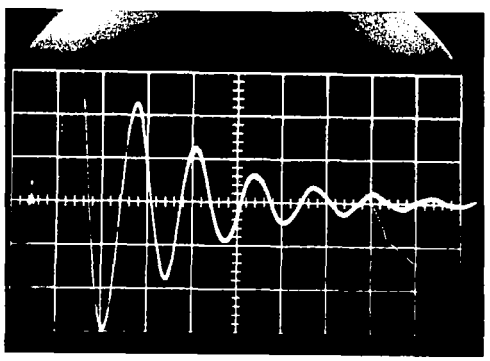

Fig. No. 32
Date: 10/18/72
Time:
Count: 4,915,166
VP:
Hor. Sw: 5 μs/cm
S/N: 15118
C: 28μf
Parameter Test

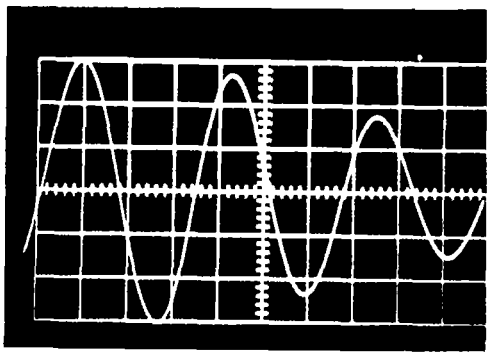

Fig. No. 33
Date: 12/21/72
Time:
Count:
VP: 2000 V
Hor. Sw: 2 μs/cm
S/N: 15117
C: 26.8μf
Engine Life Test

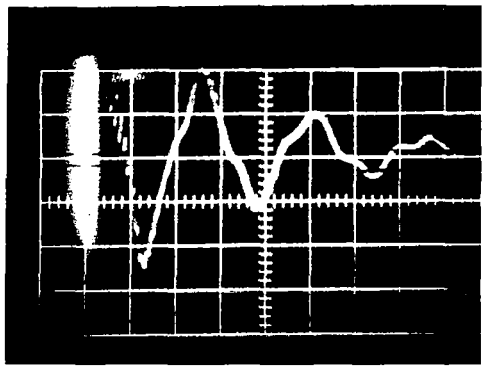

Fig. No.	34
Date:	2/14/73
Time:	
Count:	
VP:	2000 V
Hor. Sw:	2 μs/cm
S/N:	15117
C:	26.8μf

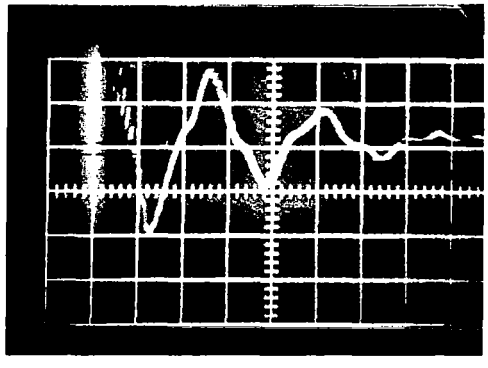

Fig. No.	35
Date:	2/14/73
Time:	
Count:	
VP:	1700 V
Hor. Sw:	2 μs/cm
S/N:	15117
C:	26.8μf

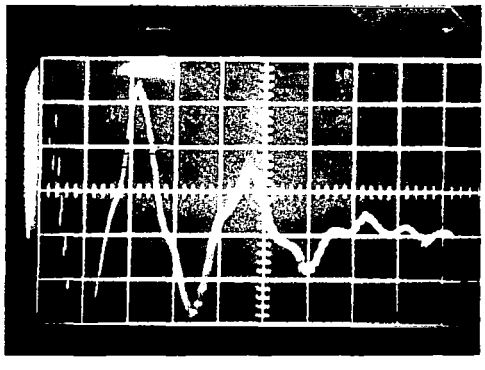

Fig. No.	36
Date:	2/14/73
Time:	
Count:	59,463
VP:	1700 V
Hor. Sw:	2 μs/cm
S/N:	15117
C:	26.8μf

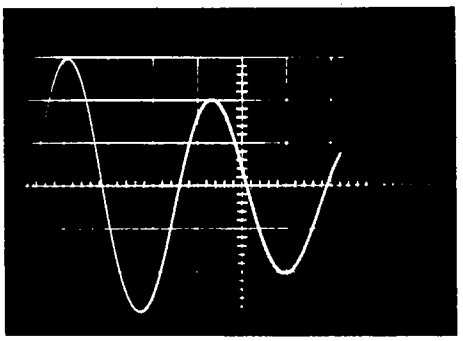

Fig. No. 37
Date: 3/01/73
Time:
Count:
VP: 1800 V
Hor. Sw: 2 μs/cm
S/N: 15121
C: 28.0 μf
Parameter Test

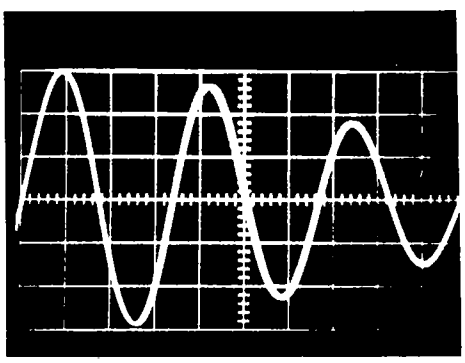

Fig. No. 38
Date: 3/01/73
Time:
Count:
VP: 2000 V
Hor. Sw: 2 μs/cm
S/N: 15117
C: 26.8 μf
Post Test

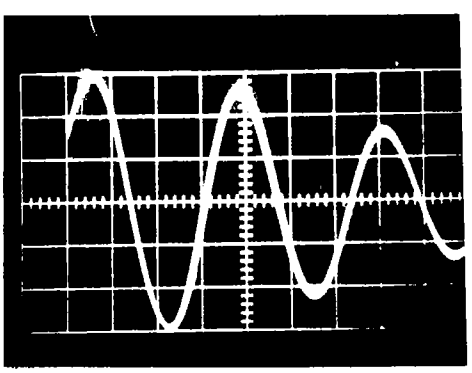

Fig. No. 39
Date: 3/05/73
Time:
Count:
VP: 1800 V
Hor. Sw: 2 μs/cm
S/N: 15122
C: 28.2 μf

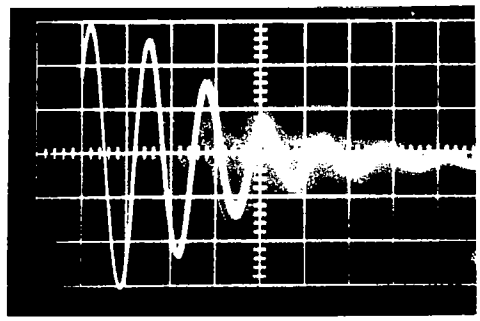

Fig. No. 40
Date: 3/05/73
Time:
Count:
VP: 1800 V
Hor. Sw: 5 μs/cm
S/N: 15122
C: 28.2 μf

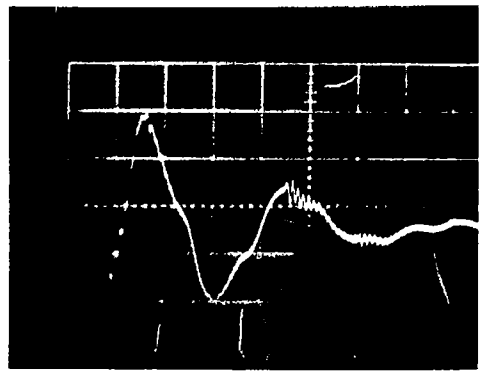

Fig. No. 41
Date: 4/18/73
Time:
Count:
VP: 1000 V
Hor. Sw: 2 μs/cm
S/N: 15122
C: 28.2 μf
System Test

TABLE D-1 MAIN CAPACITOR PARAMETERS

FIG NO.	INPUT DATA: AMP. RATIO	INPUT DATA: PERIOD U-SEC	INPUT DATA: VOLTS	CALCULATED VALUES: L U-HEN	CALCULATED VALUES: R M-OHM	CALCULATED VALUES: I K-AMP	CALCULATED VALUES: T U-SEC
1	7.15	32.00	2500.	.9264	113.9	8.41	8.000
2	4.80	32.00	2500.	.9264	90.3	9.29	8.000
3	6.00	32.00	2500.	.9264	103.7	8.78	8.000
4	5.30	32.00	2500.	.9264	96.6	9.06	8.000
5	4.80	30.00	2500.	.8142	85.1	9.90	7.500
6	4.35	32.00	2300.	.9264	85.1	8.76	8.000
7	4.80	32.00	2300.	.9264	90.8	8.54	8.000
8	1.43	7.00	10.	.0443	4.5	0.23	1.750
9	2.00	6.80	10.	.0413	8.5	0.22	1.700
10	6.00	32.00	2450.	.9264	103.7	8.61	8.000
11	2.00	7.40	10.	.0495	9.3	0.20	1.850
12	2.14	7.00	10.	.0443	9.6	0.21	1.750
13	1.80	7.20	10.	.0469	7.7	0.21	1.800
14	1.60	7.00	10.	.0443	6.0	0.22	1.750
15	5.75	31.00	2500.	.3694	93.1	9.16	7.750
16	4.10	32.00	2400.	.9264	81.7	9.27	8.000
17	4.10	32.00	2400.	.9264	81.7	9.27	8.000
18	3.70	32.00	2400.	.9264	75.7	9.51	8.000
19	3.30	32.00	2400.	.9264	77.3	9.45	8.000
20	3.50	32.00	2400.	.9264	72.5	9.65	8.000
21	2.00	7.00	10.	.0443	8.3	0.21	1.750
22	4.20	32.00	2400.	.9264	83.1	9.22	8.000
23	2.14	7.40	10.	.0495	10.2	0.20	1.850
24	5.90	15.20	2400.	.2090	48.3	17.32	3.800
25	5.55	15.40	2400.	.2145	47.3	17.36	3.850
26	1.67	7.20	10.	.0469	6.7	0.21	1.800
27	3.35	15.00	2400.	.2035	57.6	16.56	3.750
28	3.35	15.00	2400.	.2035	57.6	16.56	3.750
29	4.10	16.00	2400.	.2316	52.3	16.79	4.000
30	3.35	15.00	2400.	.2035	57.6	16.56	3.750
31	3.35	15.00	2500.	.2035	57.6	17.25	3.750
32	1.77	6.50	10.	.0332	6.7	0.23	1.625
33	1.11	7.60	10.	.0394	1.2	0.26	1.650
34	2.00	5.00	2000.	.0226	6.3	59.13	1.250
35	2.12	5.00	1700.	.0226	6.3	49.57	1.250
36	2.34	5.00	1700.	.0226	7.7	44.36	1.250
37	1.50	6.80	10.	.0413	5.0	0.23	1.700
38	1.40	6.40	10.	.0371	3.9	0.25	1.600
39	1.60	6.00	10.	.0326	5.1	0.26	1.500
40	1.55	6.00	10.	.0326	4.3	0.26	1.500
41	3.00	6.00	1000.	.0326	11.9	22.23	1.500

Where: L= Inductance in μhen (microhenries)

R= Resistance in m ohms (milliohms)

I= Peak current in K amps (kiloamperes)

T= Discharge time in μsec (microseconds)

APPENDIX E

ENGINE TEST DATA SHEETS

The following charts are in the chronological sequence of testing and present the principle test parameters as reduced from the analogue recorder traces.

DATE: 25 JAN 73

CLOCK TIME	Cum Run Time (min)	f	Thrust				Temp		Main Cap Volts	Comments
			Div mm	θ deg	Δθ deg	F μ lb_f	Div mm	°C	°F	V_m	
1015	0:00	1	Thrust not Recorded				6.5	26		0	Trigger Check V_t = 1800
1032	:17	0.1								800	Pintle (neg)
1038	:23	0.1	18 Pulses on Main				7.0	26.5		1500	
1050	:35						7.0			0	Shutdown Main Cap not Firing
1607	:00	0.1	No Thrust Record Pintle (neg)				7.0	26.5		1500	Restart V_t = 1800 missing on Main Cap
1618	:11	1.0					7.0	26.5		2000	Discharge
1623	:16	1.0					8.0	27.5		↓	Lower Charge Resistor
1624	:17	1.0					8.0	27.5			
1625	:18	0.1					8.5	28.0			Still Missing
1633	:26						7.5	24.0			Shutdown

DATE: 26 JAN 73

Clock Time	Cum Run Time (min)	f Hz	Thrust Div mm	Thrust θ deg	Thrust Δθ deg	Thrust F μ lb_f	Temp #1 Div mm	Temp #1 °C	Temp #1 °F	Main Cap Volts v	Comments
0930	0:00	1.0	Pintle (neg)				6.5	26		2000	V_f = 1800 start
0935	0:05	1.0	~ 8 Pulses on Main								Shut Down
0936	0:05	1.0	Pintle (POS)				7.0	26.5		1500	V_f = 1800 Restart
1000	0:29	1.0					24.	42.7		↓	
1023	0:52	1.0					34.0 44.5	56.8 78.2	134 170 F	↓	Press Rise; Sharp Peak in Temp Shutdown
1030	0:52	1.0					25.5	45		800	Restart
1107	1:29	↓					28.0	48.2		↓	
1136	1:58						33.0	55.2			
1141	2:03	↓					32.	53.8		↓	Shutdown
1310	2:03	1					25.	44.3		800	Restart
1401	2:54	↓					30.5	51.5		↓	
1431	3:24						32.	53.8	130		
1501	3:54						34	56.8		↓	Shutdown, Press Rise
1517	3:54						26.	45.4		↓	Restart
1549	4:26						35	58.3	137		
1554	4:31	↓					31	52.3	127	↓	Unexplained Drop in Temp on R/C #1; Not on T/C #4
1617	4:53	1					32	53.8	130	800	
1619	4:55	5								↓	
1715	5:51	↓					44.5	78.2	170	1000	
1725	6:01						47	88.	190	↓	
1730	6:06	↓					41.5	70.5		↓	Shutdown

DATE: 13 FEB. 73

Clock Time	Cum Run Time (min)	f Hz	Thrust Div mm	Thrust θ deg	Thrust Δθ deg	Thrust F μ lb_f	Temp Div mm	Temp °C	Temp °F	Main Cap Volts v	Comments
0900	0:00	1	10	.33	0		8.5	27.8		0	Trig Checkout V_t = 1800
0903	0:00									800	
1026	1:23		11.0	0.53	.20	12.3	17.0	36.			
1055	1:52		12.0	.78	.45	27.8	19.	38.			
1100	1:57										
1145	2:42		11.5	.67	.34	21.0	20.5	39.5			
1310	4:07		12.0	.78	.45	27.8	22.5	41.5			
1400	4:57		12.5	.90	.57	35.2	23.0	42.1			
1430	5:27		12.5	.90	.57	35.2	23.5	42.6			
1445	5:42		13.0	1.02	.69	42.6	24.0	43.2	109.7		
1522	6:19		13.5	1.12	.79	48.7	23.5	42.6			Shutdown
1551	6:19		12.5				20.	38.8			
1853			11.0	.53			11.5	30.7			
1853			Opened Chamber Pendulum @ +0.5° On Scale								

DATE: 14 FEB 73

Clock Time	Cum Run Time (min)	f	THRUST				TEMP			Main Cap Volts v	Comments
		Hz	Div mm	θ deg	Δθ deg	F μ lb_f	Div mm	°C	°F		
0845	:00	1	13.5	1.15			8.0	27.4		0	
0847	:00	1	13.5				8.0	27.4		1100	Trig = 1800 Checkout
0925	:38	1	↓				16.	35.0		1100	
0942	:55	1	↓				18.5	37.4		1400	
0955	1:08	1	14.0	1.25	0.10		23.0	42.2		1400	
1034	1:47	1	15.	1.50	0.35		28.5	48.7	120	1700	Double Pulses Noted
1049	2:03	1	15.5	1.60	0.45		31.	52.2	125	↓	
1100	2:14	1	14.5				32.5	54.5		↓	
1109	2:23	1	15.0	1.50	0.35		34.0	56.7		2000	
1111	2:25	1	150	1.5	0.35		36.0	60°	140	↓	Thrust; Running Free (5-10 Hz est)
1116	2:30	1	27.5	5.3	3.8	234	36.	60°		↓	Steady
			Swing up to 33.5 then down								
1117	2:31	1	23.0	3.67	7.17		36.	60		↓	
			Down to 16 then up (1.75)								
1118	2:31	1	24.5	4.18			34.5	57.7		↓	
1119	2:31	1	24.0	4.00	0		34.	56.7		800	Restart False Trig
1135	2:47	1	24.		0		32	53.7		900	
1150	3:02	1	24.		0	0	31	52.3		1100	
1205	3:17	1	25.	4.32	0.32	19.7	32	53.7		1300	
1207	3:19	1	25.		0.32	19.7	32	53.7		↓	False Trig Thrust OSC 25-28 Div Shut down
1210	3:22	1	28	5.53	1.53	94.3	34	56.7		↓	
1220	3:22	1	24.	4.00	0	0	29	49.6		1300	Restart Change Chg R From 1K to 16K no F.T.
1221	3:23	1	26	4.70	0.70	43.2	30.5	51.2		1100	
1230	3:32	1	25.5	4.50	0.50	30.8	31.5	53.		1200	
										↓	Change R_C to 10K
1231	3:33	1	25.5	4.50	0.50	30.8	32.	53.7		↓	Shutdown
1232	3:23	1	24.0	4.00	0	0	31	52.3		1200	Restart
1233	3:24	1	26.0	4.70	0.7	43.2	32	53.7		↓	
1248	3:39	1	26.0	4.70	0.7	43.2	32	↓		1300	
1250	3:41	1	26.5	4.88	0.88	54.3	32	↓		↓	Shutdown
1300	3:41	1	25.0	4.32	0		30	51.0		1300	Restart
1308	3:49	1	26.	4.70	0.38	23.4	31.5	53.0		1400	

DATE: 14 FEB 73 (cont'd)

Clock Time	Cum Run Time (min)	f Hz	Thrust Div mm	Thrust θ deg	Thrust Δθ deg	Thrust F μ lb_f	Div mm	Temp °C	Temp °F	Main Cap Volts v	Comments
1315	3:56	1	26.5	4.90	0.58	35.8	32.5	54.6		1500	
1325	4:06		26.5				33.5	54.6		1600	
1334	4:15		26.5				35.0	58.2		1400	
1345	4:26		26.5	4.90	0.58	35.8	35.0	58.2		2000	False Trig
1348	3:29		27.5	5.3	.98	60.6	36	60		1400	Reduced MCV to Control Temp.
1434	4:15		28.0	5.52	1.20	74.1	36.5	61			Thrust Trace Incr. Rapidly
1435	4:16		30.0	6.52	2.20	135.8	36.5	61			
1436	4:17		45.	16.3	11.98	740.	36.5	61			
1438	4:19		42.	13.7	9.38	579.	36.5	61			
1442	4:23		38.5	12.05	7.73	477.	37.0	61.5		1400	
1450	4:31		39.5	12.4	8.08	498.	37.0	61.5		1100	Reduced MCV to Control Control Temp
1451	4:32		36.0	10.45	6.13	378.	36.5	61.0			Drop in Thrust
1452	4:33		29.0	6.0	1.68	103.8	36.0	60			Sharp Drop in Thrust
1500	4:41		31.5	7.5	3.18	196.	36.	60			
1505	4:46		34.0	9.1	4.78	295.	36.0	60			
1510	4:51		32.0	7.85	3.53	218.	35.5	59.2			
1513	4:54		27.5	5.3	0.98	60.6	35.+	58.3			
1518	4:59		25.5	4.50	0.18	11.1	35.0	58.3		1100	
1530	5:11		25.0	4.32	0.0	0	35.0	58.3		1300	
1550	5:31		25.0	4.32	0.0	0	36.0	60		1400	
1610	5:51		25.0	4.32	0.0	0	37.5	62.2			
1616	5:57		25.5	4.50	0.18	11.1					Thrust Increasing
1619	6:00		26.0	4.70	0.38	23.4					Sharp INCR in Thrust
1620	6:01		45.0	16.3	11.98	740.					
1625	6:06		47.0	17.6	13.28	821.					
1630	6:11		45.5	16.65	12.33	762					
1634	6:15		44.5	15.97	11.65	720					
1635	6:16		26.0	4.70	0.38	23.4	37.5	62.2		1400	Drop off in Thrust
1637	6:18		26.0	4.70	0.38	23.4	38.0	63.2		0	Shutdown
1638	6:18	1	25.0	4.32	0.0	0	37.0	61.5			

Between 1638 & 1708 Thrust Curve Fluctuated from 25 to 38 mm: came to rest at 24.5 mm

After opening chamber thrust curve oscillated between 20mm & 25mm with Pendulum steady at +3.5° on scale (22.5mm = +3.5°)

DATE: 26 FEB 73

Clock Time	Cum Run Time (min)	f	Thrust				Temp			Main Cap Volts v	Comments
		Hz	Div mm	θ deg	Δθ deg	F μlb$_f$	Div mm	°C	°F		
1015	----	----	13.0	3.1	0	----	6.	25.5			
1016	:00	1	13.0	3.1	0	0	6	25.5		0	V_t = 1800 Trigger Check
1018	:00	1	13.0	3.1	0	0	6		8	800	Firing OK
1019	:01	1	14.	3.25	0.15		6.5	26		800	
1025	:07	1	13	3.1	0		8.5	28		1000	
1030	:12	1	13+	3.1	0		10.5	29.7		1200	
1033	:15	1	13+	3.1	0		12.0	31.2		1200/0	Shut down to change charging resistor
1035	:15	5	16	3.7	0.6	35.7	19.0	38.0		1200	
1036	:16	5	18.5	4.25	1.15	68.5	17.5	36.5		1200	
1041	:21	5	19.5	4.70	1.60	95.4	26.5	46.2		1200/0	Shut down to change charging resistor
1047	:21	1	15.0	3.5	0.4	23.8	20.	39.0		1200	Restart
1047+		1.	21.0	5.5	2.4	143.0	23.	42.1		↓	
1055	:29	1.	20.5	5.4	2.3	137.0	34.	51.7			
1103	:37	1.	20.5	5.4	2.3	137.0	38.5	64.2			
1103:40	:37:40	1./0	14.0	3.25	0.15	8.9	34.5	52.1		↓	Stopper firing shutdown
1135			13.5	3.20	0.1						Check torsion pendulum

+ Post Test Check shows IC in Logic Box output was "wiped out"

DATE: 28 FEB 73

Clock Time	Cum Run Time (min)	f	Thrust				Temp			Main Cap Volts	Comments
		Hz	Div mm	θ deg	Δθ deg	F μlb_f	Div mm	°C	°F	v	
0840		1	13.0	0.6			5.5	25	77	0	Trigger Checkout X_t = 1800v
0847	:00	1	13.0				5.5	25		800	Start
0850	:03	5	13.0	0.6			8.5	27.8		800	Change "f"
0900	:13	↓	13.4	0.8	0.2	11.8	25.0	44.5		1000	
0905	:18	↓	13.7	1.0	0.4	24.0	28.5	48.8		1200	
0911	:24	5	15.5	1.9	1.3	78.0	34.0	56.6		1400	Free Triggering, Chnge "f" Shutdown
			Thrust Trace Oscillating								
0915	:27	1	11.5				33.	55.3		500	Restart
0916	:28	↓	35	12.4	11.8	708				500	
0917	:29	↓	25.2	4.75	4.15	248				500	
0920	:32	↓	24.7	4.50	3.90	234	28.5	48.8		800	
0921	:33	↓	24.5	4.40	3.80	228	28.5	48.8		1100	Free Triggering
0922	:34	↓	23	3.9	3.30	197	29.0	49.5		800	N.F.T.
0926	:38	↓	23	3.9	3.30	197	27.5	47.5		0	Shutdown to Change Charge Resistor
0927	:38	↓	22.5	3.75	3.15	189	27.0	46.8		1200	Restart
0930	:41	↓	22.5	3.75	3.15		27.5	47.5		1500	
0933	:44	↓	22.5	375	3.15		28.5	48.8		1000	
0938	:49	↓	22.5	3.75	3.15	189	29.5	49.7		0	Shutdown
0955	:49	↓	20.	3.30	2.70	162	23.5	42.7			Restart
1001	:55	1	21.	3.50	2.90	173^+	27.0	46.8		0	Shutdown
1011			19.5	3.2							
1021			18.0	2.8							
1145			17.0	2.45							
1220			15.0	1.6							Chamber Door Opened

No Detectable Problem with torsion balance on visual inspection; after door was opened Trace dropped to 13^+mm

DATE: 28 FEB 73 (cont'd)

Clock Time	Cum Run Time (min)	f Hz	Div mm	Thrust θ deg	Δθ deg	F μlb_f	Div mm	Temp °C	Temp °F	Main Cap Volts v	Comments
1310 39	:00		10.	2.0			8.5	27.8			Start Pump Down
1540	:00		13^+	3.1			7.5	26.8			Trigger Checkout Pink Color to Spark
1545	:00	1	13^+	3.1	0		7.5	26.8		1000	
1555	:10	5	14	3.3	.2		12.5	31.7			
1556:20	:11:20	1	14.	↓			14.5	33.6			Shutdown to Change Chrging Resistor
1557:20	:12:20	1	14	↓			12.5	31.7			
1558	:12:40	5	15	3.50	.4		19.	38			
1606:40	:21:20	1	14.5	3.35	.25		17.	36			
1622	:36:40	1	14.	3.30	.20		11.	30			
1636	0:50:40	1	13.7	3.25	.15		10.5	29.7			Shutdown . Flashing All Over Engine Shorted

DATE: 2 MAR 73

Clock Time	Cum Run Time (min)	f Hz	Thrust Div mm	Thrust θ deg	Thrust Δθ deg	Thrust F µlb$_f$	Temp Div mm	Temp °C	Temp °F	Main Cap Volts v	Comments
1258	:00		15								
1308	:00	1	15.				6.5	26		0	Trigger Checkout All Work
1309	:06	1	8.5	1.0			6.5	26			
1316	:08	1	8.5	1.0			7.0	26.5		0	Shutdown; Reverse Polarity Pintle Neg
1318	:09	1	8.5	1.0			6.5	26.0		800	
1320	:11	5	9.5	1.4	.4	24.	8.5	27.8		800	
1327	:18	5	9.5	1.4	.4	24.	18.	37		1000	
1329	:20	5	10.5	1.75	.75	45.	20	38.9		↓	Started to Run Free Shutdown
1330	:21	5	8.5	1.0			20	38.9		↓	
1331	:21	5	8.5	1.0			17.5	36.5		1000	Restart: Polar Pintle Pos: Running Free
1334	:24	5	11.0	1.9	.9	54.	19.5	38.5		↓	
1335	:25	1	9.0	1.15	.15	9.	17.5	36.5		300	
1336	:26	↓	9.5	1.4	.4	24	18.0	37.		1000	
1338	:28		9.5	1.4	.4	24.	18.+			1200	
1340	:30		10.	1.55	.55	33.	19.	38.0		1400	
1344	:34		10.	1.55	.55	33	20.5	39.5		1600	False Pulsing
1345	:35		11.	1.9	.9	54.	21.5	40.5		1600	
1346	:36		15.5	3.15	2.15	129.	22.0	41.0		1600	
1346:10	:36:10		20.	4.30	3.30	198	21	40.		1600	Shutdown & Restart
1347	37.		7.	.35	-.65		20	38.9		1600	
1347:30	37:30		17.5	3.50	2.50	150.	22.5	41.6		1600	
1349	39		9.	1.15	.15	9	17	36.0		1600	
1351	41		10.5	1.75	.75	45	17	↓		800	
1352	42		11.	1.9	.90	54	17	↓		800	
1357	47		11.	1.9	.90	54	25	44.4		1000	
1404	51		11.5	2.1	1.10	66.	33	55.2	132	↓	
1405	52		12.	225	1.25	75.2	39	65°	149	↓	
1406:28	53:20	↓	18.5	3.8	2.8	168.					Lost Temp Trace Swings in Thrust Trace @ period of 2 min Low = 7 High = 18.5

DATE: 2 MAR 73 (cont'd)

Clock Time	Cum Run Time (min)	f Hz	Thrust Div mm	Thrust θ deg	Thrust Δθ deg	F μlb_f	F Div mm	Temp °C	Temp °F	Main Cap Volts v	Comments
1411	58		9.	1.15	.15						
1438	1:25		9	1.15	.15						
1443	1:30		9	1.15	.15						Reversed Polarity
1505	1:52		8.5	1.0							Shutdown

DATE: 7 MAR 73

Clock Time	Cum Run Time (min)	f Hz	Thrust Div mm	Thrust θ deg	Thrust Δθ deg	F μlb_f	Temp Div mm	Temp °C	Temp °F	Main Cap Volts v	Comments
0928	:00	1	9.0	+0.1			3.0	T/C not connected		0	Trig Chk Board A not firing TR Volt = 1800 Pintle is Positive
0932	:	1	8.5	-0.1			3.0			800	
0934	:04	1	8.5	-0.1			8.0	27.3		800	
0950	:20	1	9.0	+ 0.1			10.0	29.2		800	
0952	:22	1	9.				10.5	29.7		600	Time constant on main restricts chg voltage shut down to change resist
1003	:33	1	8.5	- 0.1			11.5	30.7		0	
1003:20	:33	1								800	Restart
1011	:40:40	5	9.0	+ 0.1	0	0	12.5	31.6		↓	
1015	44:40	↓	↓	↓	↓	↓	20.	38.8		↓	
1020			↓	↓	↓	↓	22.5	41.5		1000	
1025	54:40		9.0	+ 0.1	↓	↓	25.0	44.4		↓	
1035	1:04:40		11.0	+ 1.05	.95	57.	32.0	53.7		1100	
1040	1:09:40		12.+	1.50	1.40	84.	36.0	60.		↓	
1100	1:29:40		13.5	2.05	1.95	117.5	42.5	72.3			
1125	1:54:40		15.	2.55	2.45	147.0	46.5	85.7			
1142	2:11:40		18.	2.95	2.85	171.+	47.0	88.5			Running Wild
1143	2:12:40		18.	2.95	2.85	171+	48	>90		1100	Shutdown
1148	2:12:40		5.0	-2.4	-2.5		46.5	85.7		500	Restart False Triggering
1150	2:14:40	↓	6.0	-1.55			45.5	81.5			Shutdown Main
1154											Occasional Trig Flash Attempt restart. Main
1155											shows short @ 500V
1158			6.0	-1.55			44.0			0	Trig Voltage Off
1225	2:15	1	6.0				40				No visual spark from trig main running wild
1235	2:25	1	7.0	-.95			38.5			400	Change Charging "R"
1240	2:30	1	6.5	-1.30			38			400	
1245		1	7.5	.60			38			800	
1250		1	7.5				38+			1000	
1255	2:45	1	8.0	-.35			38+			1100	Spark @ Gallium Interface

DATE: 7 MAR 73 (cont'd)

Clock Time	Cum Run Time (min)	f Hz	Thrust Div mm	Thrust θ deg	Thrust Δθ deg	Thrust F μlb_f	Temp Div mm	Temp °C	Temp °F	Main Cap Volts v	Comments
1300	2:50	1	8.0				38+			1200	
1305	2:55	1	8.0				38.5			↓	Erratic Firing
1315	3:05	1/5/1	9.5	+3.5			38.5				Change to 5 Hz Back to 1 Hz
1323	3:13		8.0	-.35			38.5				Shutdown

DATE: 8 MAR 73

Clock Time	Cum Run Time (min)	f Hz	Thrust Div mm	Thrust θ deg	Thrust Δθ deg	Thrust F μlb_f	Temp Div mm	Temp °C	Temp °F	Main Cap Volts v	Comments
0950	0:00	1	10.0	+.60			8.0	27.3			Trigger chk board "A" out. Pintle is neg 200KΩ in trig chg circuit
0951	0:01		10.0							800	
0954	0:04		10.0	.60							Shutdown to change R_C in Main Cap Circuit
0955	0:04	5									Restart
1000	0:09	5	10.0	.60			10.	29.2			
1011	0:20	5	11.5	1.25	.65	40.	20.	38.8		1000	
1026	0:35		12.0	1.50	.90	55.5	26.5			1000	
1032	0:41		12.0	1.50	.90	55.5	26.5			1100	
1050	0:59		13.5	2.05	1.45	89.5	26.5				$T_{cap} \sim 124^{o}F$ Shutdown $T_C \sim 132^{o}F$ $P_C \sim 10^4$
1100	1:09		11.5	1.25	.65	40.	26.5				
			Dropped to 9.0 mm Steady State								
1139	1:09	5	9.0				26.5				Restart
1148	1:18		9.0								
			In between thrust @ 49 mm								
1310	1:18	5	9.	.15	0						Restart $T_C \approx 118^{o}F$ $42.7^{o}C$
1340	1:48	5	16	2.85	2.70	166^{+}					$T_C \approx 142^{o}F$ $61^{o}C$
1353	2:01		20	3.50	3.35	207					$T_C \approx 151^{o}F$ $66.5^{o}C$
1354	2:02		20	3.50	3.35	207					Shutdown: $P_C \sim 2 \times 10^{-4}$
1406			9.0	.15	0	0					$T_C \approx 146^{o}F$ $63.5^{o}C$

Engine Temp measurement after 1011 hrs are bad

Capacitor Temps are ok

DATE: 18 APR 73

Clock Time	Cum Run Time (min)	f	Thrust				Temp			Main Cap Volts	Comments
			Div mm	θ deg	Δθ deg	F μlb_f	Div mm	°C	°F	v	
1233	:00	1	17.5	0.5	0		27.5	26		0	V_t = 1800 B_{rd} #1 out Trigger Checkout
1234	:00	1								800	Start up $P_c = 9 \times 10^{-6}$
1240	:06	1	17.5	0.5	0		30.0	30.5		800	
1258	:24	1	18.5	0.8	0.3		31.0	32.		1000	
1334	1:00	1	19.0	0.9	0.4		33.5	36.5		1200	
1339	1:05	1	20.	1.2			34.0	37.5		1400	$P_c = 9 \times 10^{-6}$ Turned on cold
1345	1:11	1	19.5	1.1			35.0	39		1600	wall $P_c = 7 \times 10^{-6}$
1351	1:17	1	19.5	1.1			36.0	41		1800	
1400	1:26	5	18.5	0.8			37	43		1000	
1401	1:27	1	19.0	0.9			37	43		1000	
1405	1:31	1	17.5	0.5			36.5	42		↓	Turned on Engine Heater
1420	1:46	5	15.5	0.0	-0.5		40	50			Shutdown to Change Charge Resist. Restart
1435	2:01	5	15.5	0.0	-0.5		46.5	71		1200	$P_c = 3.8 \times 10^{-6}$
			Noise on All Instrumentation								
1500	2:26										Shutdown
			Gallium Blown out of Center Cavity (High Voltage Lead)								

DATE: 19 APR 73

Clock Time	Cum Run Time (min)	f Hz	Thrust Div mm	Thrust θ deg	Thrust Δθ deg	Thrust F μlb_f	Temp Div mm	Temp °C	Temp °F	Main Cap Volts v	Comments
1310	:00	1	20.0	.35	0		29.0	28.5		0	Trigger Check #1 & 3 out V_t = 1800 Startup
1311	:00		20.0				29.0	28.5		800	$P_c = 1 \times 10^{-5}$
1315	:04									1000	
1319	:08		20.5	.45	0.10		32.0	34.0		1200	
1320	:09									1400	
1322	:11									1600	
1325	:14									1700	
1326	:15						34.0	37.5		1700	Engine Heater on $P_c = 1 \times 10^{-5}$
1350	:39		22.0	9.9	.45	26.5	42.0	56.0		1700	Main Cap Temp ~ 61°C
1430	1:19		22.5	1.1	.65	38.3	48.5	80		1700	
1435	1:24		22.5	1.1	.65		48.5	80		1700	$P_c = 1 \times 10^{-5}$
1438	1:27		22.5	1.1	.65		48.5	80		1700	No change in settings Running at Half Rate
1450	1:39		21.5	0.80	.35	20.6	49.0	82		1700	Shut of Engine Heater
1515	2:04		22.0	0.9	.45	26.5	49.0	82		1700	No change: Rate Back to Normal
1521	2:10	5	21.5	0.8	.35	20.6	49.0	82		1000	Change V_c & f Shutdown to Change "R"
1522	2:10	5	21.5	0.8			49.0	82		1000	Restart
1527	2:15	1	22.0	0.9	.45	50.0	90°			1000	Main Cap Intermittent changed "f"
1531	2:19		22.0				50.0	90		1700	$P_c = 7 \times 10^{-6}$ Main Cap Temp > 80°C
1543	2:31		22.0				50.0	90		800	
1608	2:56		21.5				47.5°	75			Shutdown Main Cap Temp > 80°C

a) Gallium Frozen in Two Troughs @ 9 o'clock position of tray

b) Removed 2 temp leads to obtain 2 additional feed thrus for high voltage in Gallium Interface.

DATE: 20 APR 73

Clock Time	Cum Run Time (min)	f Hz	Thrust Div mm	θ deg	Δθ deg	F µlbf	Temp Div mm	°C	°F	Main Cap Volts v	Comments
1338	0:00	1	12.0	-2.2	0	∿	26.5	24.5			Trigger Ckout V_+ = 1800 #1 & 3 Trig Out
				Zero Position							
1339	0:00	1	12.5	-1.8	0	∿	26.5	24.5		800	Start Pintle Pos
1343	0:04	5	12.5	↓			27.0	25.0		1000	$P_c = 2 \times 10^{-5}$
1418	0:39	5	12.5	↓			43.0	58		1000	$P_c = 1 \times 10^{-5}$
1441	1:02	5	15.0	-1.2	.6	35.4	46.5	71		1000	
1450	1:11	5	15.0	-1.2	.6	35.4	47.5	75		1200	$P_c = 2 \times 10^{-5}$ Cap Temp = 75°C
1455	1:16	5	16.0	-0.8	1.0	59	48.5	80		1400	
1457	1:18	5	25	+1.8	3.6	212	49.5	85		↓	Cap Temp > 80°C Thrust Rising
1458	1:19	5	27.5	2.55	4.35	257				↓	$P_c = 2 \times 10^{-4}$
1500	1:21	1	32.0	4.85	5.65	333	49.5	85		400	1×10^{-4} False Triggering Varied
1508	1:29	1-	31.0	4.60	5.40	318	48.+	77.5		∿	Volt & freq. in this Interval
1515	1:36	5	31.0	4.60	5.40	318	49.0	82		1000	
1533	1:54	5	31.0	4.60	5.40	318	50.	90		1400	$P_c = 4 \times 10^{-6}$ Cap Temp > 90°C
1535	1:56	5	31.	4.60	5.40	318	50.	90		1400	
1538	1:59	5	31	4.60	5.40	318	50.	90			Shutdown Main Cap Appears to be shorted
1540			29	3.0	4.8		50.				Cap Temp ∿ 54.5°C
1710			29.5	3.1	4.9		35.	39.5			

Gallium had frozen in two troughs

Pendulum held at +3.° (Visual Inspection)

DATE: 7 MAY 73

Clock Time	Cum Run Time (min)	f Hz	Thrust Div mm	Thrust θ deg	Thrust Δθ deg	Thrust F̄ μlbf	Thrust Div mm	Temp °C	Temp °F	Main Cap Volts v	Comments
1720	:00	1	25.	-1.7	0	∿	27.	25		0	Trigger Checkout #1 out V_t = 1700
1721	:00		25	-1.7	0	∿	27	25		800	Startup
1730	:09						28.5	27.5		1000	
1735	:14						29.5	29.5		1200	
1800	:39						32.5			1400	
1812	:51		24.0	-2.2			36.	41		1600	
1820	:59		24.5	-1.9			38.5	46.5		1700	
1835	1:14	↓	25.0	-1.7			42.+	55.5		2000	$P_c = 1 \times 10^{-5}$
1838	1:17	5	25.0	-1.7			43.	59		1600	Thrust Increasing P_c Incr
1840	1:19	5/1	47.5	23.9	25.6	1510	49	82		800	$P_c = 1 \times 10^{-4}$ Engine quit then re-started when rate dropped to 1 Hz
1843	1:22		42.	11.5	13.2	779	45.5	67		800	Cap Temp - 52°C
1845	1:24		42	11.5	13.2	779	44.5	63		900	$P_c = 4 \times 10^{-5}$
1849	1:28		41+	10.3	12.0	708	44.	61.5		1200	$P_c = 2 \times 10^{-5}$
1855	1:34		41.0	9.9	11.6	685	44.5	63		600	False Triggering $P_c = 9 \times 10^{-5}$
1858	1:37		40.5	9.2	10.9	643	44.	61.5		600	Turned on cold wall
1905	1:44	↓	40.	8.3	10.0	590	42.5	57		800	Cap Temp = 52°C
1908	1:47	1/5/1	40	8.3	10.0	590	42.	55.5		1000	Incr pulse rate. False trig; decr pulse rate
1912	1:51	1	40	8.3	10.0	590	44.5	63		1000	P_c going crazy Shutdown
1913	1:51		39.5	7.5	9.2		44.5	63			
1917	1:51		39.5				42.5	57		500	Restart: False Trig Gallium seems Frozen
1922	1:56		↓	↓			42.5	57			Shutdown
1925	1:56		↓	↓			42.5	57		400	Restart: False Trig
1930	2:01	↓	38.5	5.9			42.5	57			Shutdown Power to Gallium Htr Incr
2016			36	3.0							Shift in Thrust Trace

TYPICAL CALIBRATION CURVE
THERMISTOR No 1.
INJECTION RING TEMPERATURE

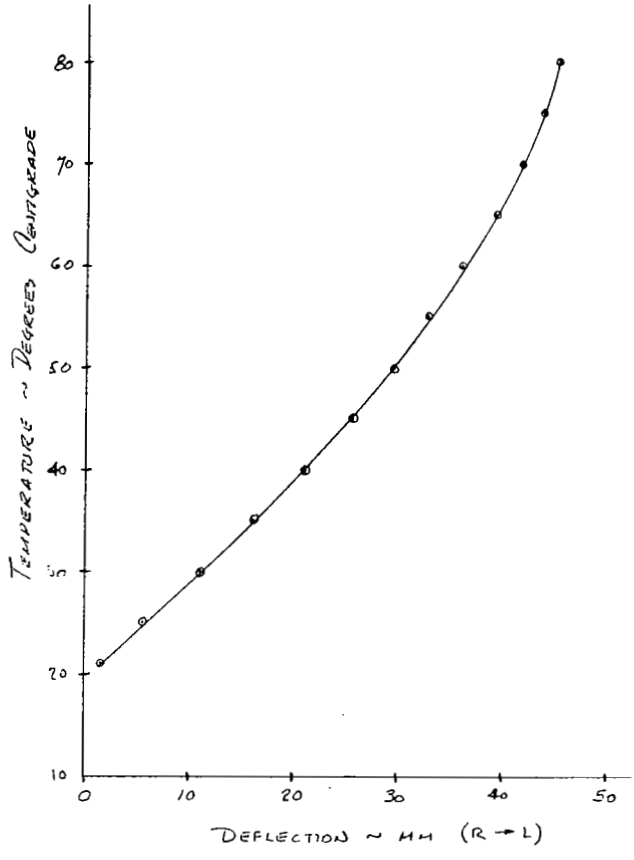

FIGURE E1 - INJECTOR RING TEMPERATURE CALIBRATION

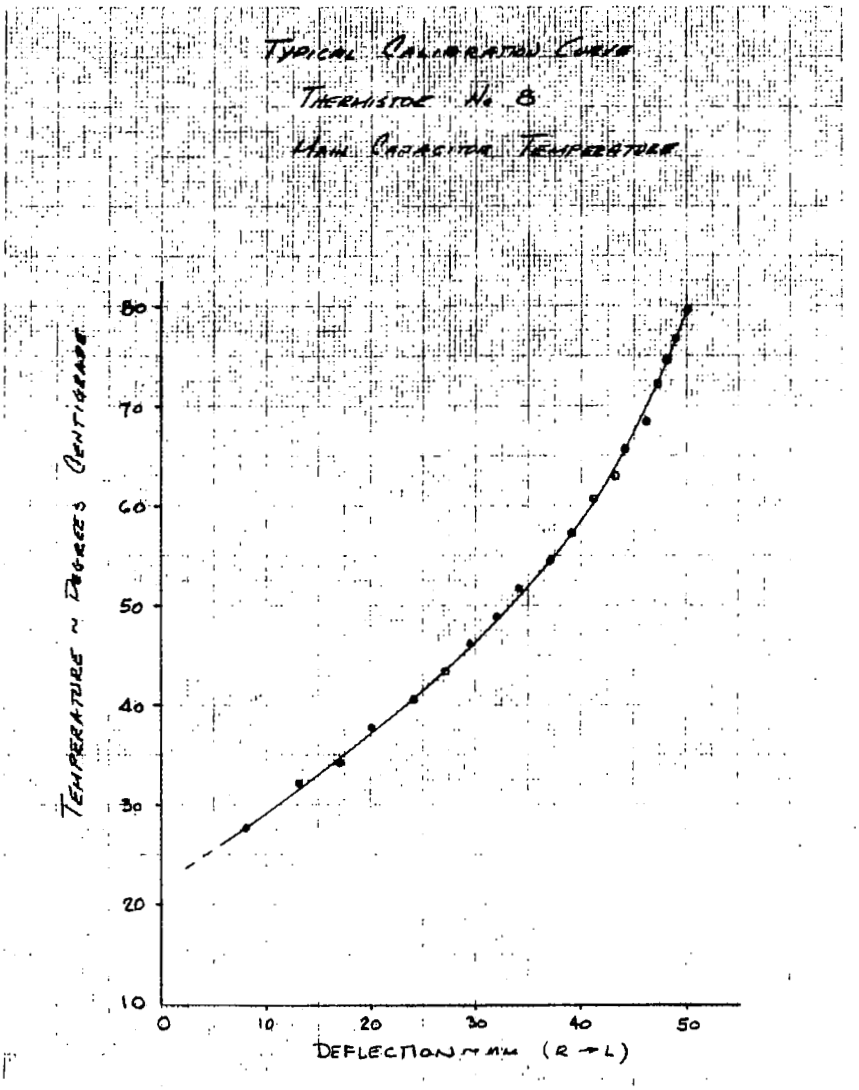

FIGURE F-2 - CAPACITOR TEMPERATURE CALIBRATION

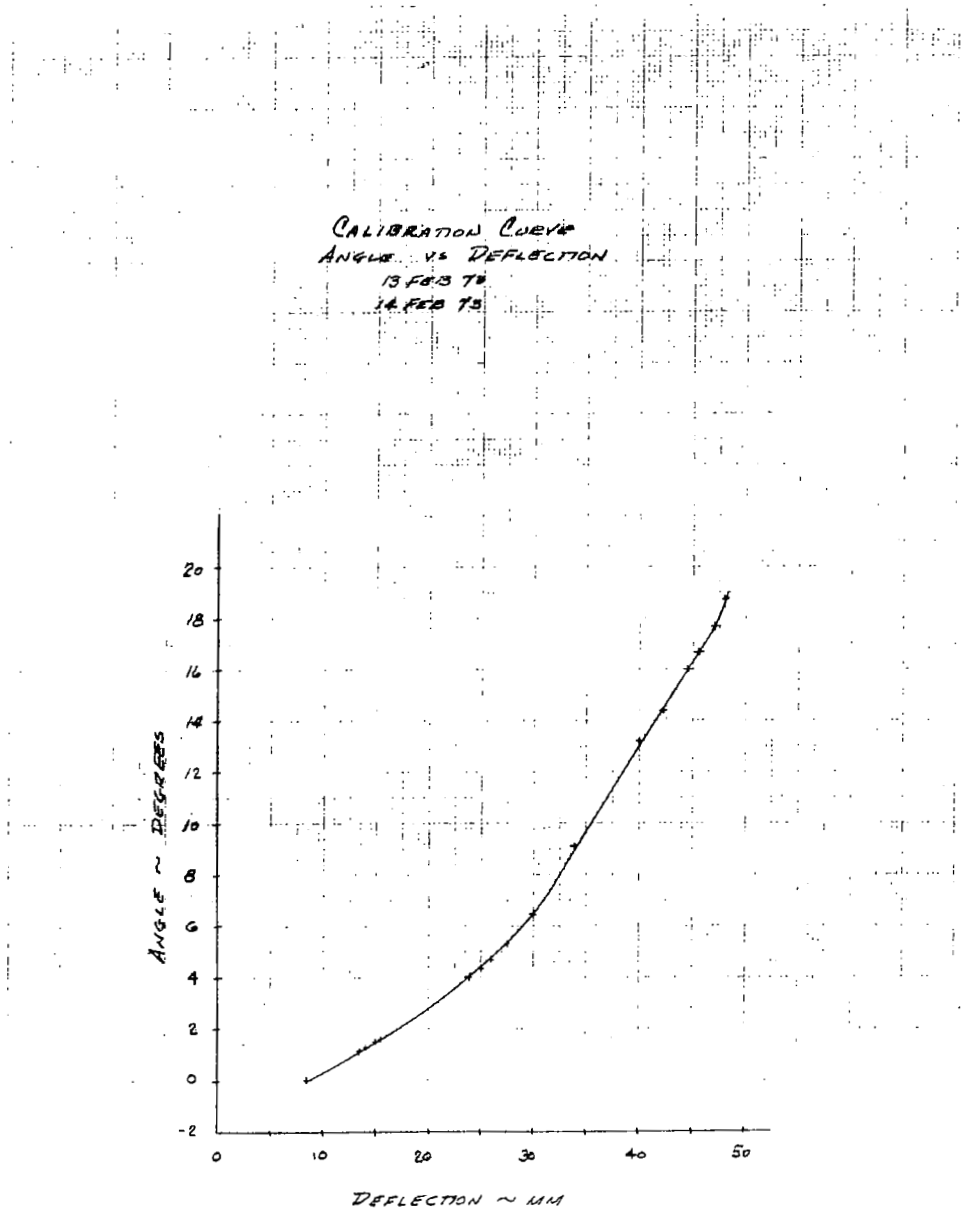

FIGURE E-3 - ANGLE vs RECORDER DEFLECTION

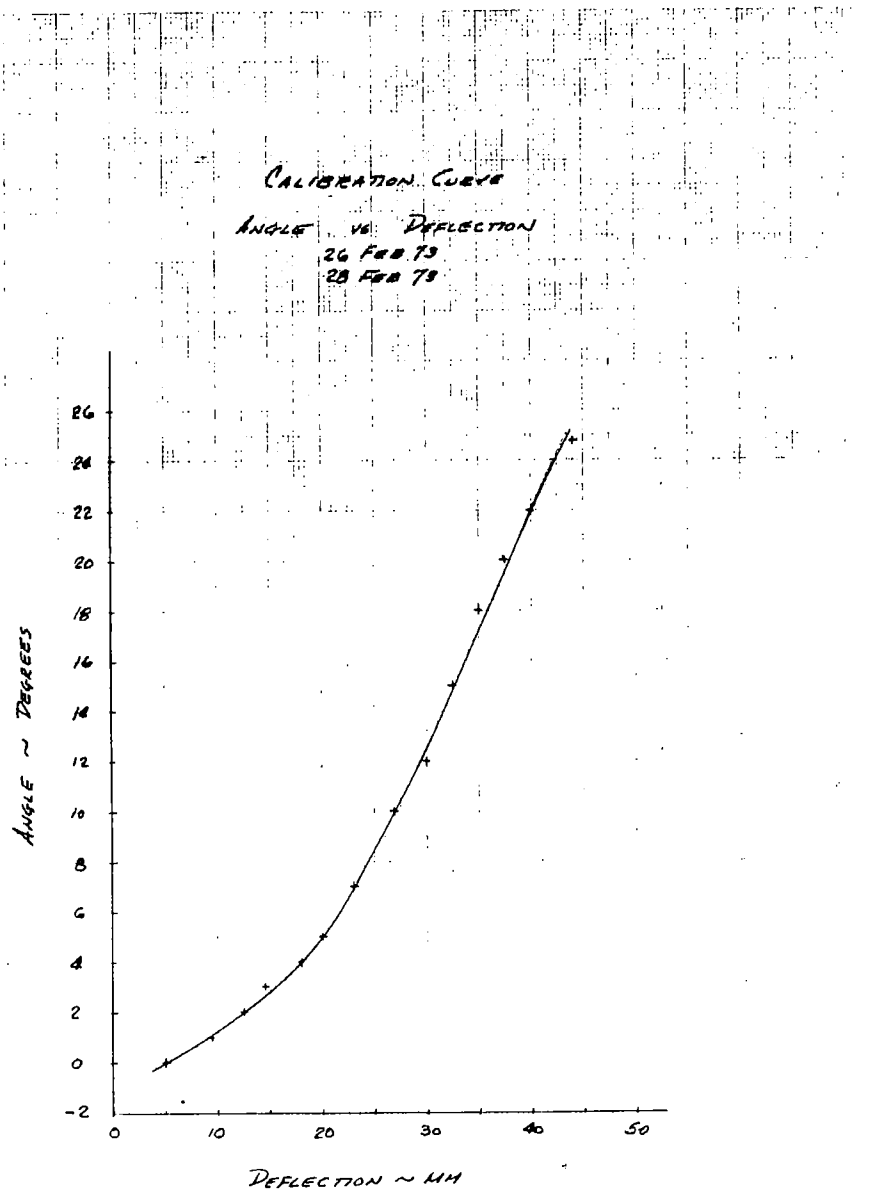

FIGURE E-4 - ANGLE vs RECORDER DEFLECTION

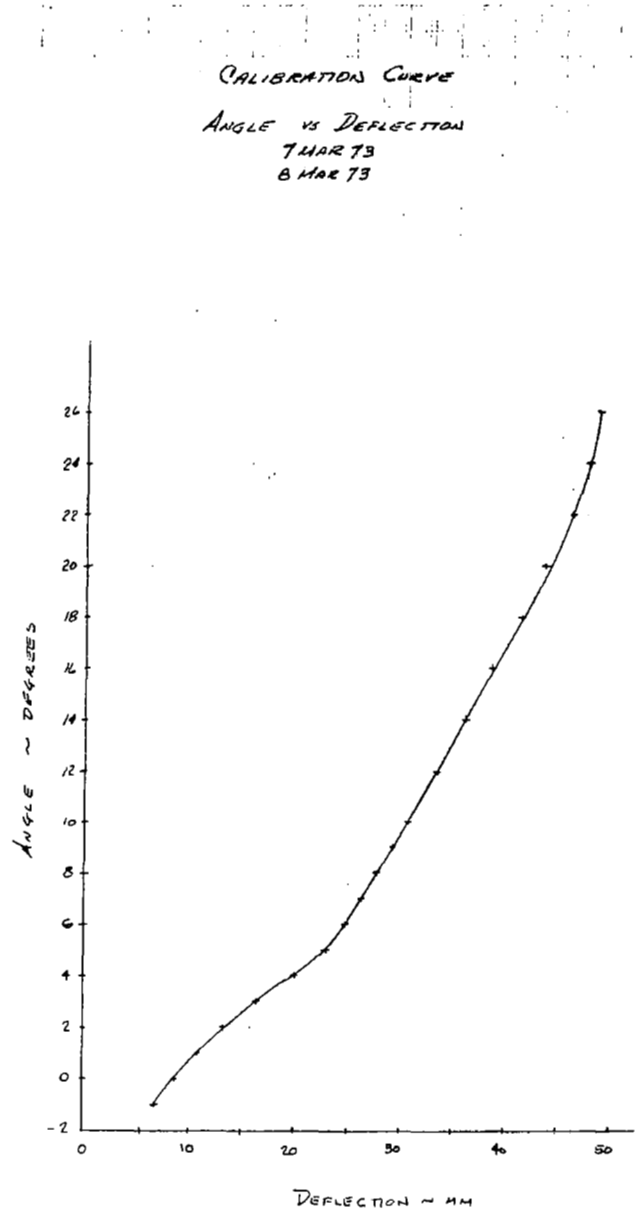

FIGURE E-5 - ANGLE vs RECORDER REFLECTION

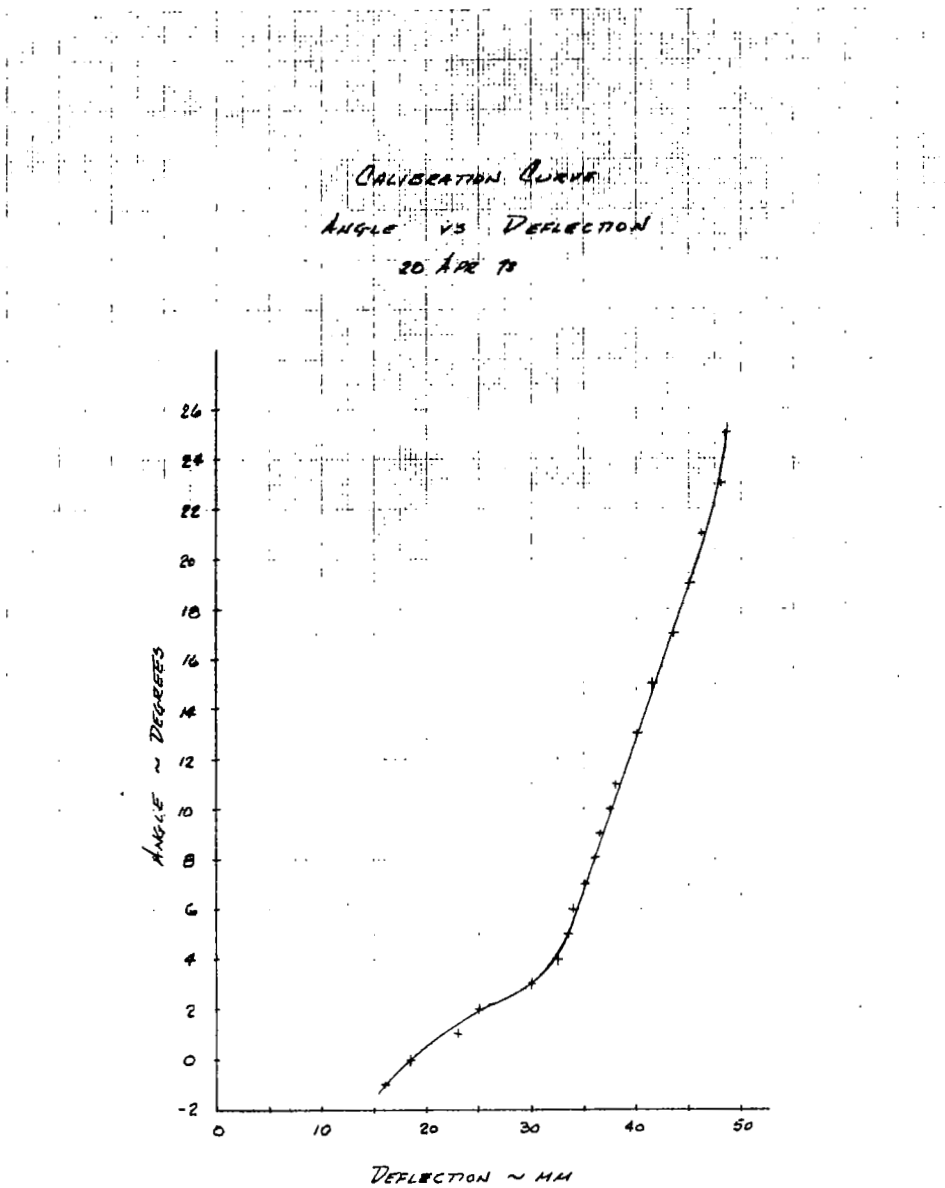

FIGURE E-6 - ANGLE vs RECORDER DEFLECTION

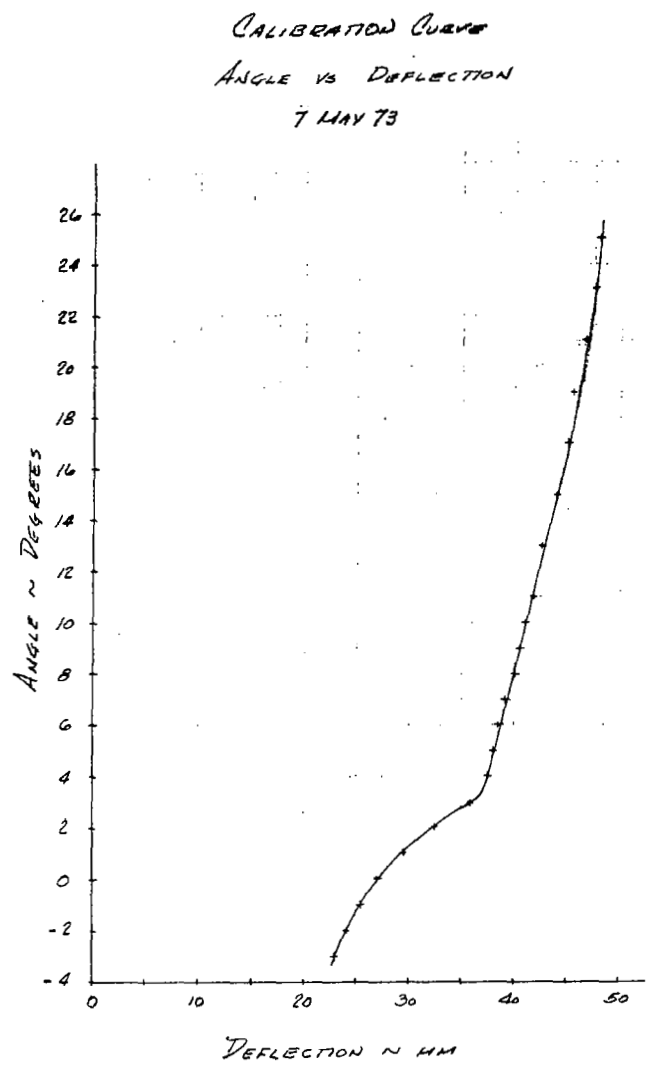

FIGURE E-7 - ANGLE vs RECORDER DEFLECTION

DISTRIBUTION LIST

CONTRACT NAS1-11382

ORGANIZATION	NUMBER OF COPIES
NASA Langley Research Center Hampton, VA 23365	
Attention: Report & Manuscript & Control Office, MS 180A	1
J. Hoell, Jr. Mail Stop 160	1
NASA Ames Research Center Moffett Field, CA 94035	
Attention: Library, Mail Stop 202-3	1
NASA Flight Research Center P.O. Box 273 Edwards, CA 93523	
Attention: Library	1
Jet Propulsion Laboratory 4800 Oak Grove Drive Pasadena, CA 91103	
Attention: Library, Mail 111-113	1
John B. Dahlgren, Mail 198-112A	10
Dr. Duane Dipprey, Mail 122-123	1
NASA Johnson Space Center 2101 Webster Seabrook Road Houston, TX 77058	
Attention: Library, Code BM6	1
NASA Marshall Space Flight Center Huntsville, AL 35812	
Attention: Library	1
Ernst Stuhlinger, AD-S	1
NASA Lewis Research Center 21000 Brookpark Road Cleveland, OH 44135	
Attention: Library, Mail Stop 60-3	1
Harold Kaufman, Mail Stop 54-1	1
NASA Goddard Space Flight Center Greenbelt, MD 20771	
Attention: Library	1
Dr. R. Hunter Code 763.0	1
R. Callens Code 763.2	1
T. Williams Code 763.2	1
Comsat Laboratories Positioning & Orientation Branch Washington, DC 20013	
Attention: Bernard Free	1
George Huson	1

DISTRIBUTION LIST (cont.)

ORGANIZATION	NUMBER OF COPIES
TRW Systems Inc. One Space Park Redondo Beach, CA 90278 Attention: Dr. C. L. Dailey	1
Air Force Weapons Laboratory Kirtland Air Force Base, NM 87417 Attention: ~~WLRC/Capt. G. F. Fritts~~ Sid	1
Thermal Mechanical Research Laboratory OAR USAF Wright-Patterson Air Force Base, OH 45433 Attention: Eric Soehngen	1
Los Alamos Scientific Laboratories P.O. Box 1663 Los Alamos, NM 87544 Attention: Dr. Stratton	1
Research and Technology Division Wright-Patterson Air Force Base, OH 45433 Attention: David Fritts, AFAPL (APIE-1)	1
United States Air Force Office Of Scientific Research Washington, DC 20025 Attention: M. Slawsky	1
NASA Scientific & Technical Information Facility P.O. Box 33 College Park, MD 20740	15 plus reproducible
Hq USAF/AFRDSD/Lt Colonel Wolfsberger Washington, DC 20330	1
Aerospace Corporation 2350 E. El Segundo Blvd. El Segundo CA 90245 Attention: J. Russi R. Doebler K. Turner John Stevens	 1 1 1 1
AFRPL/LKDA/Capt. S. Rosen, Edwards, CA 93523	1
AFRPL/LKDA Edwards, CA 93523 Attention: T. Waddell	1
Massachusetts Institute of Technology Lincoln Laboratory Lexington, MA 92173 Attention: Mr. McClellan R. Vondra	 1 2

DISTRIBUTION LIST (cont.)

ORGANIZATION	NUMBER OF COPIES
Naval Research Laboratory Attention: Mr. Beals Washington, DC 20032	1
Fairchild Industries Attention: Dr. W. Guman Farmingdale, LI, NY 11735	1
Johns Hopkins University Applied Physics Laboratory 8621 Georgia Avenue Silver Spring, MD 20910	
Attention: Mr. Fuechsel	1
S. Kowal	1
National Aeronautics & Space Administration Washington, DC 20546	
Attn: Library, KSS-10	1
RP/NASA Headquarters	1
NASA John F. Kennedy Space Center Kennedy Space Center, FL 32899 Attn: Library, IS-DOC-1L	1
GENERAL ELECTRIC CO.	
E. H. Youmans	5
J. T. Kenney	5
T. A. Jones	1
E. R. Hansen	1
P. A. Malherbe	1
G. E. DiSalle	1
R. A. Foster	1
F. J. Yocum	1
S. M. Scala	1
A. D. Cohen	1
C. K. Leonard	1
R. T. McFall	1
M. F. Sedlacek	1
T. W. Karras	1
J. Christopher	1
W. E. Johnston	1
J. H. Chestek	1
C. H. Marston	1
A. T. Tweedie	1